Investigation of the Dynamic Behavior of a Cable-Harnessed Structure

Jiduck Choi

Dissertation submitted to the faculty of the Virginia Polytechnic Institute and State University in partial fulfillment of the requirements for the degree of

Doctor of Philosophy

In

Mechanical Engineering

Daniel J. Inman, Committee Chair

Mehdi Ahmadian

Mary E. Kasarda

Pablo A. Tarazaga

Jeff T. Borggaard

May 20, 2104

Blacksburg, Virginia

Keywords: Cable-Harnessed Structure, Spectral Element Method, Damping Matrix Identification, Finite Element Model Updating

Investigation of the Dynamic Behavior of a Cable-Harnessed Structure

Jiduck Choi

ABSTRACT

To obtain predictive modeling of a spacecraft, the author investigates the effects of adding cables to a simple structure with the goal of developing an understanding of how cables interacting with a structure. In this research, the author presents predictive and accurate modeling of a cable-harnessed structure by means of the Spectral Element Method (SEM). A double beam model is used to emulate a cable-harnessed structure. SEM modeling can define the location and the number of connections between the two beams in a convenient fashion. The proposed modeling is applied and compared with the conventional FEM. The modeling approach was compared to and validated by measurement data. The validated modeling was implemented to investigate the effect of the number of connections, of the spring stiffness of interconnections, and of mass portion of an attached cable. Damping has an important role in structural design because it reduces the dynamic response, thereby avoiding excessive deflection or stress, fatigue loads, and settling times. Experimental results with some specimens indicate a clear change of damping on the main structure with the inclusion of cable dynamics. The author investigated the modification of the damping of the host structure induced by

various attached cables. The identification of a damping matrix is performed using measured data. The effect of the flexibility of a cable harness on damping is observed through experiments with various types of cables. The effect of the number of connections on damping is also investigated by changing the number of connections. Moreover, to overcome the sensitivity to noise in measured data of damping matrix identification approach, various methods are compared with a simulated lumped model and real test results. An improved damping matrix identification approach is proposed and can generate the unique damping matrix over the full frequency range of interest.

Dedication

I would like to dedicate this dissertation to my wife, Hyun Jin Kim, who sacrificed her career to support my studies. Her efforts in taking care of our lovely child, Ah-Ra Choi, enabled me to concentrate on and finish this research. She is the “best present from the God, worth more than any precious jewels”.

My wonderful daughter was there for me throughout the entire doctorate program, and refilled my energy and made me laugh.

I also dedicate this dissertation to my loving father and mother whose endless love, encouragement, prayers, and support enabled me to have much success and many honors.

I am grateful to my parent in-laws who have always encouraged me during my studies.

Acknowledgements

First of all, I would like to express my deepest appreciation and respect to my advisor, Professor Daniel J. Inman. He continually encouraged me at every time when I was stuck in some problem and convincingly conveyed a spirit of adventure with regard to research. Without his guidance and persistent help, this dissertation would not have been possible. He also gave me various opportunities to experience many places in United States where I attended conferences. He especially gave me a chance to experience research in two universities, Virginia Tech and the University of Michigan.

I appreciate the invaluable comments and suggestions from my committee members, Dr. Ahmadian, Dr. Kasarda, Dr. Borggaard, and Dr. Tarazaga. They enriched and improved my work.

I also feel grateful to my research institute, the Agency for Defense Development in Korea. They gave me a chance to study abroad without discontinuing my career.

I owe a special thanks to all of my lab colleagues for sharing their endless energy on research: Cassio Farria, Jared Hobeck, Alex Pankonien, and Kaitlin Spak.

My Korean friends were also invaluable to me. I would like to express my gratitude to Beomsuk Choi, Woonkyung Kim, Inho Kim, Hyeongjun Park, Jinwoo Seok, and Jaeheon Shim.

I acknowledge the support from the (US) *Air Force Office of Scientific Research* grant number FA9550-10-1-0427 titled "Structural Dynamics of Cable-Harnessed Spacecraft Structures" monitored by Dr. David Stargel.

Table of contents

List of figures

List of Tables

Chapter 1

Introduction

1.1 Motivation

In satellite applications, modeling is extremely important in order to predict behavior during the launch and in orbit. Today, detailed finite element models of satellite structures are accurate and agree well with experimental data. However, once the satellites are hung with cable harnesses the ability to model the system dynamics eludes modeling engineers. Previous researchers have not been able to model the effects on the dynamics of adding cables to a satellite [1]. The weight of the spacecraft becomes lighter with the improvement of structural analysis and design. However, the sensor and actuator power cables inside the structure increase in both power demand and quantity. Nowadays, cables can add up to 30% more mass to a satellite and initial attempts to simply add mass to the model have not produced acceptable results. Adding cables not only changes the mass distribution but also adds damping and, in general, changes the entire dynamic response. With this motivation, the author proposes modeling a satellite quality cable attached to a simple beam structure by the Spectral Element Method (SEM), in order to provide insight into the effects of adding cables to a structure and to produce a predictive model of a structure with a cable attached. To consider the combined distributed system connected at the discrete locations, the methodology to define the locations of the interconnections should be required. Meshing and assembly feature of SEM enable the definition and tracking of interconnections. Based on the exact dynamic stiffness matrices, the SEM can guarantee the accurate results.

The mechanism of structural damping is a complicated physical phenomenon. The damping identification is a very important task in modeling dynamic systems. In addition to controlling the amplitude of resonant vibrations, damping also has other effects, such as modifying wave attenuation and sound transmission properties through structures, reducing structural fatigue and increasing structural life [2]. Because damping is a dynamic effect it can only be determined through experimental results. Therefore, it is very difficult to develop a general model of damping. Here various damping identification methods are applied to investigate the damping alteration of a host structure induced by attached cables. Moreover, the damping identification method is proposed by a combination of model reduction and model updating with a damping matrix identification method.

1.2 Description of the problem

Figure 1 presents the inside of the satellite as an example of the lightweight cable-harnessed structure.

Figure 1 Air Force precision spacecraft with cable harnesses (Courtesy of M. I. Roberston, AFRL/RVSV).

To investigate the dynamic behavior of a cable-harnessed structure, a double beam system is presented as a simplified model of the section of a lightweight space structure as shown in Figure 2. The main structure is modeled as a beam with rectangular cross section. The cable attachment is treated as a circular beam. The interconnections between beams can be defined by means of their locations and spring constants.

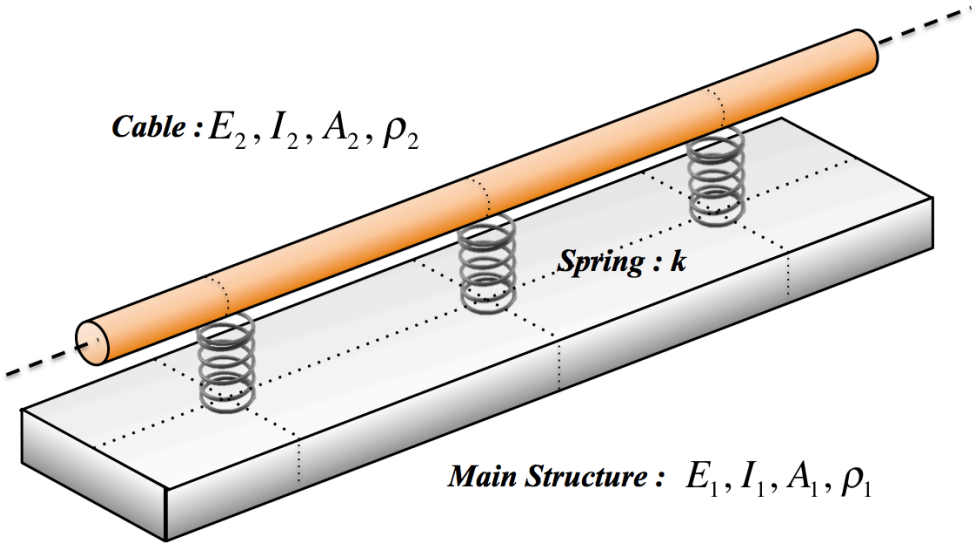

Figure 2 The model of a cable-harnessed structure

By utilizing this model, the spectrally formulated modeling for a combined system will be compared with the FEM results and validated experimentally. Furthermore, the double-beam system is also utilized in experimental configuration for validating the modeling and identifying the damping. In addition, the spring constant of interconnection structure is obtained from these experiments.

1.3 Dissertation outline

The dissertation is organized as follows: In chapter 1, the background of this research and the literature reviews are presented to introduce the various methods to investigate

the dynamic behavior of a cable-harnessed structure. In chapter 2, the spectrally formulated models of a single beam and a double-beam system are presented. The spectrally formulated models are validated by experimental results in chapter 3. The spring stiffness of interconnection structure is experimentally obtained too. The simulation results reveal the effects of number of interconnections, of the spring stiffness of interconnections, and of the mass portion of an attached cable in chapter 4. In chapter 5, the change of damping is investigated in two points of view: a number of interconnections and type of an attached cable. The damping matrix is identified using Kim's method. And the effect of the flexibility of an attached cable on damping is observed using lumped system. Then IV method is applied to identify the damping ratios and validate the flexibility effect on damping with reduction of noise in measurement. The new damping identification procedure is proposed by a combination the FE model reduction and updating with the full measured FRF matrix in chapter 6. Chapter 7 presents conclusions and discusses the future work.

1.4 Literature survey

1.4.1 Modeling approaches for a combined system

There are many approaches to modeling a combined dynamic system in the literature. The response of a single beam has an exact solution, which can be obtained in various ways [3]. However, when a secondary beam is attached to the main beam by means of several spring connections, obtaining the solution of a system becomes more complicated. Several authors have investigated double-beam systems that are elastically combined by a distributed spring in parallel. Seelig and Hoppman II [4] have worked out the solution of the differential equation of elastically connected parallel beams. Gürgöze

[5], [6] has dealt with the derivation of the frequency equation of a clamped-free Euler Bernoulli beam with several spring-mass systems attached in the mid span by means of the Lagrange multipliers method. An exact method has presented for the vibration of a double-beam system subject to harmonic excitation by Vu et al. [7]. The system consists of a main beam with an applied force, and an auxiliary beam, with a distributed spring k and damper c in parallel between the two beams. Wu and Chou [8] have considered a beam connected to several two degree-of-freedom (DOF) systems at specific locations. Rao [9] has considered the free response of several Timoshenko beam systems connected elastically.

Our approach here is to apply the Spectral Element Method (SEM) to the combined distributed system. Doyle [10] and Doyle & Farris [11] have presented spectrally formulated elements for rods and beams. Gopalakrishnan et al. [12] have considered an assembly of dynamic stiffness matrices of the Timoshenko beam, similarly for conventional finite elements. Lee [13] has introduced a general approach to spectral element formulation for one-dimensional structures, in which the spectral element matrix is computed numerically directly from the transfer matrix formulated from the state vector equation of motion of a structure. Lee et al. [14] have presented the spectral element model formulated for the axially moving Timoshenko beam under a uniform axial tension. The excellent texts have also presented the spectral element method by Doyle [15] and Lee [16]. Doyle has introduced the basic formulation of the spectral element matrix by using an Euler-Bernoulli beam. Lee has summarized the various ways to derive the spectral element matrix for structural elements such as an Euler beam, a Timoshenko beam and a plate. Lee has also presented several practical applications of

SEM. Many authors have used the dynamic stiffness approach to modeling, which is very closely related to the SEM approach. Aït-Djaoud et al. [17] have presented the dynamic stiffness matrix method for beam element to include the effect of concentrated masses. The quantitative effect of concentrated on masses to the natural frequencies of the structure was assessed. Banerjee [18] and Chen [19] have used the dynamic stiffness matrix for a beam with attached two DOF systems. Li and Hua [20], [21] have considered elastically connected two and three parallel beams by using dynamic stiffness analysis. Jiao et al. [22] have investigated the Euler beam with an arbitrary cross section. Choi and Inman [23, 24, 25] considered applying the SEM to a double beams system as a simplified model of a cable-harnessed structure and validated it experimentally on a combined system.

1.4.2 Damping matrix identification

Most mechanical systems under vibrating environments experience the dissipation of energy by damping. The identification of damping in a real physical system is a very important task in modeling the dynamics of the system. But the extensive modeling of damping still remains an unsolved problem. In most methods of modeling damping, the damping matrix is expressed by using a simple model such as viscous, structural, or proportional for mathematical convenience. However, the actual physical system has damping due to boundary conditions, the spatial distribution of the damping, and many other effects that are typically ignored and/or difficult to model. To present the proper damping matrix dealing with both the physical mechanism and spatial distribution of damping, various approaches have been proposed. Pilkey and Inman [26] have presented the excellent reviews of damping matrix identification approaches. Pradhan and Modak

[27] have also given good reviews of damping matrix identification methods. They have also presented an excellent categorization of the damping matrix identification methods. The damping matrix identification methods can be classified into three main groups.

1) FRF-based direct method

The first group is known as a direct method based on the measured Frequency Response Functions (FRFs). In this group, the system matrices can be obtained directly from the measurement data without the effort to find the modal parameters. However, this group requires the measurement of the full FRF matrix that can cause a significant experimental complexity.

Caravani and Thomson's method

Caravani and Thomson [28] have explained a numerical approach that identifies the optimal damping coefficient of a multidimensional system. The identification is performed in an iterative manner. They have assumed that the mass and stiffness matrices M and K are known. Only the viscous damping is considered. In general, there is the distinction between the ideal system and real system. The damping coefficients are obtained by minimizing the difference between the responses of the ideal and the real system. The damping vector $\mathbf{d}_k$ is identified by repeatedly minimizing the cost function L_k.

$$L_K = \sum_{i=1}^{k} \left[\left(\mathbf{X}_{i,k} - \overline{\mathbf{X}}_i \right) \mathbf{A}_i \left(\mathbf{X}_{i,k} - \overline{\mathbf{X}}_i \right) + \left(\mathbf{d}_k - \mathbf{d}_0 \right)^T B_i \left(\mathbf{d}_k - \mathbf{d}_0 \right) \right] \tag{1}$$

Where $\mathbf{X}$ and $\overline{\mathbf{X}}$ are response vectors, $\mathbf{A}_i$ is treated as an inverse covariance matrix and $\mathbf{B}_i$ is the penalty function. In each iteration procedure, the vectors $\mathbf{X}_{i,k}$ are related to $\mathbf{d}_k$ by the nonlinear relationship. $\mathbf{X}_{i,k}$ and $\mathbf{d}_k$ are expressed by

$$\mathbf{d}_k = \mathbf{d}_{k-1} + \left[\sum_{i=1}^{k}\left(\mathbf{J}_{i,k-1}^T \mathbf{A}\mathbf{J}_{i,k-1} + B_i\right)\right]^{-1} \times \left[\sum_{i=1}^{k}\left(\mathbf{J}_{i,k-1}^T \mathbf{A}(\overline{\mathbf{X}}_i - \mathbf{X}_{i,k-1}) + B_i(\mathbf{d}_0 - \mathbf{d}_{k-1})\right)\right] \qquad (2)$$
$$\mathbf{X}_{i,k} = \mathbf{X}_{i,k-1} + \mathbf{J}_{i,k-1}(\mathbf{d}_k - \mathbf{d}_{k-1})$$

where $\mathbf{J}_{i,k-1}$ is the Jacobian matrix $\left[dX/dc\right]_{d=d_{k-1}}$. In most cases, **B** is set to zero to reach the coefficient to their stationary values. If the obtained coefficients are not physically correct, then one must gradually increase the **B** matrix and repeat the iteration process. Thomson and Caravani [29] have extended their work to non-proportional damping.

Chen, Ju, and Tsuei's method

Chen et al. [30, 31] have presented the *Normal FRF method* to obtain the damping matrix separately from mass and stiffness matrix. The equation of motion with viscous damping is expressed as

$$\mathbf{M}\ddot{x}(t) + \mathbf{C}\dot{x}(t) + \mathbf{K}x(t) = f(t) \qquad (3)$$

For the harmonic excitation, equation (1) is written as

$$\left[\mathbf{K} - \omega^2\mathbf{M}\right]X(\omega) + j\omega\mathbf{C}X(\omega) = F(\omega) \qquad (4)$$

Considering H^N as the frequency response function from the normal modes $\left[\mathbf{K} - \omega^2\mathbf{M}\right]^{-1}$, pre-multiplying equation (4) by H^N yields

$$\left[I + j\omega H^N(\omega)\mathbf{C}\right]X(\omega) = F(\omega) \qquad (5)$$

The measured FRF matrix is denoted as complex frequency response function, H^C. The normal FRF is derived from H^C such as,

$$H^N(\omega) = H_R^C(\omega) - G(\omega)H_I^C(\omega) \qquad (6)$$

where the transformation equation $G(\omega)$ is defined as

$$G(\omega) = -H_I^C(\omega)\left[H_R^C(\omega)\right]^{-1} \tag{7}$$

For a noise-free case, an exact solution for damping matrix can be obtained directly from equation (2) by

$$C = -\frac{1}{\omega_j}\left[H^N(\omega_j)\right]^{-1} G(\omega_j) \tag{8}$$

In practice, the FRFs are contaminated with noise and the *Least Squares Method* (LS) is employed to solve for the damping matrix. Chen et al. have considered that the identification results could be improved by the separation of the damping matrix from mass and stiffness matrices, because the order of magnitude of damping matrices is smaller than that of stiffness and mass matrices.

Lee and Kim's method

Lee and Kim [32, 33, 34] have proposed the direct identification of a damping matrix by using the *Dynamic Stiffness Matrix* (DSM), the inverse of the measured *Frequency Response Matrix* (FRM). The procedure to obtain the damping matrices can be summarized as the following. The equation of motion of a dynamic system with damping is:

$$\mathbf{M}\ddot{x}(t) + \mathbf{C}\dot{x}(t) + (\mathbf{K} + \mathrm{j}\mathbf{D})x(t) = f(t) \tag{9}$$

where M, K, C and D are the mass, stiffness, viscous damping and structural damping matrices. For the harmonic excitation, equation (9) is written as

$$\left[\left(\mathbf{K} - \omega^2\mathbf{M}\right) + \mathrm{j}\left(\omega\mathbf{C} + \mathbf{D}\right)\right]X(\omega) = F(\omega) \tag{10}$$

The dynamic stiffness matrix (DSM) is expressed as

$$H^c(\omega)^{-1} = \left(\mathbf{K} - \omega^2\mathbf{M}\right) + \mathrm{j}\left(\omega\mathbf{C} + \mathbf{D}\right) \tag{11}$$

where $H^c(\omega)$ is the complex frequency response matrix (FRM) from the measurement. The DSM is expressed as an inverse of measured complex FRM. FRM is much easier to measure than DSM. After obtaining the DSM by inverting the FRM, equation (11) can be expressed as

$$\text{real}\left[H^c(\omega)\right]^{-1} = \mathbf{K} - \omega^2\mathbf{M}, \qquad \text{Imag}\left[H^c(\omega)\right]^{-1} = \omega\mathbf{C} + \mathbf{D} \tag{12}$$

where *imag* and *real* represent the imaginary and real part. From the imaginary part of equation (12) with least-square sense, the damping matrices can be obtained as

$$\begin{bmatrix} \mathbf{D} \\ \mathbf{C} \end{bmatrix}_{2n\times n} = \begin{bmatrix} \mathbf{I} & \omega_1\mathbf{I} \\ \mathbf{I} & \omega_2\mathbf{I} \\ \vdots & \vdots \\ \vdots & \vdots \\ \mathbf{I} & \omega_k\mathbf{I} \end{bmatrix}^{+}_{2n\times kn} \begin{bmatrix} \text{Imag}\left[H^c(\omega_1)\right]^{-1} \\ \text{Imag}\left[H^c(\omega_2)\right]^{-1} \\ \vdots \\ \text{Imag}\left[H^c(\omega_k)\right]^{-1} \end{bmatrix}_{kn\times n} \tag{13}$$

where '+' denotes the pseudo-inverse of the matrix. Ozgen and Kim [35] have investigated the DSM-based method further and presented an experimental setup to reduce the noise effect on DSM. Ozgen and Kim have proposed the expansion of the identified damping matrix to the size of the analytical model. The expanded damping matrix was combined with analytical stiffness and mass matrices to build an experimental–analytical hybrid model.

Instrumental Variable (IV) method

Fritzen [36] has optimized a loss function to estimate the system parameters. The output error (ε_{OE}) is defined as

$$\varepsilon_{OE} = X(s) - X_m(s) = X(s) - (s^2\mathbf{M} + s\mathbf{C} + \mathbf{K})^{-1}F(s) \tag{14}$$

The unknown system parameters **M**, **K** and **C** appear as nonlinear in equation (14). Thus, Fritzen has considered the equation error (ε_{EE}) that has the advantage that the unknown matrices appear linear in the error equation as shown in equation (15).

$$\varepsilon_{EE} = F(s) - (s^2\mathbf{M} + s\mathbf{C} + \mathbf{K})X(s) \tag{15}$$

A vector **p,** the parameter vector, is defined and its components are mass, stiffness and damping matrices. The dimension of **p** is $N < 3n$. Then, the error equation is expressed as

$$\varepsilon = \mathbf{b} - \mathbf{A}\mathbf{p} \tag{16}$$

where ε is an error and **b** is a force vector. The **A** matrix is shown as

$$\mathbf{A} = \begin{bmatrix} s_1^2 X_1^T(s_1) & s_1 X_1^T(s_1) & X_1^T(s_1) \\ s_2^2 X_1^T(s_2) & s_1 X_1^T(s_1) & X_1^T(s_2) \\ \vdots & \vdots & \vdots \\ s_v^2 X_\mu^T(s_1) & s_v X_\mu^T(s_v) & X_\mu^T(s_v) \end{bmatrix} \tag{17}$$

The solution of equation (17) in the sense of least squares means minimization of the loss function $J = \left\| e^T e \right\|$. The equation can be expressed in normal equation as $\mathbf{A^T A p = A^T b}$ where **p** is the solution vector. To solve this equation, the *Instrumental Variable* (IV) method is applied. The IV method was developed for parameter estimation in econometrics and summarized by Kendall and Stuart [37]. An iterative procedure is used to solve for the unknown parameter vector *p*. First, a least squares estimate is used to find an initial **p**. Then, a new **p** is estimated by $\mathbf{p = (W^T A)^{-1} W^T b}$**.** After convergence has been achieved, the damping matrix is derived from the elements of *p*. One problem with the Instrumental Variable (IV) method is that the choice of the **W** matrix is not straightforward. Young [38] has suggested building up **W** from the undisturbed output signals of the system. Fritzen has created an additional auxiliary model that produces as

output Instrumental Variables X_{aux}. These are composed to the matrix **W** by equation (17).

Wang [39] has combined the weighted FRF with the IV method. An error of FRF, $\Delta H(\omega)$ is weighted by the Dynamic Stiffness Matrix, $\mathbf{S}(\omega)$ such as

$$\left[\Delta H(\omega)\right]\left[\mathbf{S}(\omega)\right] = [H_M(\omega)][\mathbf{S}(\omega)] - \mathbf{I} \tag{18}$$

The IV method proves to be effective in reducing or eliminating the noise effect in identification.

2) Modal parameters based method

The second group is the method based on modal parameters. This group uses experimentally identified modal parameters, frequencies, damping ratios and mode shape vectors, to find the damping matrix. These approaches require modal parameter estimation of measurement FRF data before the identification. The system parameters are extracted using modal parameters such as natural frequencies and mode shapes derived from the FRF data. However, the structural parameters estimated by these methods can be affected by several factors including the inaccuracy of FRFs, the errors in the extracted modal parameters and the incompleteness of the modal information.

Lancaster's method

Lancaster [40] has proposed the identification method of mass, stiffness and damping matrices directly from complex modal parameters such as eigenvalues and eigenvectors. The complex modes are normalized by

$$\psi_j^T\left[2\lambda_j\mathbf{M} + \mathbf{C}\right]\psi_j = 1 \tag{19}$$

Then the system matrices can be identified as

$$\begin{aligned}
\mathbf{M} &= \left[\Phi\Lambda\Phi^T + \overline{\Phi\Lambda}\Phi^*\right]^{-1} \\
\mathbf{K} &= -\left[\Phi\Lambda^{-1}\Phi^T + \overline{\Phi\Lambda^{-1}}\Phi^*\right]^{-1} \\
\mathbf{C} &= -\mathbf{M}\left[\Phi\Lambda^2\Phi^T + \overline{\Phi\Lambda}^2\Phi^*\right]\mathbf{M}
\end{aligned} \tag{20}$$

where the Λ and Φ represents the matrix of eigenvalues and eigenvectors. The over-bar means complex conjugate and the * is the complex conjugate transpose. The weakness of this method is that normalization process in equation (19) requires the mass and damping matrices themselves that are the targets of calculation. Adhikari [41] has proposed a method, based on the poles and residues of the measured transfer functions, to overcome this basic difficulty associated with Lancaster's method.

Hasselman's method

Hasselman [42] has dealt with the viscous damping only. The viscous damping is typically assumed that the modal damping matrix is taken to be diagonal. Considering the linear viscous damping, the damping matrix is diagonalized by a transformation to modal coordinates. The diagonal terms are related to the percent of critical damping of each mode. However, non-proportional damping in general does not diagonalize. And the off-diagonal terms exist with the same order as the diagonal terms.

$$\begin{aligned}
\mathbf{C}_{jj} &= -2\sigma_j\mathbf{M}_{jj} \\
\mathbf{C}_{jk} &= \omega_j\delta\left(\phi_j^{\mathrm{Im}}\right)^T m\phi_k^{\mathrm{Re}} + \omega_k\left(\phi_j^{\mathrm{Re}}\right)m\delta\phi_k^{\mathrm{Im}}
\end{aligned} \tag{21}$$

where $\phi = \phi^{\mathrm{Re}} + \delta\phi^{\mathrm{Re}} + j\delta\phi^{\mathrm{Im}}$. The $\delta\phi^{\mathrm{Im}}$ can be obtained from the co-quad technique. The response of a given point on a structure is separated into coincident and quadrature components (co and quad). These are used to construct the off-diagonal term $\mathbf{C}_{jk}$ in damping matrix if sufficient pure modes are obtainable.

Ibrahim's method

Ibrahim [43] has illustrated a state space formulation that uses a partial set of identified complex modes together with an analytical FE model of the structure to estimate improved system matrices. First, the normal modes are calculated from the given complex modes. The improved mass matrix is computed by incorporating extracted normal modes in the mass orthogonality equation.

$$\mathbf{u}_\mathbf{N}^\mathbf{T}\mathbf{M}\mathbf{u}_\mathbf{N} = \mathbf{M}_\mathbf{A} \tag{22}$$

where $\mathbf{M_A}$ is the analytical mass matrix, $\mathbf{M}$ is an improved mass matrix, and $\mathbf{u_N}$ are the extracted normal modes. Then, the damping matrix can then be obtained by

$$\mathbf{C} = \mathbf{M}\left[\mathbf{M}^{-1}\mathbf{C}\right] \tag{23}$$

In equation (22), the improved mass matrix $\mathbf{M}$ is obtained from equation (21). The $\mathbf{M}^{-1}\mathbf{C}$ term is found from the following relations as a combination of measured complex modes and analytical modes:

$$\begin{aligned}
\begin{bmatrix} \mathbf{M}^{-1}\mathbf{K} & \mathbf{M}^{-1}\mathbf{C} \end{bmatrix}\begin{bmatrix} \psi_i \\ \lambda_i\psi_i \end{bmatrix} &= \left\{-\lambda^2\psi_i\right\} \; i = 1..m \\
\begin{bmatrix} \mathbf{M}^{-1}\mathbf{K} & \mathbf{M}^{-1}\mathbf{C} \end{bmatrix}\begin{bmatrix} \phi_j \\ \lambda_j\phi_j \end{bmatrix} &= \left\{-\lambda^2\phi_j\right\} \; j = m+1..n
\end{aligned} \tag{24}$$

where m is the number of experimental modes and the ψ, ϕ are the measured complex mode shapes and analytical mode shapes respectively. The limitation is that the order of the improved matrices cannot exceed the number of elements in the measured eigenvectors.

Minas and Inman's method

Minas and Inman [44] have proposed a method for identifying the damping matrix of a structure from incomplete experimental data combined with a reasonable representation of the analytical mass and stiffness matrices developed by finite element methods. The mass and stiffness matrices are then reduced to the size of the modal data measured by using standard model reduction techniques. Rearranging the eigenvalue problem yields

$$\mathbf{C}\mathbf{u}_i = -(1/\lambda_i)(\lambda_i^2\mathbf{M} + \mathbf{K})\mathbf{u}_i = \mathbf{f}_i \tag{25}$$

where λ_i and $\mathbf{u}_i$ are the measured eigenvalues and eigenvectors and the matrices **M** and **K** are assumed to be known. Its complex conjugate transpose is $\mathbf{u}_i^*\mathbf{C} = \mathbf{f}_i^*$ which can be solved by separating the real and imaginary parts and rearranging them, obtaining the equation

$$\mathbf{G}_i\mathbf{d} = \mathbf{b}_i \tag{26}$$

where the entries of $\mathbf{G}_i$ are the real and imaginary parts of $\mathbf{u}_i$ and $\mathbf{b}_i$ is given by

$$\mathbf{b}_i = \begin{bmatrix} \mathrm{Re}(\mathbf{f}_i) \\ -\mathrm{Im}(\mathbf{f}_i) \end{bmatrix} \tag{27}$$

As the damping matrix is assumed to be symmetric, the number of unknowns in the *n*x*n* damping matrix **d** can be reduced to (n^2+n)/2. Equation (26) can be solved using the least-squares approach or other optimization procedures depending on the size of the modal data available, which can lead to an over-determined or underdetermined problem.

Pilkey and Inman's method

Pilkey and Inman [45,46,47] proposed the iterative and direct versions of damping identification methods based on Lancaster's normalization formula in equation (19). In the iterative method, assuming that the mass matrix and the eigensystem are predefined,

the initial damping matrix is guessed. Then the eigenvectors are normalized using the initial guess $\mathbf{C}_0$ for the viscous damping matrix such as

$$\psi_j^T\left[2\lambda_j\mathbf{M}+\mathbf{C}_0\right]\psi_j=1 \tag{28}$$

Next, the matrix $\mathbf{C}_1$ is computed using Lancaster's formula

$$\mathbf{C}_1=-\mathbf{M}\left[\Phi\Lambda^2\Phi^T+\overline{\Phi\Lambda}^2\Phi^*\right]\mathbf{M} \tag{29}$$

and compared to the initial guess according to convergence criteria. If the criteria are not satisfied, a new normalization is performed using $\mathbf{C}_1$ as $\psi_j^T\left[2\lambda_j\mathbf{M}+\mathbf{C}_1\right]\psi_j=1$ repeatedly until convergence is reached.

The direct method avoids the iteration. It can be performed on the basis of accurate knowledge of the mass and stiffness matrices. The eigenvalue problem can be written as

$$\psi_j^T\mathbf{C}\psi_j=-\psi_j^T\left[\mathbf{M}\lambda_j+\mathbf{K}(1/\lambda_i)\right]\psi_j \tag{30}$$

Substituting the equation (30) into equation (28) yields a new normalization condition such as

$$\psi_j^T\left[\mathbf{M}\lambda_j-\mathbf{K}\right]\psi_j=\lambda_j \tag{31}$$

Finally, the normalized eigenvectors are used to construct a symmetric damping matrix $\mathbf{C}$ by equation (29).

Adhikari and Woodhouse's method

Adhikari and Woodhouse [48,49] have introduced a damping identification method based on perturbation analysis. This method can be described by the following steps:

1. Measure a set of transfer functions $H_{ij}(\omega)$.

2. Choose the number m of the modes to be retained in the study. Determine the complex natural frequencies λ_j and complex mode shapes z_j from the transfer functions $H_{ij}(\omega)$, for all $j=1\sim m$. Obtain the complex mode shape matrix $\mathbf{Z} = [\ \mathbf{z}_1 \quad \mathbf{z}_2 \quad \cdots \quad \mathbf{z}_m\ ]$.

3. Estimate the undamped natural frequencies as $\omega_j = \mathrm{Re}(\lambda_j)$.

4. Set $\mathbf{U} = \mathbf{Re(Z)}$ and $\mathbf{V} = \mathbf{Im(Z)}$ and obtain $\mathbf{W} = \mathbf{U}^{\mathbf{T}}\mathbf{U}$ and $\mathbf{S} = \mathbf{U}^{\mathbf{T}}\mathbf{V}$.

5. Denote $\mathbf{B} = \mathbf{W}^{-1}\mathbf{S}$

6. From the **B** matrix, C'_{kj} is calculated by

$$\mathbf{C}'_{kj} = \frac{(\omega_j^2 - \omega_k^2)\mathbf{B}_{kj}}{\omega_j} \ (j \neq k) \text{ and } \mathbf{C}'_{jj} = 2\lambda_j \tag{32}$$

7. Finally, the damping matrix in physical coordinates can be obtained as

$$\mathbf{C} = \left[\left(\mathbf{U}^{\mathbf{T}}\mathbf{U}\right)^{-1}\mathbf{U}^{\mathbf{T}}\right]^{\mathbf{T}} \mathbf{C}' \left[\left(\mathbf{U}^{\mathbf{T}}\mathbf{U}\right)^{-1}\mathbf{U}^{\mathbf{T}}\right] \tag{33}$$

The damping matrices **C** and $\mathbf{C}'$ are not symmetric in general. Thus Adhikari and Woodhouse [50] have modified their formulation to obtain the symmetric damping matrix **C**.

3) FE model updating based method

The third group is based on the FE model updating. The damping matrix is identified during the finite element model updating procedure. Detailed review of FE model updating is summarized in the next section.

1.4.3 Finite element model updating

The conventional finite element model (FEM) is the most well-known and powerful modeling method. However, the finite element predictions are often in conflict with the

measurement results from experiments. The error between FEM and measurement mainly comes from several key reasons. First, the order of measurement and the FE model is much smaller than the degrees of freedom of real structure. Thus the analytical model can be only considering part of the real complex structure. Second, the complex connection between structural components and boundary conditions are usually hard to be expressed precisely in analytical model. Third, the uncertainty such as nonlinear behavior of the real physical system cannot be expressed in the equation of motions. Therefore the finite element model updating is concerned with the correction of finite element models based on dynamic response from test structures. The various approaches have been proposed as shown in the surveys by Imregun & Visser [51], Mottershead & Friswell [52]. The excellent text by Friswell and Mottershead [53] gives a very detailed review of finite element model updating methods. The model updating methods can be classified into two broad groups: direct updating and iterative updating.

1) Direct model updating

Direct updating methods do not require an iteration procedure. Thus excessive computational costs can be avoided. This group updates the mass and stiffness matrices directly. Direct methods can reproduce the measured data exactly. However, the physical meaning of the updated system matrices is often not preserved. Baruch [54] has considered the mass matrix to be accurate as the reference of updating. If the measured eigenvectors are corrected, the orthogonality can be used to update the stiffness matrix. The measured modes will not be orthogonal to the analytical mass matrix because the real test structure is distinct from the analytical model. If the mass matrix is exact then the eigenvector matrix may be corrected to enforce orthogonality. The corrected modal

matrix can be used to update the analytical stiffness matrix with two constraints: reproduction of the measured modal data and preservation of symmetry condition. Berman and Nagy [55] have considered the measured modal data as a reference to update the mass and stiffness matrices. Baruch [56] has defined these kinds of methods as the *Reference Basis* methods. Caesar [57, 58] has proposed updating methods with a wide set of selection of the references. Wei [59] has investigated the approach to update the mass and stiffness simultaneously using the measured eigenvector matrix as the reference. Friswell et al. [60] have extended the method of Baruch [56], which deals with the stiffness matrix only, to the direct updating of stiffness and damping matrices. Minas and Inman [61, 62] have applied the eigenstructure assignment technique to the model updating method, based on the control theory. This method can correct the parameters more accurately. However it requires a large amount of calculation, and thus is not suitable for the model updating of large-scale structure. The complete input and output matrix are hard to be obtained in reality. Furthermore, the updating results may not have the physical insight. Tarazaga et al. [63, 64] have proposed a model updating procedure by using the quadratic compression method. This method requires the proper selection of the principal submatrices that reflect the physical system to be updated. Cavalho et al. [65] have introduced the direct model updating method that can handle the incomplete measured data without using standard modal expansion or reduction techniques. The completed eigenvector matrix is such that it is mass normalized with respect to the analytical mass matrix. The method is also capable of preserving a large number of eigenvalues and eigenvectors without a spillover effect.

2) Iterative model updating

Iterative methods are based on minimizing a penalty function that is generally a non-linear function of selected updating parameters to improve the correlation between the measured data and the analytical model. Iterative methods can choose the wide range of updating parameters. Physical connections can easily be reflected. However, it requires engineering insight in selecting the updated parameters to reduce the computation time and avoid the divergence. Iterative updating methods include eigensensitivity methods and frequency response function (FRF) methods. Lin and Ewins [66] propose the response function method (RFM) without any modal parameter extraction. The RFM has been further developed by Lin & Zhu (2006) [67] to identify damping matrices of structural systems, as well as mass and stiffness matrices. The method uses both analytical and experimental FRFs for computation of FRF sensitivity. In order to overcome the complexity problem of measured modes, complex model updating formulations using measured FRF data (such as FRF sensitivity with respect to damping constants) is derived to directly identify damping coefficients and to simultaneously update mass and stiffness modeling errors. Arora et al. [68, 69] have proposed that a damped updating procedure is a two-step procedure. In the first step, mass and stiffness matrices are updated using the RFM. In the second step, the damping matrix is identified using updated mass and stiffness matrices by the direct damping identification method by Pilkey and Inman [45,46]. Lin [70] presents a model updating method using multiple FRFs analysis. The method calculates the required modal parameters by solving eigenvalue problem of an equivalent eigensystem derived from the measured FRFs. All measured FRFs are used simultaneously to construct the equivalent eigensystem matrices

from which natural frequencies, damping ratios, and modeshape vectors of interest are solved. Since the identification problem is reduced to an eigenvalue problem of an equivalent system, natural frequencies and damping ratios identified are consistent.

1.5 Key contributions

The contributions of this dissertation on the investigation of dynamic behavior of a cable-harnessed structure are summarized as follows:

- *The development of the Spectral Element Method based predictive and accurate modeling*: The SEM uses the exact solution as its basis function, thus it presents an accurate result with a minimum number of elements in higher frequencies range. Moreover, SEM has the meshing and assembly feature that make it possible to track the location of interconnections.
- *Experimental validation of proposed modeling in the combined distributed system*: There are very few previously published results that validate the modeling of a combined distributed system by experimental results. The proposed SEM based modeling approach is validated by several experiments.
- *Defining the value of interconnection structures by the experiments*: In the proposed SEM-based method, the interconnections are modeled as springs. Thus, defining the spring stiffness of connection structure is a key task to establish the modeling of a combined system. The spring stiffness of interconnection is obtained by the experiments and validated.
- *Investigation on the effect of interconnections*: After experimental validation, the proposed modeling approach is applied to investigate the change of dynamic

behavior such as changes in natural frequencies. The effect of the number of interconnections and the connection stiffness is modeled and predicted.

- *The Development of modified damping matrix identification:* The combination of the model updating method (Incomplete Data Handling Method: IDHM) and the model reduction method (System Equivalent Reduction Expansion Process: SEREP) with the full measured FRF matrix is developed considering the broad frequency range of interest. The proposed method is validated with a multi degree-of-freedom lumped mass system.
- *The effect of the attached cable on damping*: The alteration of damping is investigated by analyzing the experiments. That reveals the effect of number of connections and the type of attached cables on damping. Especially, the effect of flexibility of attached cables is studied further with a lumped mass system.

1.6 Publications and presentations

Based the research result in this dissertation, the following papers are published and the presentation is presented:

- **Journals**
  1) J. Choi, D.J. Inman, Spectrally formulated modeling of a cable-harnessed structure, Journal of Sound and Vibration, 333 (2014) 3286-3304. (Published)
  2) J. Choi, D.J. Inman, Two-step damping identification approach, (in preparation)
- **Conferences**
  1) J. Choi, D.J. Inman, Development of modeling for Cable Harnessed Structures, 54th SDM 2013, Boston, MA, 2013.

2) J. Choi, D.J. Inman, Spectral Element Method for Cable Harnessed Structure, IMAC XXXI, Orange County, CA, 2013.

3) J. Choi, D.J. Inman, Investigation on damping of the host structure induced by an attached cable, IMAC XXXII, Orlando, FL, 2014.

- **Technical presentation**

1) J. Choi, Modeling Dynamics and Experimental Validation of Cable Harnessed Structures, 2013 SEM international student paper competition, Chicago, IL, 2013.

Chapter 2

Spectrally formulated model

2.1 Introduction

SEM is an element-based method that combines the generality of the finite element method with the accuracy of spectral techniques. The SEM approach delivers excellent accuracy using a small number of elements especially at higher frequencies, because the SEM is based on the exact solution of the governing differential equation of the element. The exact dynamic stiffness matrices are used as the element matrices in the Finite Element Method (FEM). Thus it is possible to generate the meshes on geometric domains of concern. The spectral element can be assembled in the same methodology of the FEM. After assembly and the application of the boundary conditions, the global matrix can be solved for a response of the model, repeatedly at all discrete frequencies because the dynamic stiffness matrices are computed at each frequency.

In this section, the spectral formulations of a single beam and a double beam model are presented. A cable-harnessed structure is modeled as double beams connected in several places by springs as shown in section 1.2. Previous authors ([4], [7], [9], [20], [22]) considered two or three beams with continuous connections such as an adhesive layer between the beams. The case in which the connections exist only at certain locations in limited numbers has not previously been considered. The limited number of connections requires separating the beams into several parts. By utilizing meshing-assembly features of SEM, the locations and number can be defined conveniently without loss of accuracy.

Therefore, this proposed simplified model presents a more accurate representation of an actual component.

2.2 Euler-Bernoulli beam

A single beam can be considered as the Euler-Bernoulli beam or a long slender beam if the width and thickness are 10 times less than length [3]. For the Euler beam, the shear deformation can be neglected. Thus we can consider only the transverse displacement. The bending moment of the beam and shear force can be defined by

$$M(x,t) = EI(x)w''(x,t) \quad V(x,t) = -M'(x,t) = -EI(x)w'''(x,t) \tag{34}$$

If *EI(x)* and A are assumed to be constant and no external force exists, the free vibration of the beam is governed by

$$EIw''''(x,t) + \rho A\ddot{w}(x,t) = 0 \tag{35}$$

Assume the solution of equation (35) in spectral form to be

$$w(x,t) = \frac{1}{N}\sum_{n=0}^{N-1} W_n(x)\, e^{i\omega_n t} \tag{36}$$

Substitute equation (36) into (35), and we get the eigenvalue problems at the specific frequency $\omega = \omega_n$:

$$EIW''''(x) - \omega^2 \rho A W(x) = 0 \tag{37}$$

Assume the general solution of equation (37) is

$$W(x) = a_1 \cos\beta x + a_2 \sin\beta x + a_3 \cosh\beta x + a_4 \sinh\beta x \tag{38}$$

Substituting equation (38) into (37) yields the following dispersion relation equation by

$$\beta^4 - \frac{\rho A \omega^2}{EI} = 0 \tag{39}$$

The nodal displacement and slope at both ends can be expressed by

$$\{\mathbf{d}\} = \begin{pmatrix} W(0) \\ W'(0) \\ W(L) \\ W'(L) \end{pmatrix} = \begin{bmatrix} 1 & 0 & 1 & 0 \\ 0 & \beta & 0 & \beta \\ \cos\beta L & \sin\beta L & \cosh\beta L & \sinh\beta L \\ -\beta\sin\beta L & \beta\cos\beta L & \beta\sinh\beta L & \beta\cosh\beta L \end{bmatrix} \{\mathbf{a}\} \tag{40}$$

where $\{\mathbf{a}\} = \begin{bmatrix} a_1 & a_2 & a_3 & a_4 \end{bmatrix}^T$ and

$$[\mathbf{D}(\omega)] = \begin{bmatrix} 1 & 0 & 1 & 0 \\ 0 & \beta & 0 & \beta \\ \cos\beta L & \sin\beta L & \cosh\beta L & \sinh\beta L \\ -\beta\sin\beta L & \beta\cos\beta L & \beta\sinh\beta L & \beta\cosh\beta L \end{bmatrix} \tag{41}$$

And the transverse shear force and bending moments at the nodal points are given by

$$\{\mathbf{f}\} = \begin{Bmatrix} V(0) \\ M(0) \\ -V(L) \\ -M(L) \end{Bmatrix} = EI \begin{bmatrix} 0 & -\beta^3 & 0 & \beta^3 \\ \beta^2 & 0 & -\beta^2 & 0 \\ -\beta^3\sin\beta L & \beta^3\cos\beta L & -\beta^3\sinh\beta L & -\beta^3\cosh\beta L \\ -\beta^2\cos\beta L & -\beta^2\sin\beta L & \beta^2\cosh\beta L & \beta^2\sinh\beta L \end{bmatrix} \{\mathbf{a}\} \tag{42}$$

where

$$[\mathbf{F}(\omega)] = EI \begin{bmatrix} 0 & -\beta^3 & 0 & \beta^3 \\ \beta^2 & 0 & -\beta^2 & 0 \\ -\beta^3\sin\beta L & \beta^3\cos\beta L & -\beta^3\sinh\beta L & -\beta^3\cosh\beta L \\ -\beta^2\cos\beta L & -\beta^2\sin\beta L & \beta^2\cosh\beta L & \beta^2\sinh\beta L \end{bmatrix} \tag{43}$$

From the equation (40)~(43), the relation between $\{\mathbf{f}\}$ and $\{\mathbf{d}\}$ can be obtained as

$$[\mathbf{S}]\{\mathbf{d}\} = \{\mathbf{f}\}, \quad [\mathbf{S}] = [\mathbf{F}][\mathbf{D}]^{-1} \tag{44}$$

Finally, the spectral element matrix of the Euler Bernoulli beam is given by

$$[\mathbf{S}] = EI \begin{bmatrix} \mathbf{S}_{11} & \mathbf{S}_{12} & \mathbf{S}_{13} & \mathbf{S}_{14} \\ \mathbf{S}_{12} & \mathbf{S}_{22} & \mathbf{S}_{23} & \mathbf{S}_{24} \\ \mathbf{S}_{13} & \mathbf{S}_{23} & \mathbf{S}_{33} & \mathbf{S}_{34} \\ \mathbf{S}_{14} & \mathbf{S}_{24} & \mathbf{S}_{34} & \mathbf{S}_{44} \end{bmatrix} \tag{45}$$

where

$$\begin{aligned} \kappa &= \frac{1}{1-\cos(\beta L)\cosh(\beta L)} \\ \mathbf{S}_{11} &= \mathbf{S}_{33} = \kappa(\beta L)^3\left(\cos(\beta L)\sinh(\beta L)+\sin(\beta L)\cosh(\beta L)\right) \\ \mathbf{S}_{22} &= \mathbf{S}_{44} = \kappa\beta L^3\left(-\cos(\beta L)\sinh(\beta L)+\sin(\beta L)\cosh(\beta L)\right) \\ \mathbf{S}_{12} &= -\mathbf{S}_{34} = \kappa\beta^2 L^3\sin(\beta L)\sinh(\beta L) \\ \mathbf{S}_{13} &= -\kappa(\beta L)^3\left(\sin(\beta L)+\sinh(\beta L)\right) \\ \mathbf{S}_{14} &= -\mathbf{S}_{23} = \kappa\beta^2 L^3\left(-\cos(\beta L)+\cosh(\beta L)\right) \\ \mathbf{S}_{24} &= \kappa\beta L^3\left(-\sin(\beta L)+\sinh(\beta L)\right) \end{aligned} \tag{46}$$

After obtaining the spectral element matrix, we can assemble elements to generate the global spectral matrix. And we apply the boundary conditions to the global system. The global system can be expressed by

$$\left[\mathbf{S}_{\mathbf{g}}\right]\left\{\mathbf{d}_{\mathbf{g}}\right\} = \left\{\mathbf{f}_{\mathbf{g}}\right\} \tag{47}$$

Owing to usage of the exact dynamic stiffness matrix to formulate the spectral element matrix, we can solve the system characteristics with a minimum number of element matrices exactly. Now, we can calculate the natural frequencies by solving the eigenvalue problem for the spectral element model given by

$$\left[\mathbf{S}_{\mathbf{g}}\right]\left\{\mathbf{d}_{\mathbf{g}}\right\} = \mathbf{0} \tag{48}$$

Similar to the regular eigenvalue problem, we need to consider that the determinant of spectral element matrix $[\mathbf{S}_g]$ is zero, $\det(\mathbf{S}(\omega_n)) = 0$, to find the natural frequencies. However, the spectral element matrix consists of transcendental functions such as sine,

cosine, hyperbolic cosine (cosh), and hyperbolic sine (sinh). We cannot use the linear eigensolver such as 'eig' in MATLAB. Several approaches to find the eigenvalues are summarized by Lee [16].

2.3 Timoshenko beam

The equation of motion of the Timoshenko beam can be expressed as

$$\begin{aligned} &\kappa GA\left(w'' - \theta'\right) - \rho A\ddot{w} = 0 \\ &EI\theta'' + \kappa GA\left(w' - \theta\right) - \rho I\ddot{\theta} = 0 \end{aligned} \tag{49}$$

where w and θ are the transverse deflection and the slope respectively. The solutions to equation (49) in spectral form are:

$$w\left(x,t\right) = \frac{1}{N}\sum_{n=0}^{N-1} W_n\left(x\right)e^{\mathrm{j}\omega_n t},\ \theta\left(x,t\right) = \frac{1}{N}\sum_{n=0}^{N-1} \Theta_n\left(x\right)e^{\mathrm{j}\omega_n t} \tag{50}$$

The spatial solutions $W\left(x\right)$ and $\Theta\left(x\right)$ can be written as

$$\begin{aligned} W\left(x\right) &= a_1 e^{-\mathrm{j}\beta_1 x} + a_2 e^{-\mathrm{j}\beta_2 x} + a_3 e^{-\mathrm{j}\beta_3 x} + a_4 e^{-\mathrm{j}\beta_4 x} \\ \Theta\left(x\right) &= a_1 b_1 e^{-\mathrm{j}\beta_1 x} + a_2 b_2 e^{-\mathrm{j}\beta_2 x} + a_3 b_3 e^{-\mathrm{j}\beta_3 x} + a_4 b_4 e^{-\mathrm{j}\beta_4 x} \end{aligned} \tag{51}$$

where β_i and b_i are denote the wave number and the wave mode ratio respectively. Substituting the equation (50) into (49) yields

$$\begin{bmatrix} \kappa GA\beta_i^2 - \rho A\omega^2 & -\mathrm{j}\kappa GA\beta_i \\ \mathrm{j}\kappa GA\beta_i & EI\beta_i^2 + \kappa GA - \rho I\omega^2 \end{bmatrix} \begin{Bmatrix} 1 \\ b_i \end{Bmatrix} = \begin{Bmatrix} 0 \\ 0 \end{Bmatrix} \quad \left(i = 1,2,3,4\right) \tag{52}$$

Equation (52) results in the following dispersion relation:

$$\kappa GAEI\beta_i^4 - \left(\rho AEI + \kappa GA\rho I\right)\omega^2\beta_i^2 - \rho A\left(\kappa GA - \rho I\omega^2\right)\omega^2 = 0 \tag{53}$$

By solving equation (53), we obtain the wave number β_i as a function of frequencies ω. From equation (52), the wavemode ratio b_i can also be obtained as

$$b_i = \frac{\kappa GA\beta_i^2 - \rho A\omega^2}{\mathrm{j}\kappa GA\beta_i} \tag{54}$$

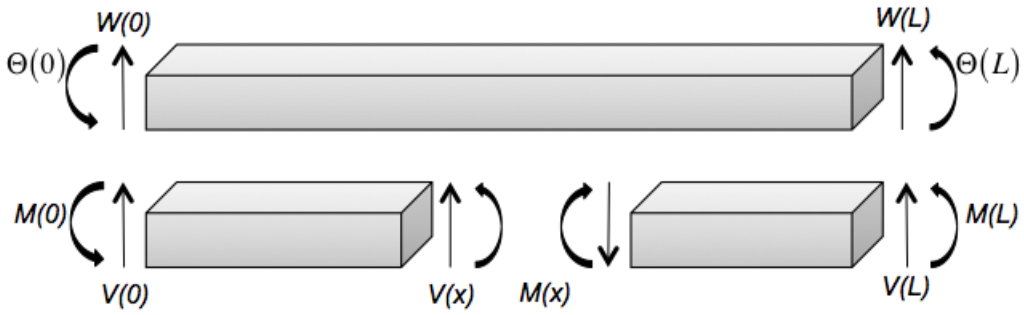

Figure 3 Free body diagram of the Timoshenko Beam

Figure 3 is the free body diagram of a Timoshenko beam and shows the sign convention of the shear force and bending moment. The shear force and bending moments are $V(x) = \kappa GA\left(W'(x) - \Theta(x)\right)$ and $M(x) = EI(x)\Theta'(x)$. The nodal displacement and rotation at both ends can be expressed by

$$\{\mathbf{d}\} = \begin{Bmatrix} W(0) \\ \Theta(0) \\ W(L) \\ \Theta(L) \end{Bmatrix} = \begin{bmatrix} 1 & 1 & 1 & 1 \\ b_1 & b_2 & b_3 & b_4 \\ e^{-\mathrm{j}\beta_1 L} & e^{-\mathrm{j}\beta_2 L} & e^{-\mathrm{j}\beta_3 L} & e^{-\mathrm{j}\beta_4 L} \\ b_1 e^{-\mathrm{j}\beta_1 L} & b_2 e^{-\mathrm{j}\beta_2 L} & b_3 e^{-\mathrm{j}\beta_3 L} & b_4 e^{-\mathrm{j}\beta_4 L} \end{bmatrix} \begin{Bmatrix} a_1 \\ a_2 \\ a_3 \\ a_4 \end{Bmatrix} = [\mathbf{D}(\omega)] \begin{Bmatrix} a_1 \\ a_2 \\ a_3 \\ a_4 \end{Bmatrix} \tag{55}$$

The transverse shear force and bending moments at the nodal points are given by

$$\begin{aligned} \{\mathbf{f}\} &= \begin{Bmatrix} -V(0) \\ -M(0) \\ V(L) \\ M(L) \end{Bmatrix} = [\mathbf{F}(\omega)] \begin{Bmatrix} a_1 \\ a_2 \\ a_3 \\ a_4 \end{Bmatrix} \\ &= \begin{bmatrix} -\kappa GA(b_1 - \mathrm{j}\beta_1) & -\kappa GA(b_2 - \mathrm{j}\beta_2) & -\kappa GA(b_3 - \mathrm{j}\beta_3) & -\kappa GA(b_4 - \mathrm{j}\beta_4) \\ \mathrm{j}EI\beta_1 b_1 & \mathrm{j}EI\beta_2 b_2 & \mathrm{j}EI\beta_3 b_3 & \mathrm{j}EI\beta_4 b_4 \\ \kappa GA(b_1 - \mathrm{j}\beta_1)e^{-\mathrm{j}\beta_1 L} & \kappa GA(b_2 - \mathrm{j}\beta_2)e^{-\mathrm{j}\beta_2 L} & \kappa GA(b_3 - \mathrm{j}\beta_3)e^{-\mathrm{j}\beta_3 L} & \kappa GA(b_4 - \mathrm{j}\beta_4)e^{-\mathrm{j}\beta_4 L} \\ \mathrm{j}EI\beta_1 b_1 e^{-\mathrm{j}\beta_1 L} & \mathrm{j}EI\beta_2 b_2 e^{-\mathrm{j}\beta_2 L} & \mathrm{j}EI\beta_3 b_3 e^{-\mathrm{j}\beta_3 L} & \mathrm{j}EI\beta_4 b_4 e^{-\mathrm{j}\beta_4 L} \end{bmatrix} \begin{Bmatrix} a_1 \\ a_2 \\ a_3 \\ a_4 \end{Bmatrix} \end{aligned} \tag{56}$$

The relation between the force vector $\{\mathbf{f}\}$ and the displacement vector $\{\mathbf{d}\}$ is

$$[\mathbf{S}]\{\mathbf{d}\} = \{\mathbf{f}\} \tag{57}$$

Substituting the equations (55), (56) into (57), finally the spectral element matrix becomes

$$[\mathbf{S}] = [\mathbf{F}][\mathbf{D}]^{-1} \tag{58}$$

After assembling the spectral elements and applying boundary conditions, the global spectral matrix can be obtained as shown in equation (47).

2.4 Spectral formulation for a combined system

As spacecraft become lighter, the cables may cause a more appreciable change in the dynamic behavior of the main structure. Thus the key to modeling the combined system precisely is to use a good model for the cable itself. Coombs [1] described the procedure to manufacture a cable bundle and Spak and Inman [71] presented excellent reviews of the modeling of cable. The cables are twisted in pairs, bundled and bound by lacing cord, and wrapped in a single layer of Kapton tape with 50% overlap. To predict the material properties of cables is a difficult matter. Thus experiments were conducted to obtain the material properties of the cable. The material properties of a cable bundle obtained by Coombs are shown in Table 1. Based on this data, the natural frequencies are compared by utilizing the SEM of the Euler-Bernoulli beam and Timoshenko Beam as derived in section 2.2 and 2.3.

Table 1 Material properties of the attached cable

	L (m)	A (m^2)	I (m^4)	E (GPa)	G (MPa)	ρ (Kg/m3)	κ
Cable	0.5334	1.2323e-05	1.9566e-10	4.1	97.83	13630	0.889

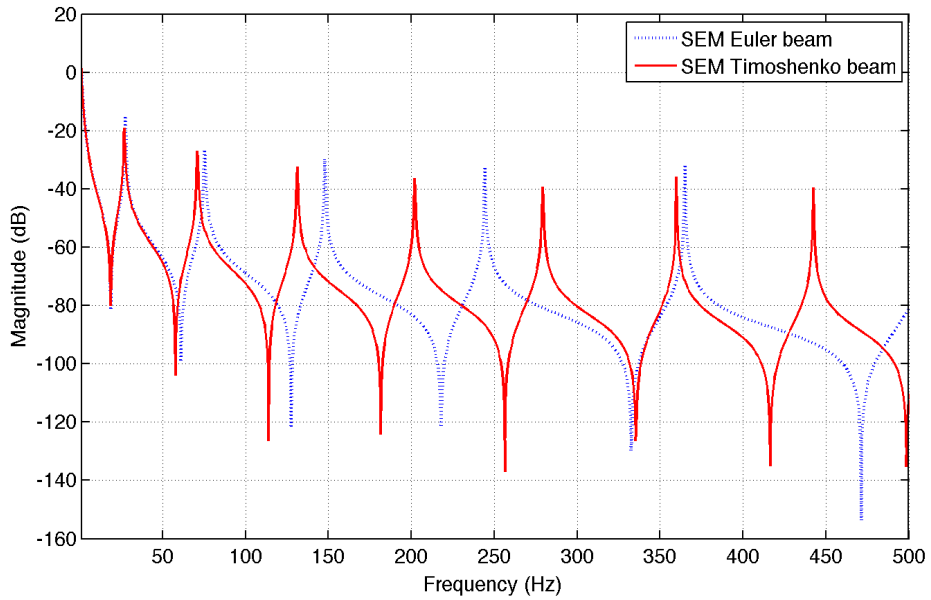

Figure 4 FRFs of FEM and SEM with Timoshenko and Euler-Bernoulli beams

As shown in Figure 4, the Timoshenko beam model includes all of the relevant frequencies, whereas the Euler Bernoulli beam does not. From these results, it can be concluded that the cable should be modeled as a Timoshenko beam to capture all natural frequencies as described by Coombs [1]. Thus, the Timoshenko beam model is utilized to formulate a combined system. Figure 5 illustrates the double beam model with the interconnections at the specific nodal points. $W_{i,j}$ and $\Theta_{i,j}$ are the transverse displacement and rotation at the node '*i*' of the beam '*j*', and N is the total number of nodes at each beam.

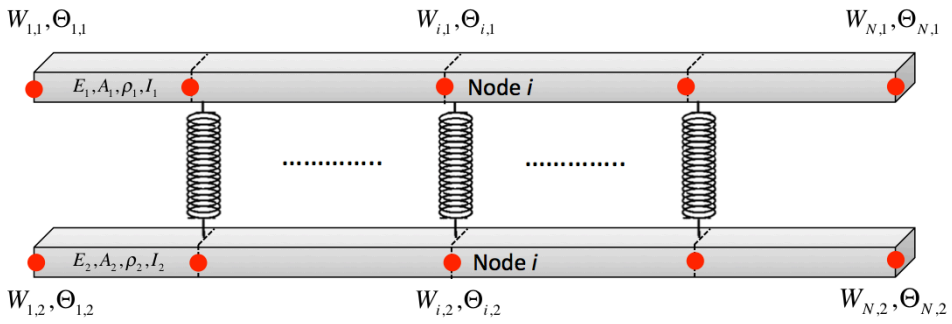

Figure 5 Double beam model showing the connectors and coordinates

Considering the double beam system in Figure 5, each beam is *2N* DOF system. The interconnections exist between the i^{th} nodes of beam 1 and 2. From the relation between nodal displacement and force, the combined global stiffness matrix without the spring connections is:

$$\begin{bmatrix} [\mathbf{S}_1] & 0 \\ 0 & [\mathbf{S}_2] \end{bmatrix} \begin{Bmatrix} \mathbf{d}_1 \\ \mathbf{d}_2 \end{Bmatrix} = \begin{Bmatrix} \mathbf{f}_1 \\ \mathbf{f}_2 \end{Bmatrix} \tag{59}$$

where

$$\begin{aligned} \{\mathbf{d}_1\} &= \begin{Bmatrix} W_{1,1} & \Theta_{1,1} & \cdots & W_{i,1} & \Theta_{i,1} & \cdots & W_{N,1} & \Theta_{N,1} \end{Bmatrix}^T \\ \{\mathbf{f}_1\} &= \begin{Bmatrix} V_{1,1} & M_{1,1} & \cdots & V_{i,1} & M_{i,1} & \cdots & V_{N,1} & M_{N,1} \end{Bmatrix}^T \\ \{\mathbf{d}_2\} &= \begin{Bmatrix} W_{1,2} & \Theta_{1,2} & \cdots & W_{i,2} & \Theta_{i,2} & \cdots & W_{N,2} & \Theta_{N,2} \end{Bmatrix}^T \\ \{\mathbf{f}_2\} &= \begin{Bmatrix} V_{1,2} & M_{1,2} & \cdots & V_{i,2} & M_{i,2} & \cdots & V_{N,2} & M_{N,2} \end{Bmatrix}^T \end{aligned} \tag{60}$$

The global stiffness matrices of each beam, $[\mathbf{S}_1]$ and $[\mathbf{S}_2]$, are *2N×2N* matrices and the global displacement and force vector $\{\mathbf{d}_1\}, \{\mathbf{d}_2\}, \{\mathbf{f}_1\}$ and $\{\mathbf{f}_2\}$ are *2N×1* vectors. The force F_i between the i^{th} nodes of beam 1 and beam 2, due to the spring connection, is expressed as

$$F_i = k(W_{i,1} - W_{i,2}) \tag{61}$$

Considering the relation of force and displacement, the total combined system can be expressed as

$$\begin{aligned} [\mathbf{S}_1]\{\mathbf{d}_1\} + \sum_{i=1}^{p} F_i &= \{\mathbf{f}_1\} \\ [\mathbf{S}_2]\{\mathbf{d}_2\} - \sum_{i=1}^{p} F_i &= \{\mathbf{f}_2\} \end{aligned} \tag{62}$$

where p is the total number of connections. Let $\{\mathbf{L}_i\}$ denote a locator vector defining the location of the i^{th} connector. The vector $\{\mathbf{L}_i\}$ is 4N×1 vector corresponding to $\{\mathbf{d}_1\ \mathbf{d}_2\}^T$. The $2i\text{-}1^{th}$ component of $\{\mathbf{L}_i\}$ is '1' and the $2N+2i\text{-}1^{th}$ component of $\{\mathbf{L}_i\}$ is '-1' and the remainders are zero. Then equation (62) can be written as

$$\begin{bmatrix} [\mathbf{S}_1] & 0 \\ 0 & [\mathbf{S}_2] \end{bmatrix} \begin{Bmatrix} \mathbf{d}_1 \\ \mathbf{d}_2 \end{Bmatrix} + \sum_{i=1}^{p} k\{\mathbf{L}_i\}\{\mathbf{L}_i\}^T \begin{Bmatrix} \mathbf{d}_1 \\ \mathbf{d}_2 \end{Bmatrix} = \begin{Bmatrix} \mathbf{f}_1 \\ \mathbf{f}_2 \end{Bmatrix} \tag{63}$$

Lastly, after assembly, the global spectral matrix can be expressed by

$$[\mathbf{S}_g]\{\mathbf{d}_g\} = \{\mathbf{f}_g\} \tag{64}$$

where

$$[\mathbf{S}_g] = \left[\begin{bmatrix} [\mathbf{S}_1] & 0 \\ 0 & [\mathbf{S}_2] \end{bmatrix} + \sum_{i=1}^{p} k\{\mathbf{L}_i\}\{\mathbf{L}_i\}^T \right],\ \{\mathbf{d}_g\} = \begin{Bmatrix} \mathbf{d}_1 \\ \mathbf{d}_2 \end{Bmatrix} \text{ and } \{\mathbf{f}_g\} = \begin{Bmatrix} \mathbf{f}_1 \\ \mathbf{f}_2 \end{Bmatrix} \tag{65}$$

Owing to the usage of the exact dynamic stiffness matrix to formulate the spectral element matrix, we can solve exactly for the system characteristics with a minimum number of element matrices. Now, we can calculate the natural frequencies by solving the eigenvalue problem for spectral element model given by

$$[\mathbf{S}_g]\{\mathbf{d}_g\} = 0 \tag{66}$$

Similar to the normal eigenvalue problem, setting the determinant of the global spectral matrix $[\mathbf{S}_g]$ to zero, $\det(\mathbf{S}_g(\omega_n)) = 0$, yields the natural frequencies ω_n.

2.5 Accuracy and efficiency of the spectral formulation

It is very important to predict the dynamic behavior and characteristics of a structure accurately and efficiently. The conventional FEM is the most common and powerful method in modeling a structural system. The FEM uses an approximate polynomial shape function as its basis. Thus, in order to capture higher frequencies, a large number of elements are required. The higher number of elements used to capture higher frequencies then requires model reduction, which in turn requires an additional procedure. On the other hand, SEM is based on the exact solution. Thus the SEM can capture all necessary modes, in the high frequency range without using a large order model. Because SEM does not require model reduction, which makes it difficult to keep track of the connections, the SEM model allows for a more precise study of the effect of the interconnections between the cable and structure. Here we focus on the accuracy and efficiency of the SEM in modeling a cable-harnessed structure. The conventional FEM and the SEM will be compared using simulation results to validate the accuracy and efficiency of the SEM against a standard modeling method.

2.5.1 Comparison between FEM and SEM in the frequency domain

The equation of motion of a general multiple degree-of-freedom (MDOF) system is

$$[\mathbf{M}]\{\ddot{x}(t)\}+[\mathbf{K}]\{x(t)\}=\{f(t)\} \tag{67}$$

where [**M**] and [**K**] are the usual mass and stiffness matrices. Assuming harmonic motion of the system, the displacement and external force are expressed as

$$\{x\}=\{\mathbf{X}\}\sin\omega t,\quad \{f\}=\{\mathbf{F}\}\sin\omega t \tag{68}$$

Substituting the equation (68) into (67) will yield

$$\left([\mathbf{K}]-\omega^2[\mathbf{M}]\right)\{\mathbf{X}\}=\{\mathbf{F}\} \tag{69}$$

The matrix $\left([\mathbf{K}]-\omega^2[\mathbf{M}]\right)$ is the *dynamic stiffness matrix* of the MDOF system and is denoted as $[\mathbf{Z}(\omega)]$. Thus equation (69) can be written as

$$[\mathbf{Z}(\omega)]\{\mathbf{X}\}=\{\mathbf{F}\} \tag{70}$$

The inverse of the matrix $[\mathbf{Z}(\omega)]$ is defined as the *receptance FRF matrix*, $[\alpha(\omega)]$. In the spectral domain, the FRF matrix obtained by the inverse of $[\mathbf{S}(\omega)]$ in the SEM will be compared with $[\alpha(\omega)]$ of the conventional FEM and the experimental FRF results.

2.5.2 Single beam

First, we considered the free vibration of a single free-free beam. The properties of the beam are shown in Table 2. From the characteristic equation of a free-free beam [3], $\cos(\beta L)\cosh(\beta L)=1$, the exact natural frequencies are calculated. Root-finding algorithms [19] are used to find the natural frequencies, ω_n, in the SEM.

Table 2 Model properties

	Dimension	E (GPa)	ρ (Kg/m^3)
Al Beam	$1.2192\times0.0254\times0.003175$ (m)	70	2700

Table 3 Natural frequencies (Hz) of exact solution, SEM and FEM

Mode	ω_{exact}	ω_{SEM}	ω_{FEM} (10)	ω_{FEM} (30)	ω_{FEM} (50)
1	0	0	0.00001	0.00009	0.0002
2	11.1794	11.1794	11.1798	11.1794	11.1794
3	30.8165	30.8165	30.8242	30.8166	30.8165
4	60.4127	60.4127	60.4683	60.4135	60.4128
5	99.8654	99.8654	100.1052	99.8687	99.8658
6	149.5272	149.5272	149.9387	149.1928	149.1831
7	208.3612	208.3612	210.2857	208.3915	208.3652
8	277.4040	277.4040	281.5237	277.4749	277.4134

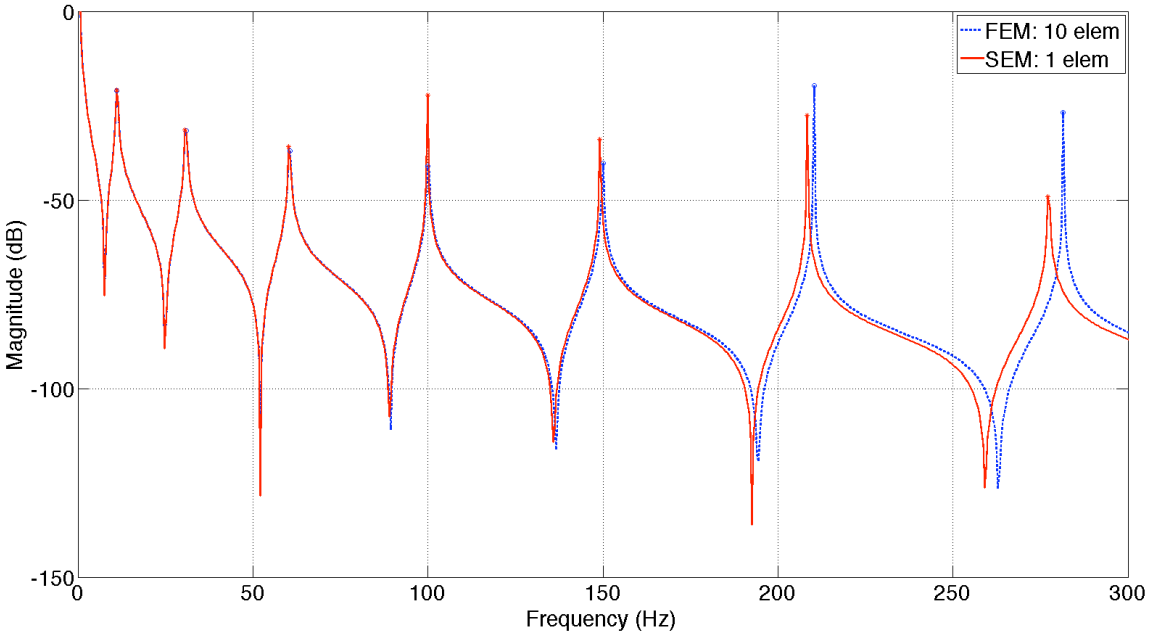

Figure 6 FRF of SEM (1 element) and FEM (10 elements)

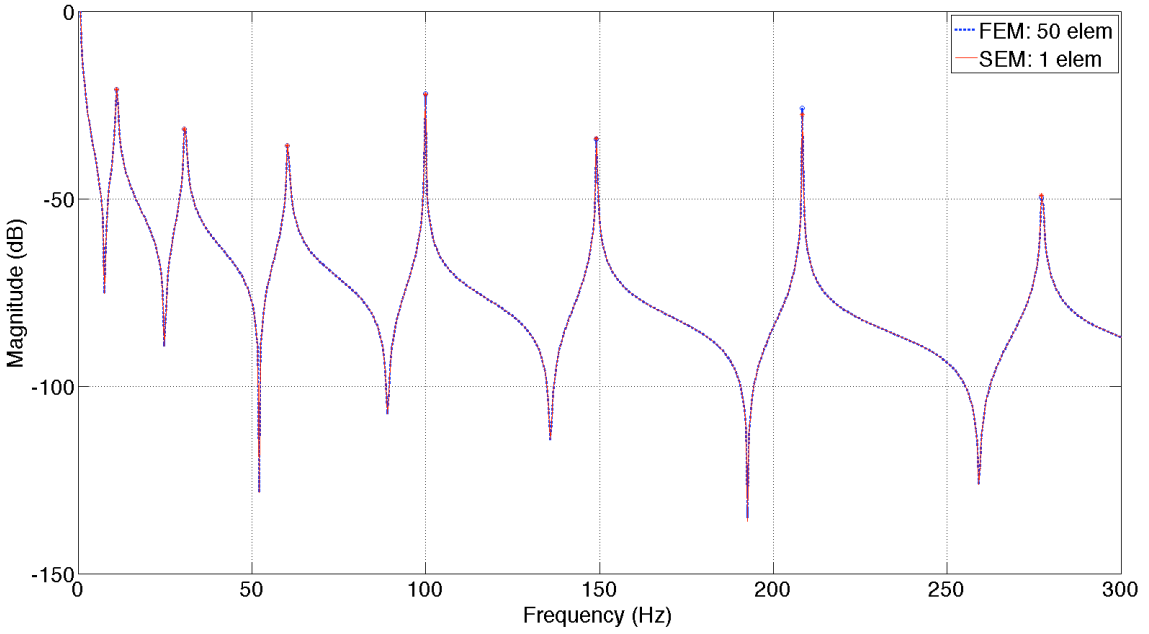

Figure 7 FRF of SEM (1 element) and FEM (50 elements)

The natural frequencies of the free-free beam are compared in Table 3. The SEM results are identical to the exact solution. In Figure 6, the 10-element FEM cannot capture

all resonance frequencies. But the SEM can capture all natural frequencies with only one element. Fifty FEM elements were used in Figure 7. All of the natural frequencies are almost identical with the SEM natural frequencies. As the number of elements is increased, the FEM results get closer to the SEM result and the exact solution. Considering the higher frequency range, the FEM will need many more elements to present accurate results. However the SEM produces accurate results with a minimum number of elements.

2.5.3 Double-beam system

The accuracy and efficiency of the SEM were also investigated in a double beam system. The spectral formulation in section 2.5 was used in modeling the double beams system. The double-beam systems with 3 and 5 interconnections were simulated using the material properties in Table 4.

Table 4 Model parameters of double beams

	L (m)	A (m^2)	I (m^4)	E (N/m^3)	ρ (kg/m^3)
Beam1	1.2192	8.0645×10^{-5}	6.7746×10^{-11}	7×10^{10}	2700
Beam2	1.2192	4.03225×10^{-5}	2.7098×10^{-12}	2.333×10^{10}	540

The calculated first 11 modes are summarized in Table 5. In Figure 8 and Figure 10, 12-element FEM was used and the SEM used a minimum number of elements (4 and 6). The FRFs plots shows that the 12 elements of FEM are not sufficient to capture all modes of interest compared with the SEM result. In Figure 9 and Figure 11, the number of FEM elements was increased to 120. With 30 times more elements than the SEM, the FEM can produce all of the desired natural frequencies. As mentioned in single beam analysis, considering the higher frequency range, the FEM will need many more elements to

present an accurate result. Again, the SEM produces accurate results with a minimum number of elements and allows for simple record keeping of the connection points.

Table 5 Natural frequencies (Hz) for double beam

Mode	3 spring connections		5 spring connections	
	FEM 120	SEM 4	FEM 120	SEM 6
1	0.0025	0.0119	0.0006	0.0053
2	6.8085	6.8085	10.5753	10.5753
3	7.1844	7.1844	15.7602	15.7603
4	11.1687	11.1687	16.2981	16.2982
5	29.5254	29.5254	30.1176	30.1176
6	34.6464	34.6464	58.0927	58.0927
7	44.8028	44.8028	69.8780	69.8780
8	58.4510	58.4506	84.7031	84.7031
9	58.8538	58.8545	94.2957	94.2947
10	66.7777	66.7782	106.1145	106.1145
11	99.6240	99.6240	121.6623	121.6622

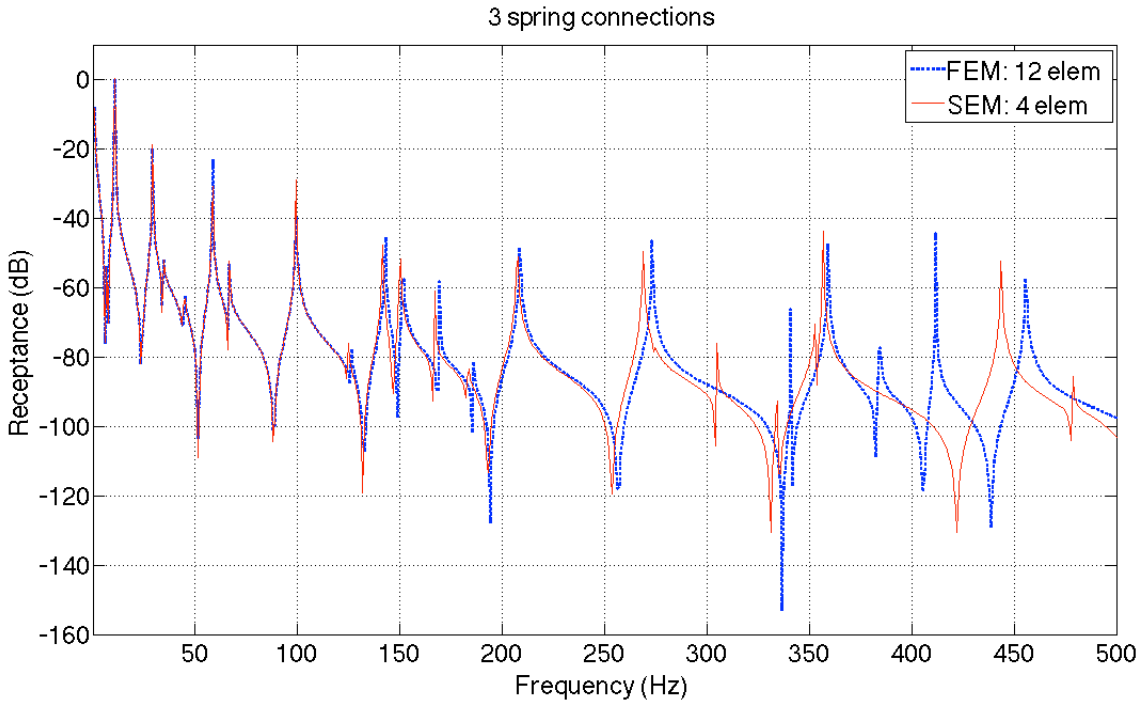

Figure 8 FRFs of SEM (4 element) and FEM (12 elements) with 3 connections

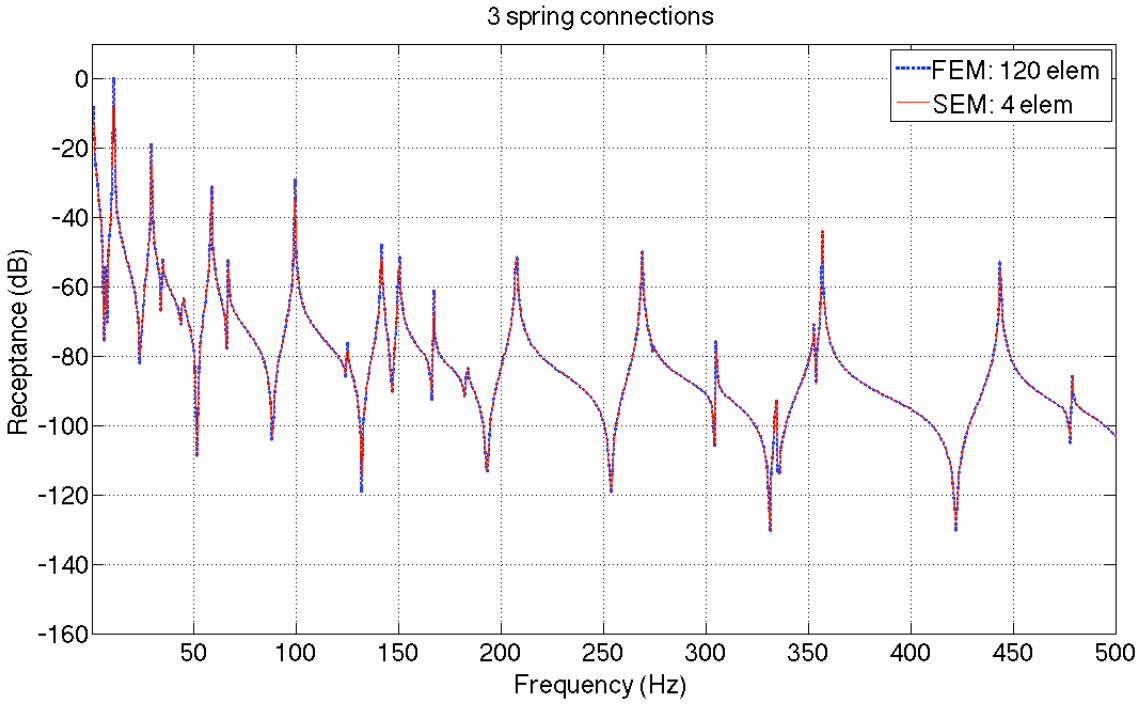

Figure 9 FRFs of SEM (4 element) and FEM (120 elements) with 3 connections

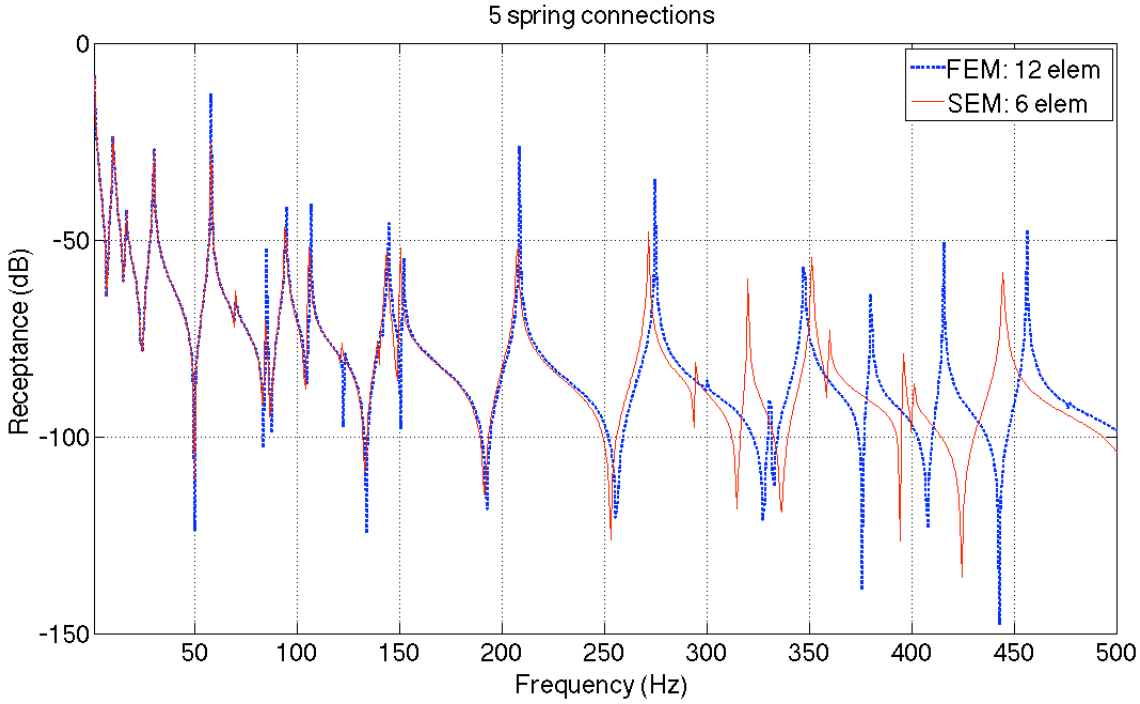

Figure 10 FRFs of SEM (6 element) and FEM (12 elements) with 5 connections

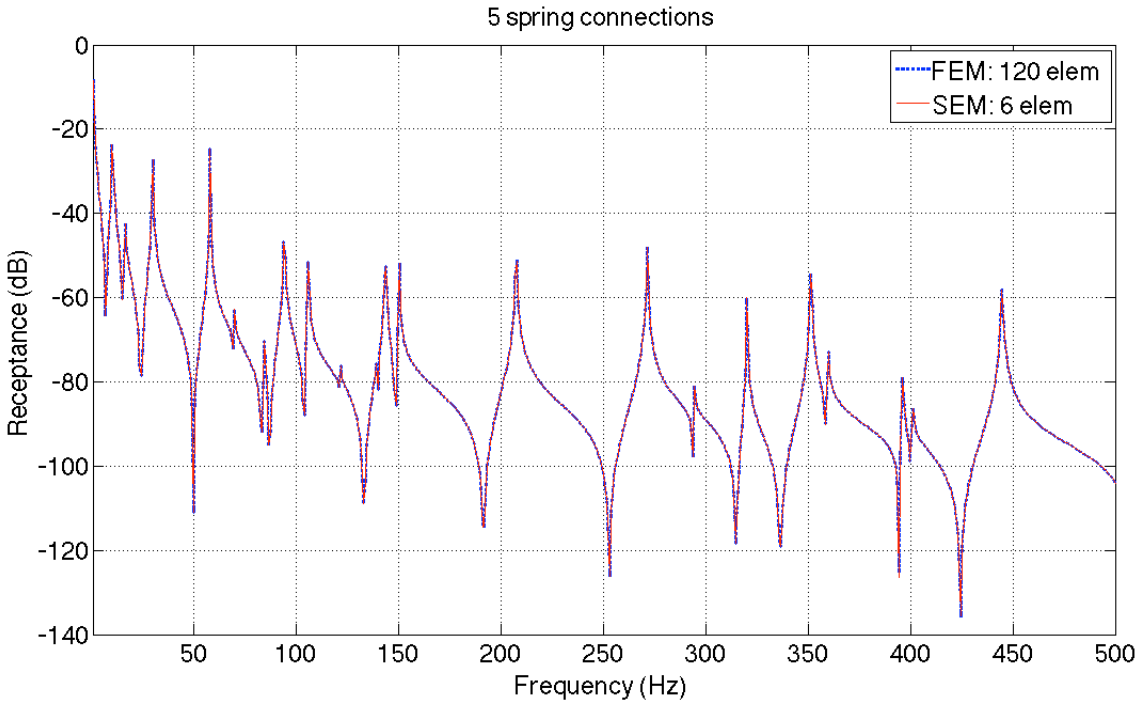

Figure 11 FRFs of SEM (6 element) and FEM (120 elements) with 5 connections

Chapter 3

Experimental validation

3.1 Introduction

In the previous section, the SEM formulation for a cable-harnessed structure was presented. The accuracy and efficiency of the SEM was verified by comparing it with the conventional FEM. In this section, the SEM approach was validated with experimental results.

In the previously published literature, the SEM was applied to model a single beam and compared with the single beam test. There are very few attempts at modeling a combined distributed system by means of the SEM, as shown in the literature, and none that experimentally validate SEM on a more complex structure such as a double beam system. In a double beam system, there are interconnections between beams by using zip-tie and tie-down structure and they are modeled as the springs. One of the key tasks in the experimental validation of the SEM approach is to define the value of spring stiffness of a real interconnection structure. In this section, the spring stiffness of the interconnections was also determined experimentally. With the defined spring stiffness of interconnections, we can compare SEM prediction with the measured FRF. In analyzing the results, nonlinear behavior was ignored because the excitation levels are such that the response remained in the linear region. In practice, the most significant nonlinear response would come from slack cables slapping against the host structure, but this is not examined here. Ignoring nonlinear effects is validated by looking at the experimental FRF plots, which clearly indicate linear behavior.

3.2 Single beam

First, the experiments were conducted with a single beam. The FRFs were measured with the experimental setup as shown in Figure 12. The experiment was conducted with a PCB impact hammer, the Polytec Laser vibrometer and its controller, and RT Pro Measurement Software [72]. The test specimen was a 0.8636-meter long Al beam with a cross section of a 0.0254-meter width and a 0.003175-meter thickness. The material properties of the specimen are shown in Table 6. The velocities were measured at total of 9 points and the 9×9 full mobility FRF matrix was measured.

Table 6 Material properties of Al single beam

	L (m)	A (m^2)	I (m^4)	E (GPa)	G (GPa)	ρ (Kg/m^3)	κ
Al Beam	0.8636	8.0645e-05	6.7746e-11	70	25	2700	0.889

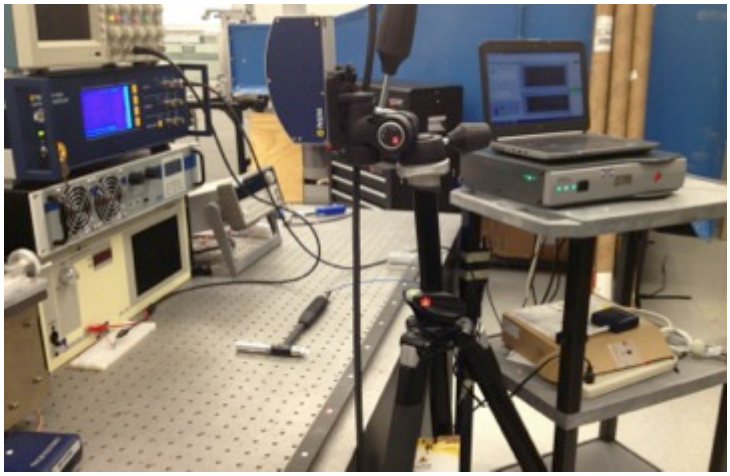

Figure 12 Experimental configuration

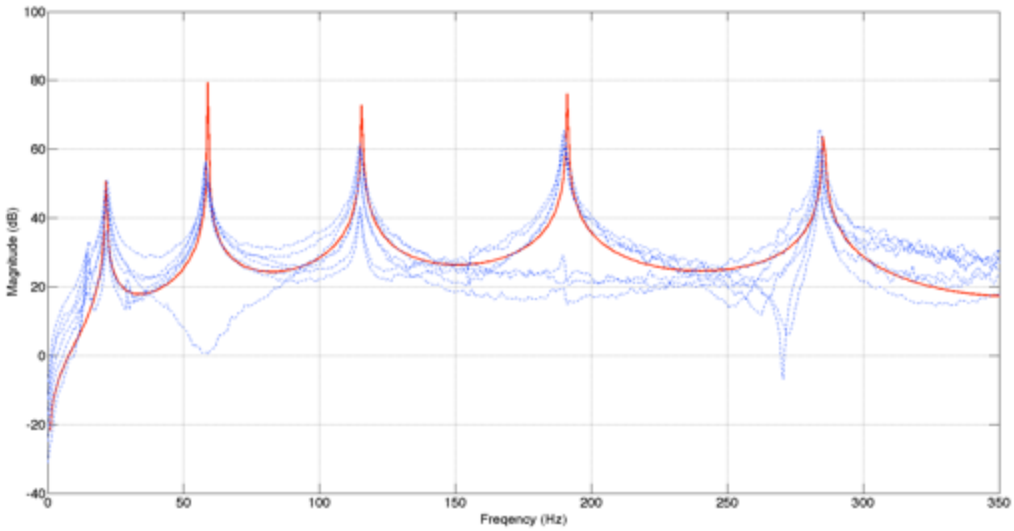

Figure 13 FRFs from measurement (blue dotted line) and SEM (solid red line)

Figure 13 shows the mobility FRFs from the measurement data and the SEM. The peaks present the natural frequencies showing that the analytical SEM model predicts the experimental data very well. In the frequency range of interest, the SEM results show a good coherence with the measured FRFs.

3.3 Spring stiffness of the interconnection structure

Before testing the double beam system with the real connections (tie-down and zip-tie), the spring stiffness of the connection has to be defined. The tie-down structure is shown in the left-hand side of Figure 14. The tie-down is attached to the host structure and the cable is fixed by using the zip-tie shown in the right-hand side of Figure 14. A two DOFs system was used to define the stiffness of the connection shown in Figure 15. The 'green circle' represents the cross section of a short piece of copper beam and M_2 is the measured weight. From the modal test, the measured FRF shows the natural frequencies of a system.

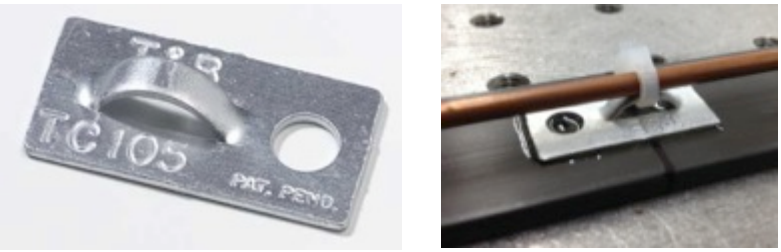

Figure 14 Tie-down structure (T&B TC 105) and an actual connection

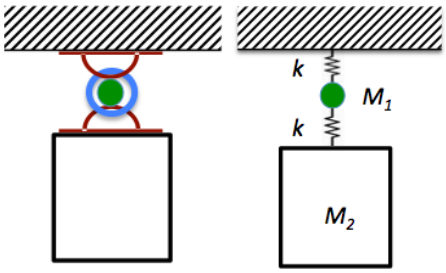

Figure 15 Modeling of experiment setup

In Figure 15, the mass M_1 of a cooper beam piece is 2g and the mass of M_2 is 500g. The accelerometer was attached at the bottom of the mass M_2 as shown in Figure 16. The impact was applied at the center of mass M_2.

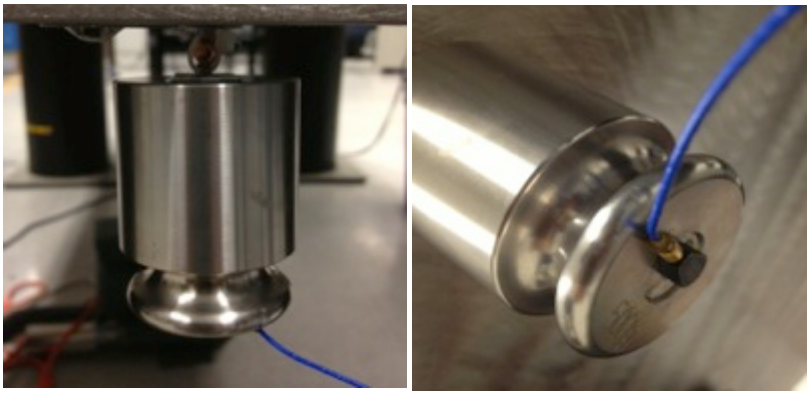

Figure 16 Experiment setup for measuring the tie stiffness

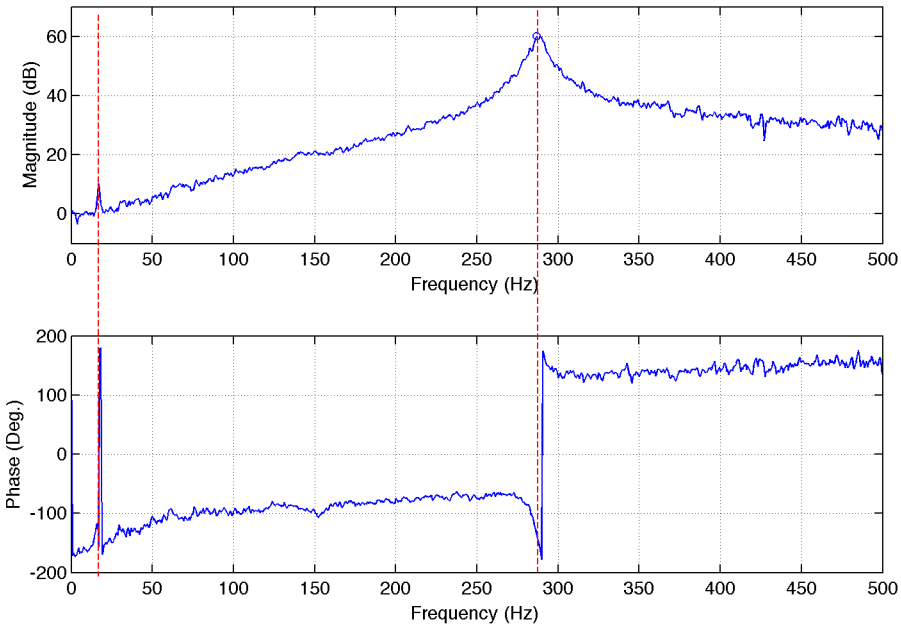

Figure 17 FRF results: Magnitude (upper) and Phase (lower)

The mass matrix of two DOFs system can be defined from the free-body diagram. From the accelerance FRF as shown in Figure 17, two natural frequencies were obtained. The first resonance peak shows small magnitude but it was considered as the first natural frequencies based on the phase plot. Based on the known mass matrix and natural frequencies, the stiffness can be calculated. The results are summarized in Table 7.

Table 7 Stiffness calculations

Mode	Natural frequency (Hz)	Connection stiffness, *k* (N/m)
1	16.88	11.238
2	286.88	3245.7

Considering the physical behavior of connection structure, the spring stiffness, 3245.7 N/m, is an acceptable value because it is equivalent to the force of 330 kgf required for 1-meter extension.

3.4 Double-beam system

In this section, to validate the SEM modeling approach for the double beam system, modal tests were conducted to obtain the FRF from the two double beam systems.

3.4.1 Experiment 1: two identical beams connected by 5 springs

The experimental configuration is shown in Figure 18. Using a hanging configuration, free-free boundary conditions apply to this experiment. Two identical aluminum beams were used and connected by 5 springs. In this case, the spring has a predefined spring stiffness of k=10 N/m and the flat ends that enable it to be attached onto the surface of beams easily. The springs were attached by using Epoxy adhesive. The material properties are summarized in Table 8.

Table 8 Material properties of Aluminum beams

	L (m)	A (m^2)	I (m^4)	E (GPa)	G (GPa)	ρ (Kg/m^3)	κ
Al Beam	1.2192	8.0645e-05	6.7746e-11	70	25	2700	0.889

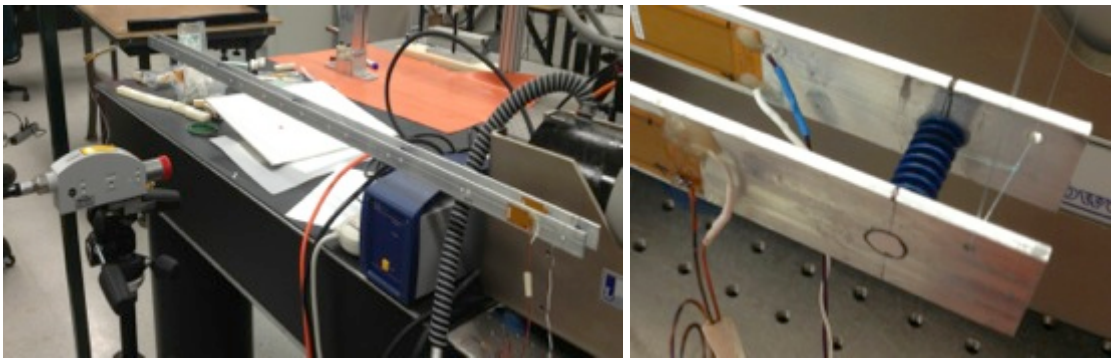

Figure 18 Experimental configuration

To validate that both beams work as a combined system, a lightweight Macro Fiber Composite (MFC) actuator was used to drive the second beam with 'Chirp wave' and the mobility FRF was measured with the laser vibrometer focused on the first beam. Figure

19 shows the mobility FRF measurement. From the FRF, it was found that the two beams work together as a double beam system. The measurement and SEM show very close resonance frequencies in the FRF plot. Clearly the SEM approach developed here predicts an accurate frequency response.

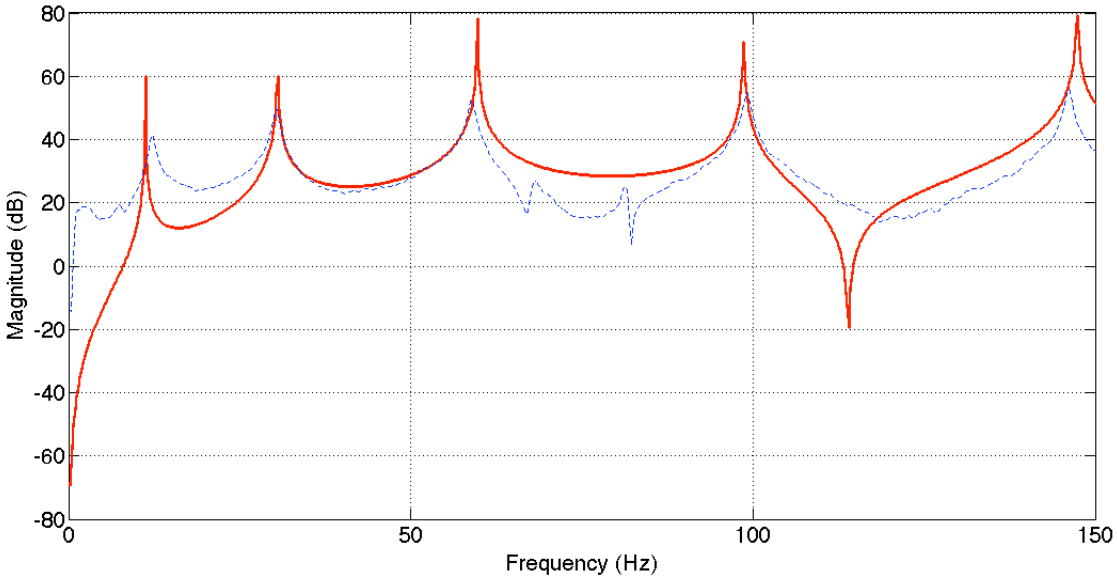

Figure 19 FRF from measurement (blue dotted line) and SEM (solid red line)

3.4.2 Experiment 2: an aluminum beam with copper beam connected by tie-down and zip-tie

The experimental setup is shown in Figure 20. The input force was applied by using Labworks mini shaker (ET-132). The PCB force sensors (PCB 208C02) were attached to the Al beam. The output was measured at 7 nodal points with PCB accelerometers (PCB 352C67). A free-free boundary condition was used in this experiment. In this experiment, a real connection was applied as shown in Figure 15. The material properties of the Al beam and copper beam are summarized in Table 9. The T&B TC105 tie-down is relatively stiffer than zip-tie. Thus the spring-like behavior of interconnection comes from the zip-tie. Considering the material of the zip-tie, the spring stiffness of

connections was applied with the value of k=3245.7 N/m, based on the results in section 3.3. FRFs were measured with 7 points.

Table 9 Material properties of Al beam and Copper beam

	L (m)	A (m^2)	I (m^4)	E (GPa)	G (MPa)	ρ (kg/m^3)	κ
Al Beam	0.762	3.0242e-04	2.2864e-09	70	25	2700	0.889
Copper Rod	0.762	9.9315e-07	3.0079e-13	117	46	8940	0.343

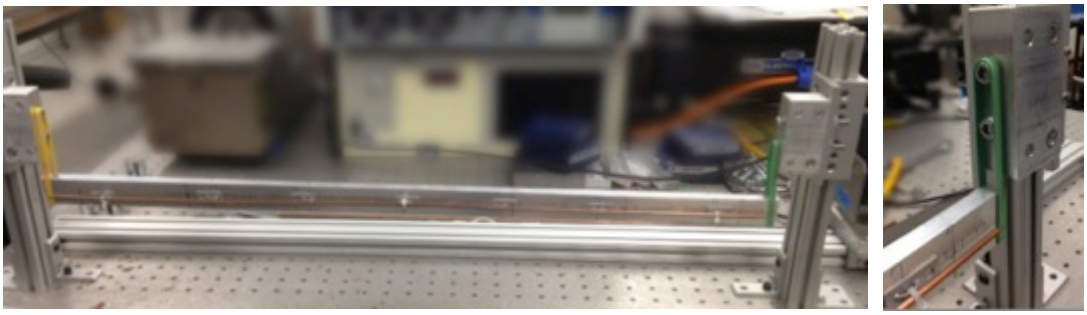

Figure 20 Experimental setup and free-free boundary condition

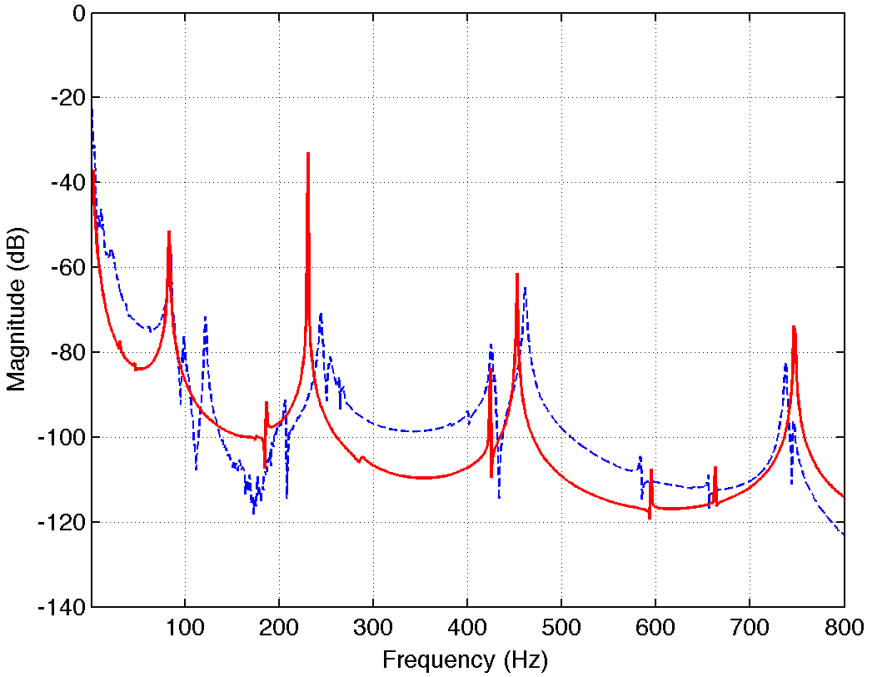

Figure 21 H_{25} FRFs of from measurement (blue, dashed line) and SEM (red, solid line)

Figure 21 shows the H_{25} FRFs from both of the measurement and the SEM. Both results show good agreement of resonance frequencies and magnitude. Thus the proposed SEM modeling approach provides an accurate prediction of the dynamic characteristics of a cable-harnessed structure.

Chapter 4

The change of dynamic characteristics

4.1 Introduction

In section 3, the spectrally formulated modeling for a cable-harnessed structure is validated by experiments. In this section, the proposed modeling approach is utilized to look into the change of the dynamic behavior of a cable-harnessed structure, mainly considering the stiffness of the connection structure, the number of connections and the mass portion of an attached cable.

4.2 Effect of spring stiffness, *k*

The interconnections between two beams are modeled by a spring connection as shown in Figure 5. And the spring constant k can be changed for the various types of connections. In this section, 5 values of k (10, 10^2,10^3,10^4,10^5) are used to investigate the effect on the dynamic behavior. The following material properties are used.

Table 10 Material properties of Aluminum beam and Copper beam

	L (m)	A (m^2)	I (m^4)	E (GPa)	G (MPa)	ρ (kg/m^3)	κ
Al Beam	1.2192	8.0645e-05	6.7746e-11	70	25	2700	0.889
Copper Rod	1.2192	7.9173e-06	4.9856e-12	117	46	8940	0.343

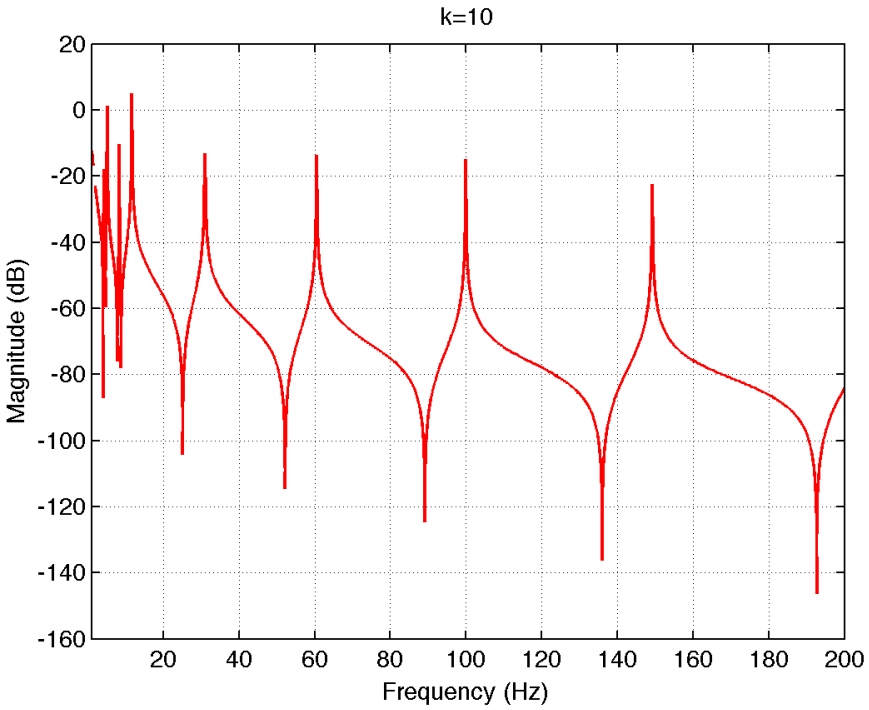

Figure 22 FRFs of double beams (connection stiffness *k*=10)

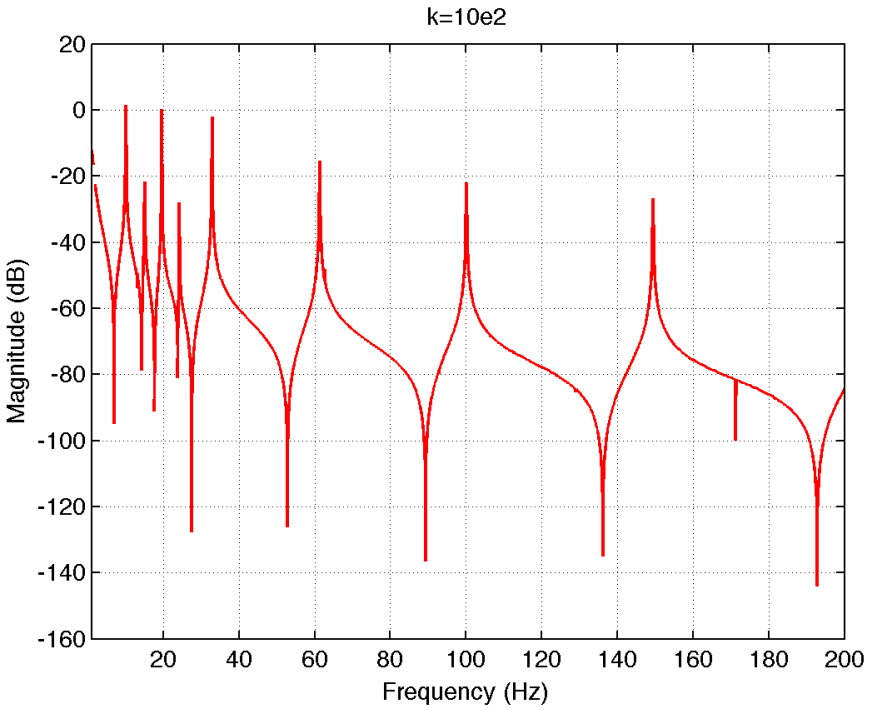

Figure 23 FRFs of double beams (connection stiffness *k*= 10^2 N/m)

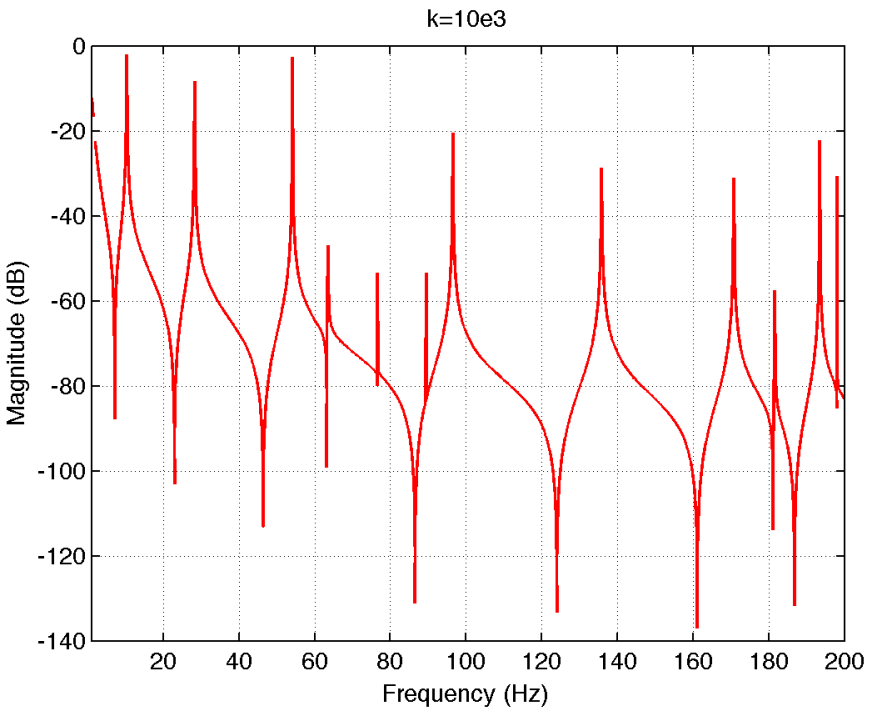

Figure 24 FRFs of double beams (k=10^3 N/m)

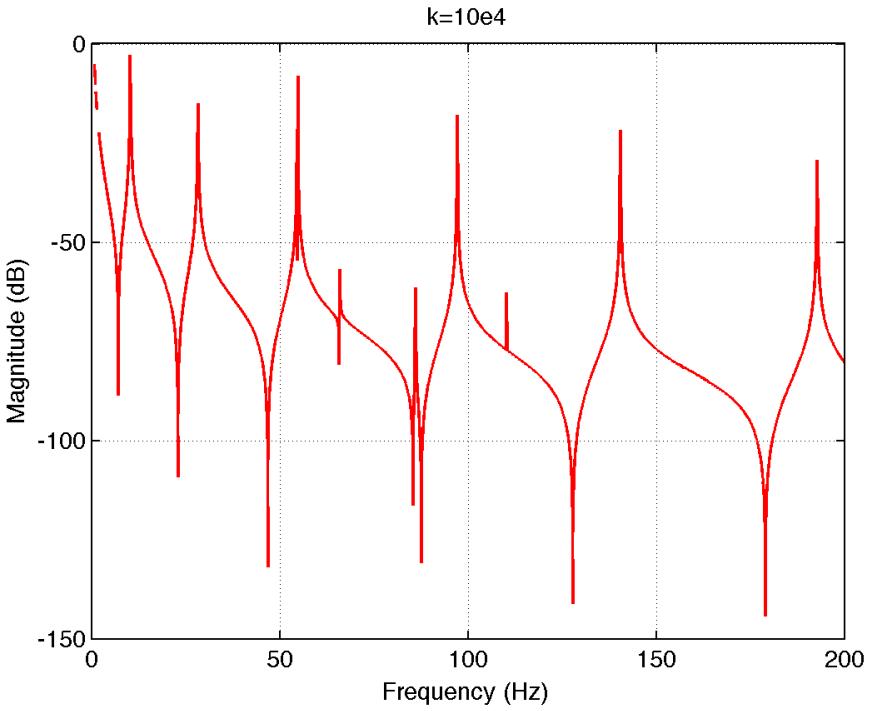

Figure 25 FRFs of double beams (k= 10^4 N/m)

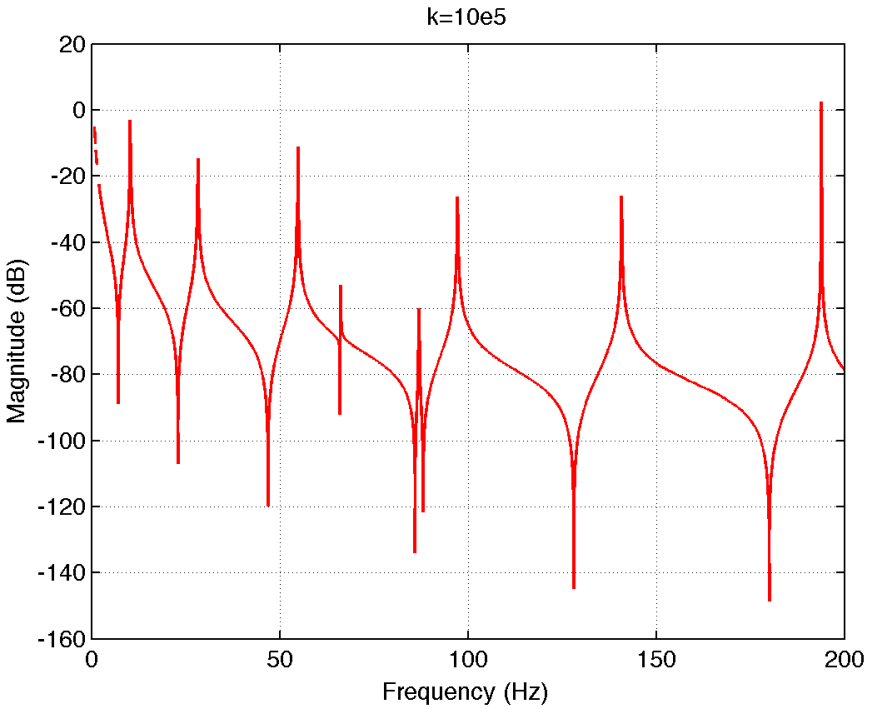

Figure 26 FRF of double beams (k=10^5 N/m)

Table 11 Natural frequencies of 5 cases

Mode	k=10	k=10^2	k=10^3	k=10^4	k=10^5
1	4.2983	10.029	10.268	10.268	10.268
2	5.134	13.074	28.237	28.237	28.297
3	8.298	14.984	54.086	54.803	54.862
4	11.641	19.521	63.459	65.907	66.145
5	19.641	24.178	76.593	86.025	86.98
6	30.983	32.834	89.487	97.129	97.188
7	60.474	40.893	96.472	110.2	112.59
8	99.875	62.564	135.81	140.47	140.77
9	149.19	92.771	170.74	192.71	193.84
10	208.41	100.05	181.54	213.24	213.6

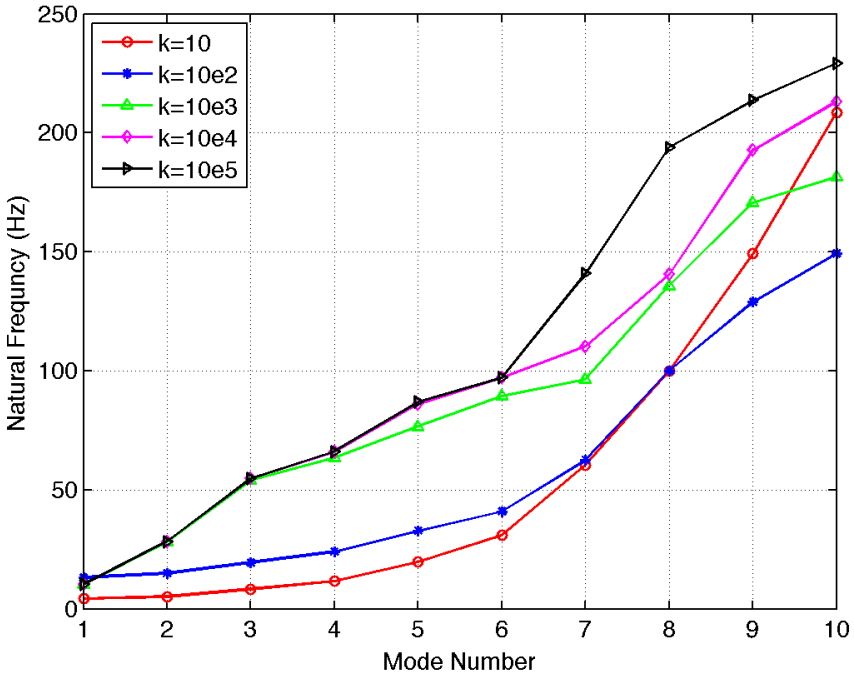

Figure 27 Change in the natural frequencies by connection stiffness

The frequency response function is obtained for each case as shown in Figure 22~Figure 26. **Error! Reference source not found.** summarized the obtained natural frequencies from FRFs. Figure 27 indicates that the natural frequencies of a combined system increase as the spring stiffness of the interconnections increases. Moreover, the natural frequencies start to converge in the low frequency range for larger values of *k*. These results reveal that the effect of stiffness moves to a higher frequency range as the stiffness become larger. This also shows that the dynamic characteristics of a cable-harnessed structure are totally changed by the stiffness of the interconnections.

4.3 Effect of the number of interconnections

By using the validated SEM modeling method, the effect of the interconnections in the combined system is investigated in double-beam systems with 1, 3, 5, 7 and 9

connections. Figure 28 shows the location of nodal points of the SEM. The locations of the connections for each case can be summarized in Table 12. An aluminum beam with copper beam is used and the material properties are shown in Table 10, and the spring constant k is 10^5 (N/m). The SEM uses a minimum number of elements, with one element between the nodes, to obtain the exact natural frequencies.

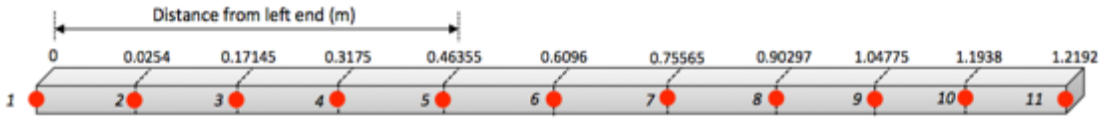

Figure 28 A simplified beam and locations of nodal point

Table 12 Locations of connections

Num. of Connections	1	3	5	7	9
Locations of Connections	6	2,6,10	2,4,6,8,10	2,4,5,6,7,8,10	2,3,4,5,6,7,8,9,10

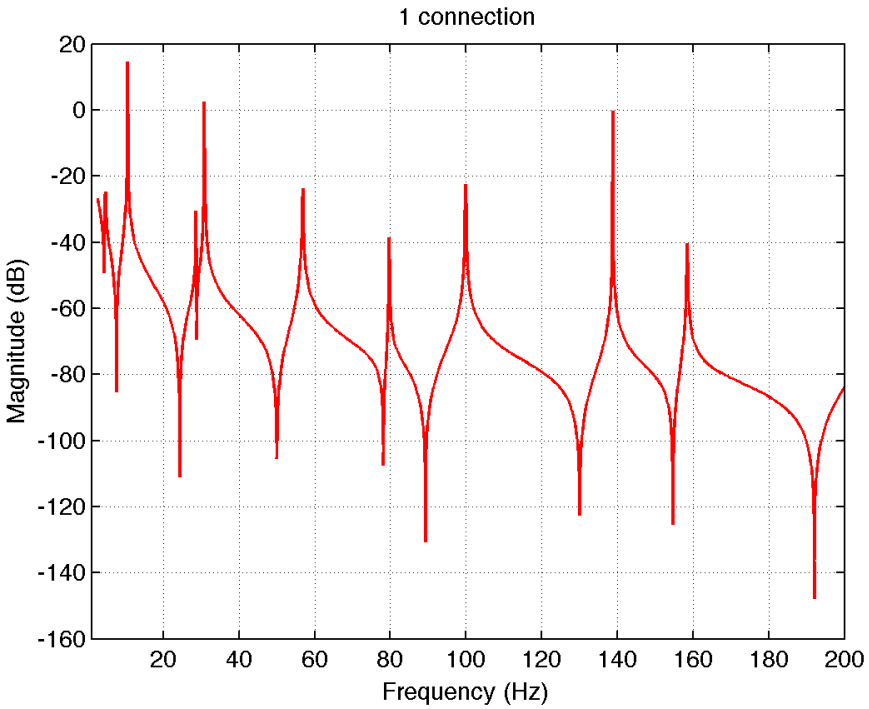

Figure 29 FRFs of double beam with 1 connection

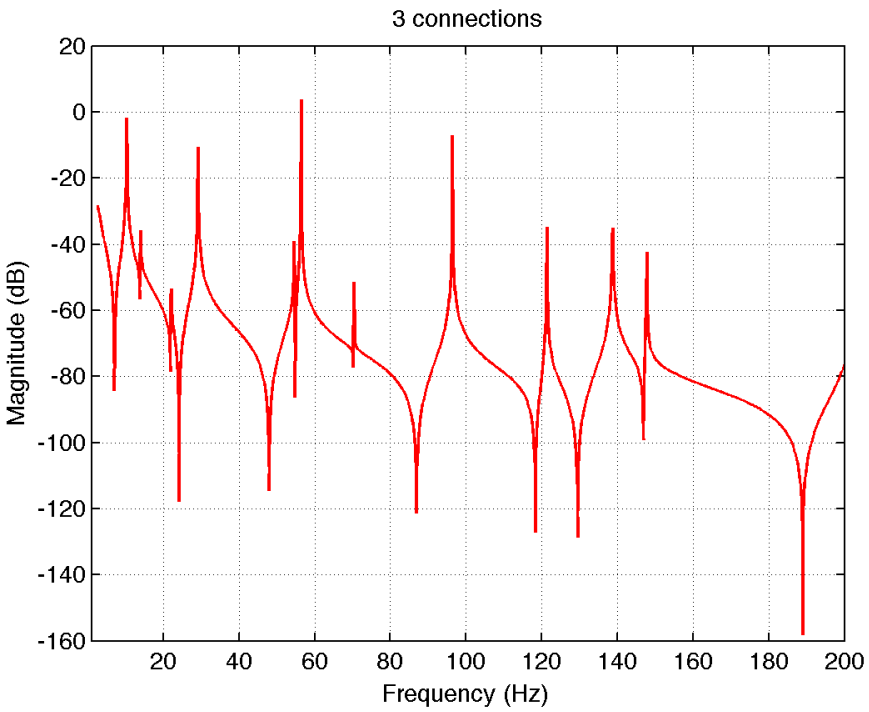

Figure 30 FRFs of double beam with 3 connections

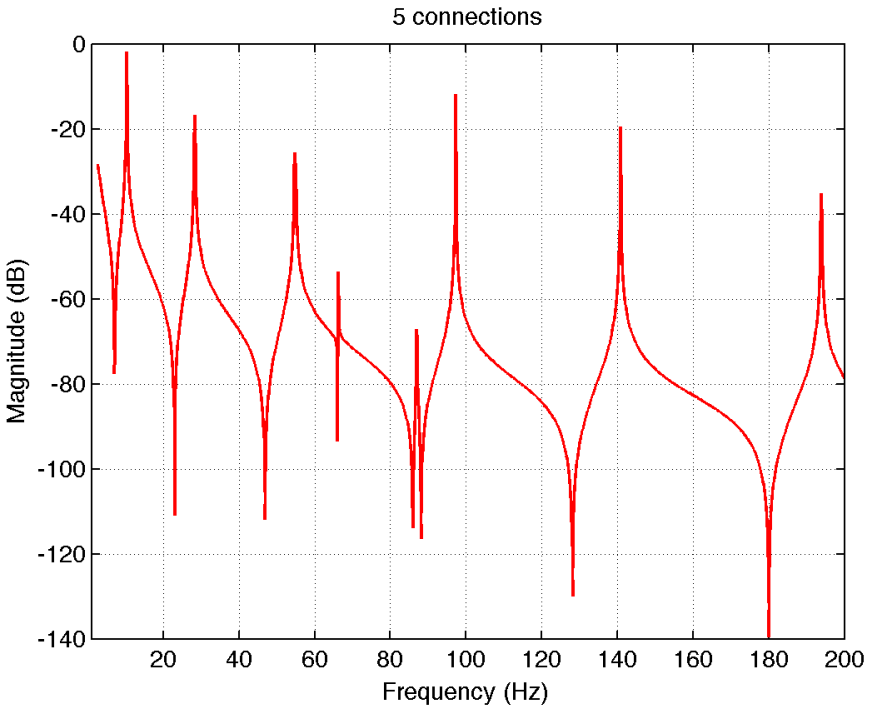

Figure 31 FRFs of double beam with 5 connections

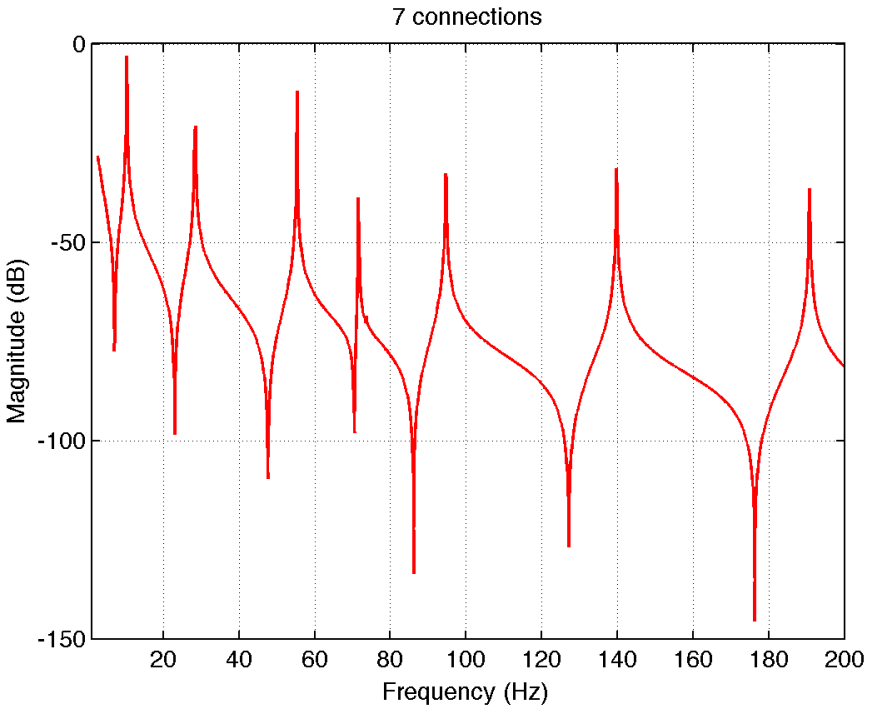

Figure 32 FRFs of double beam with 7 connections

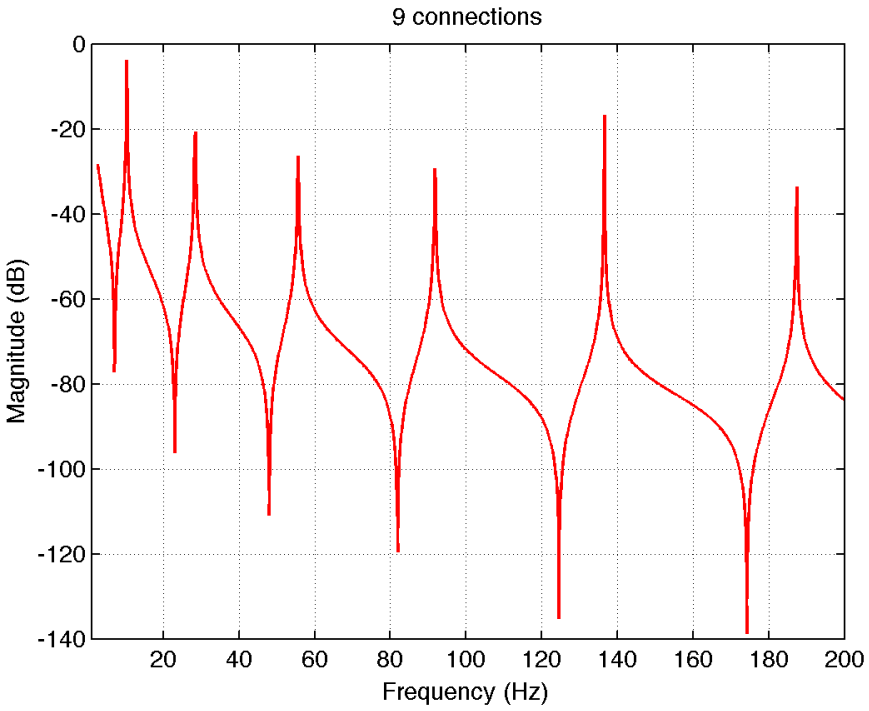

Figure 33 FRF of double beam with 9 connections

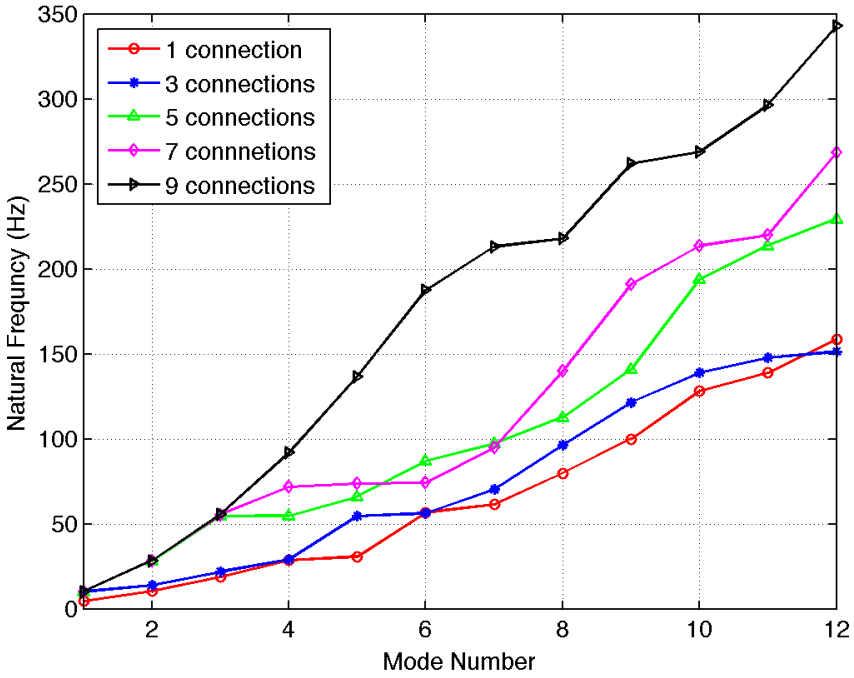

Figure 34 Change in the natural frequencies related to the number of connections

Table 13 Natural frequencies for 5 cases

Modes	Number of connections				
	1	3	5	7	9
1	4.5967	10.268	10.268	10.268	10.268
2	10.507	13.910	28.297	28.357	28.357
3	18.966	22.029	54.564	55.280	55.579
4	28.536	29.133	54.862	71.578	91.756
5	30.804	54.624	66.145	73.548	136.53
6	56.773	56.355	86.980	74.026	187.33
7	61.458	70.324	97.188	94.621	213.18
8	79.697	96.353	112.65	139.75	217.84
9	99.875	121.37	140.77	190.79	261.81
10	128.21	138.74	193.84	213.54	268.81
11	138.8	147.69	213.72	219.63	296.47
12	158.44	151.39	229.3	268.34	343.03

The calculation resulting in the first 12 natural frequencies are summarized in Table 13. Figure 34 illustrates the change in the natural frequencies as the number of connections changes. The natural frequencies increase as the number of interconnections increases. However, the first three modes converge for cases with three or more connections. The lower natural frequencies start to converge when there are more interconnections between beams. This means that the natural frequencies increase due to the connections but finally converge, from the lower frequency range to the higher frequency range.

4.4 Effect of the mass portion of an attached cable

In a cable-harnessed structure, the mass portion of an attached cable has increased up to 30% of total mass of the system. In this section, the effect of the mass portion of an attached cable is investigated. The material properties of two beams are summarized in Table 14. Two beams are connected by the spring (k=3250N/m) at 5 points in Table 12.

Table 14 Material properties of aluminum beam and copper beam

	L (m)	A (m^2)	I (m^4)	E (GPa)	G (MPa)	ρ (kg/m^3)	κ
Al Beam	1.2192	8.0645e-05	6.7746e-11	70	25	2700	0.889
Cu beam (30%)	1.2192	7.9173e-06	4.9856e-12	117	46	8940	0.343
Cu beam (20%)		5.2753e-06	2.2146e-12				
Cu beam (10%)		2.6377e-06	5.5364e-13				
Cu beam (5%)		1.3188e-06	1.3841e-13				
Cu beam (1%)		2.6377e-07	5.5364e-15				

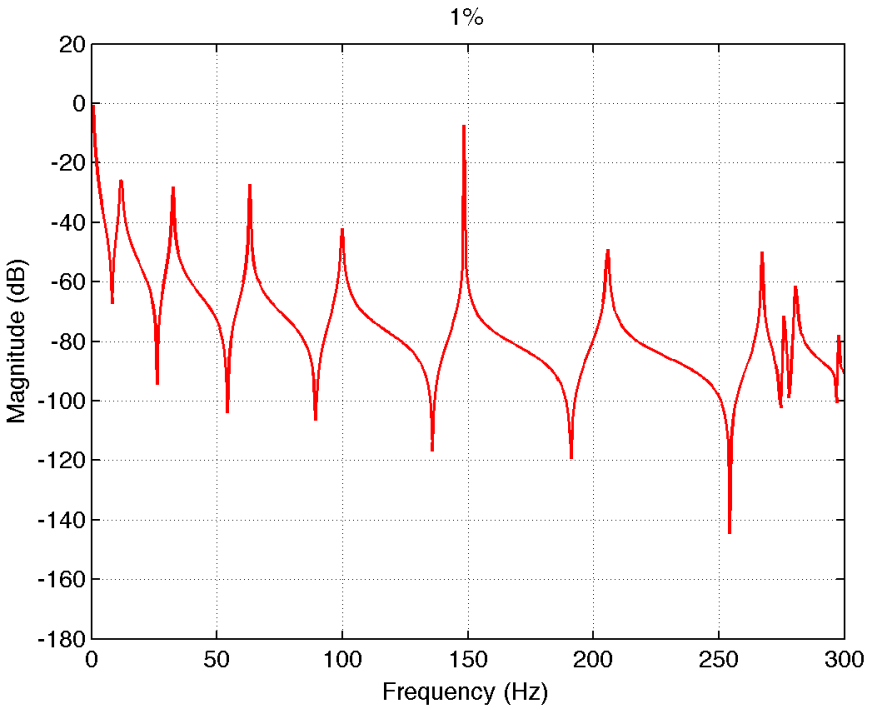

Figure 35 FRF of Double beam with 1% mass portion of an attached cable

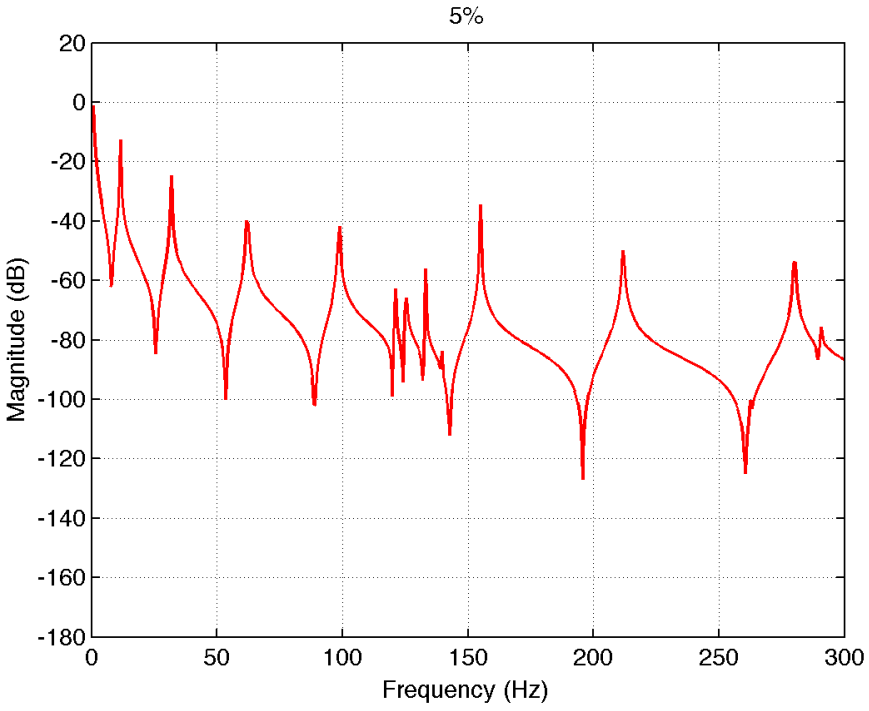

Figure 36 FRF of Double beam with 5% mass portion of an attached cable

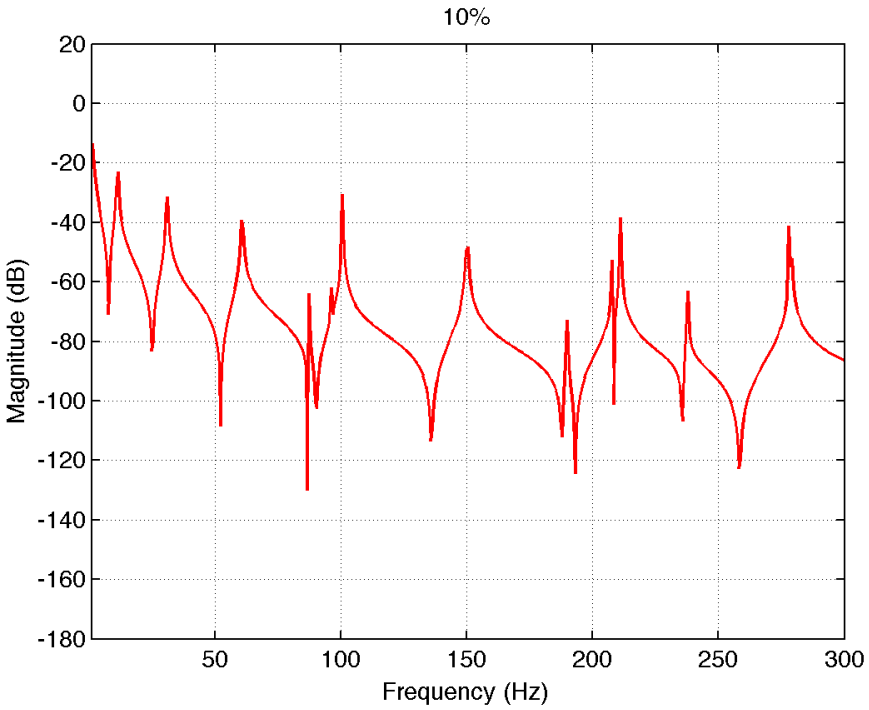

Figure 37 FRF of Double beam with 10% mass portion of an attached cable

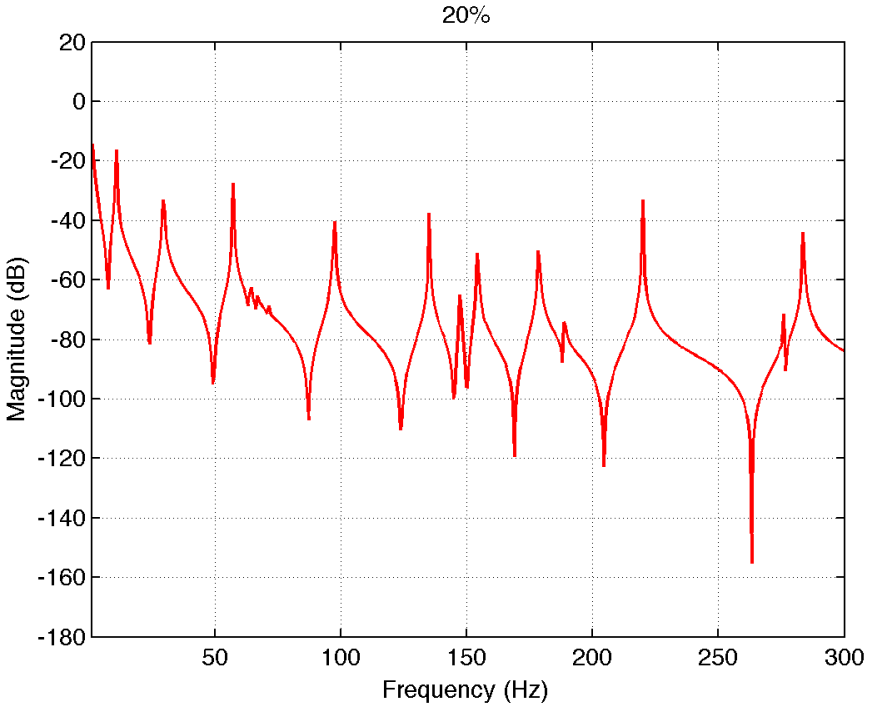

Figure 38 FRF of Double beam with 20% mass portion of an attached cable

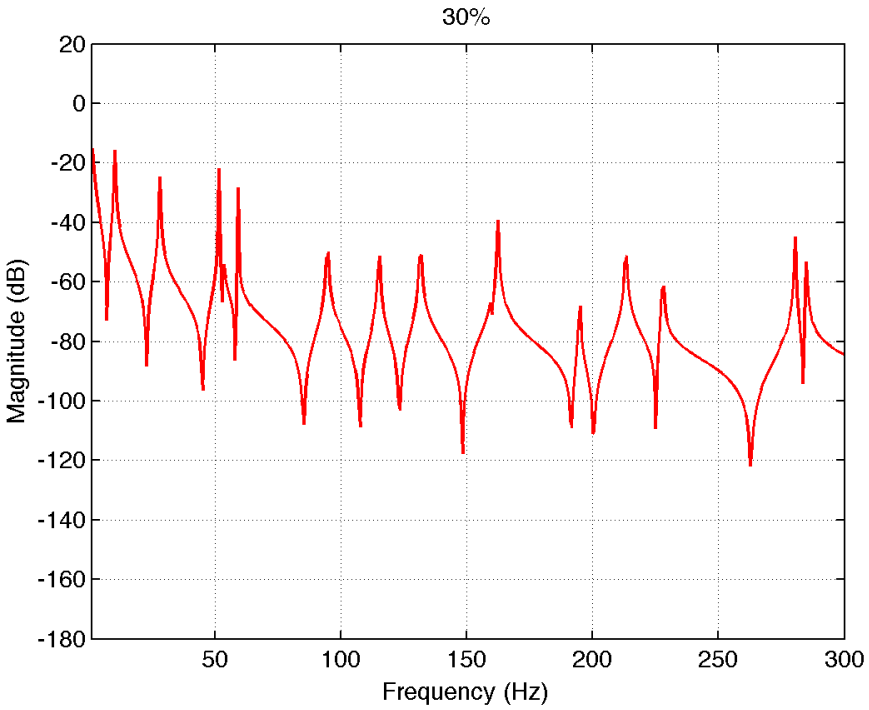

Figure 39 FRF of Double beam with 30% mass portion of an attached cable

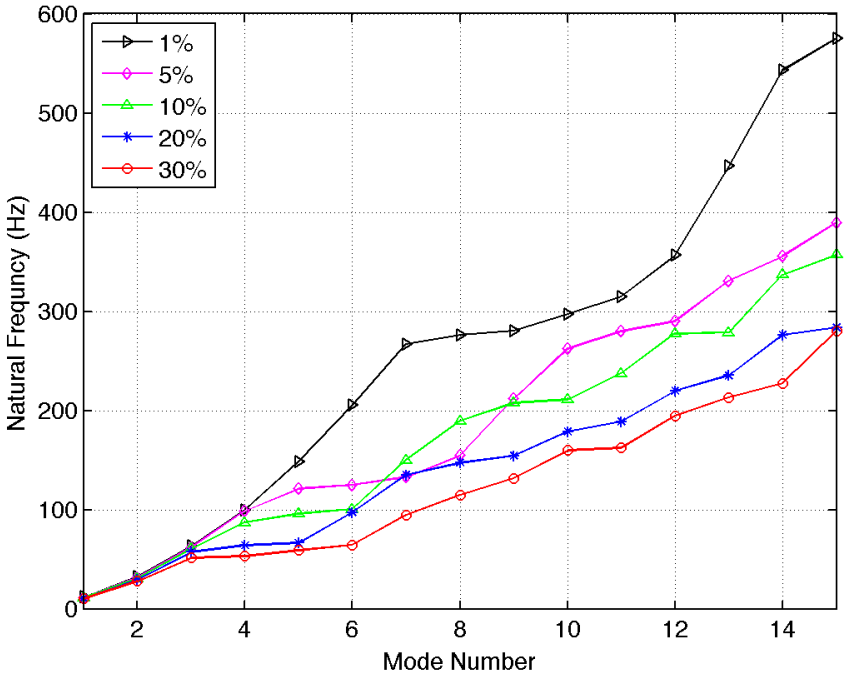

Figure 40 Change in the natural frequencies due to the mass portion

Table 15 Natural frequencies with 5 different mass portions.

Modes	Mass portion of an attached cable				
	1%	5%	10%	20%	30%
1	11.783	11.465	11.146	10.828	10.191
2	32.484	31.847	30.892	29.618	28.025
3	63.057	62.101	60.828	57.324	51.592
4	99.681	98.725	87.261	64.012	53.184
5	148.41	121.02	96.178	66.560	59.235
6	205.73	125.16	100.64	97.452	64.331
7	267.20	133.12	150.00	135.03	94.585
8	276.11	154.78	189.81	147.45	114.97
9	280.57	211.78	207.64	154.46	131.53
10	297.45	262.42	211.15	178.66	159.87
11	314.97	279.93	237.58	188.85	162.42
12	356.37	290.13	277.71	219.74	194.90
13	446.49	330.89	278.98	235.35	213.06
14	542.99	355.73	337.26	276.11	227.71
15	575.16	389.49	357.32	283.76	280.25

Figure 35~Figure 39 shows the FRF of each mass ratio of an attached cable. The first 15 natural frequencies are summarized in Table 15. In Figure 40 the natural frequencies of 5 cases are compared. The results show that more modes appear as the mass portion of attached cable increases in the lower frequency range. This mainly comes from fact that the attached cables increase the total mass of the combined system.

4.5 Summary

With the SEM based modeling approach, the change of dynamic characteristics is investigated, mainly concentrating on the natural frequencies of a combined system, in three aspects: stiffness of interconnection, number of interconnections, and the mass ratio of an attached cable. First, the numerical result indicates that the larger stiffness of interconnection will increase the natural frequencies. Next, an increment of a number of

interconnections will increase the natural frequencies of a combined system. In the end, the eigenfrequencies will converge from the lower frequency range to the higher frequency range. Last, the heavier attached cable will increase the total mass of a combined system. This diminishes the natural frequencies of a total system. Therefore, more modes appear in in the lower frequency range. In conclusion, attaching a cable to the system will change the dynamic behavior of a total system significantly.

Chapter 5

Damping alteration of a cable-harnessed structure induced by an attached cable

5.1 Introduction

The author has considered the possibility that attached cables would affect the natural frequency and damping of a combined system significantly. The changes of natural frequencies are observed by presenting the SEM-based modeling approach with experimental validation in section 2~4. In this chapter, the alteration of damping in an entire structure induced by an attached cable is investigated by using the DSM-based identification approach. The typical example of the DSM-based method is Kim's method [32-34]. The effect of the number of connections and type of attached cables on the damping of a total structure is observed with Kim's method. Additionally, to verify the effect of the flexibility of attached cables, the simplified lumped mass-spring system is used and compared with damping identification results.

Kim's method is very straightforward and hence attractive. However it does not result in accurate damping matrices when noise is present. Damping matrix identification approaches are mostly based on the inverse problem of the measured FRF. Even a small level of noise can make a significant effect on the inversed matrices. A survey of damping identification methods reveals the Instrumental Variable (IV) method [36, 39] is a good approach to reduce the noise effects on identified damping matrices. The IV method is also applied to identify the damping and is compared with DSM base methods.

5.2 Damping in the cable-harnessed structure

By using Kim's matrix identification method, the author has investigated the effect of the number of interconnections between the cable and host structure first. After that, the effect of the type of attached cable has been examined.

5.2.1 Experimental setup

The experimental setup is shown in Figure 41. An aluminum beam with the dimensions of 30-inches in length, 1¼-inches in width and 3/8-inches in thickness formed the test structure. The input force was applied by a mini shaker (Labworks, ET-132) and measured by the force sensor (PCB 208C02). The output was acquired by using accelerometers (PCB 352C67). To prevent the measurement of torsional vibration, the shaker, force sensor and accelerometer were attached at the centroid of the aluminum beam, as shown in Figure 42. A Vibrant laser USB shaker controller and RT pro software were also used. The test specimen was hung by rubber bands at both ends to emulate the free-free boundary condition as shown Figure 42. A 7x7 Full accelerance FRF matrix was measured for each test.

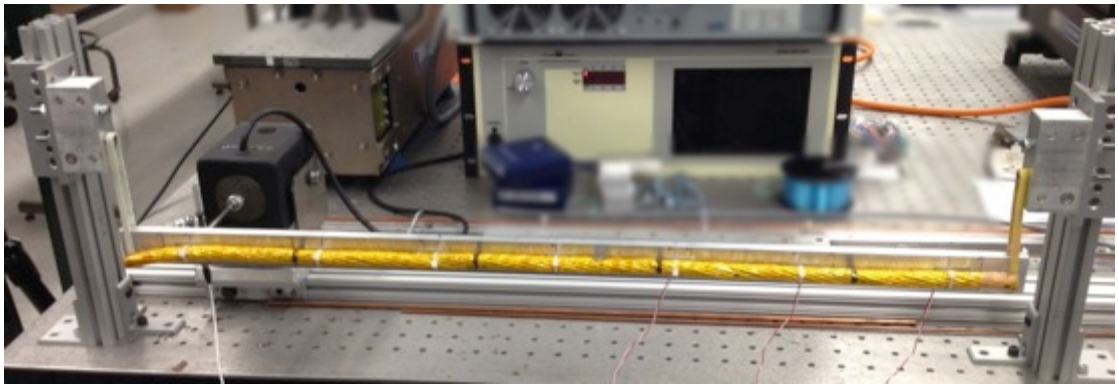

Figure 41 Experimental setup

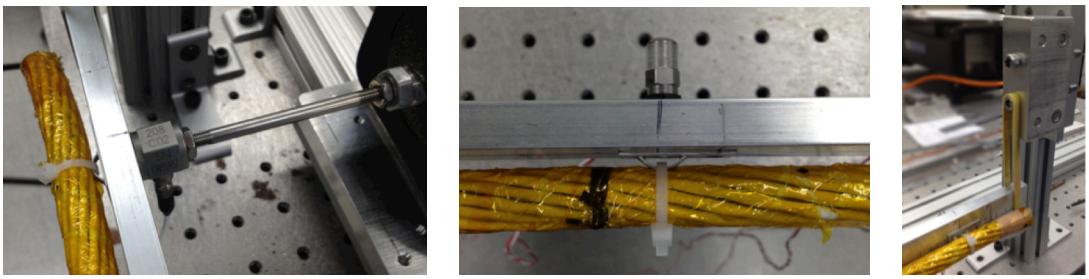

Figure 42 Shaker with force sensor, accelerometer and boundary Condition

5.2.2 The effect of number of interconnections on damping

The effect of the number of interconnections has been investigated with four different connection cases (bare beam and 3, 5 and 7 connections). Figure 43 shows the specimen with 7 interconnections. An aluminum beam with an actual satellite cable tied to it was used in the tests.

Figure 43 Test specimen (7 connections)

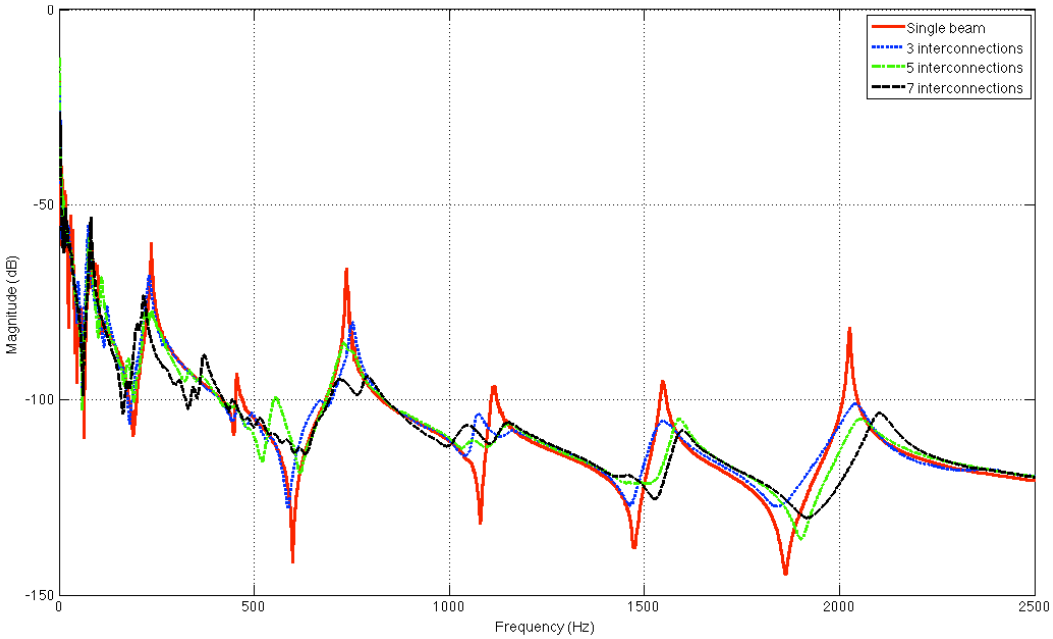

Figure 44 Driving point FRFs, measured at 3rd point

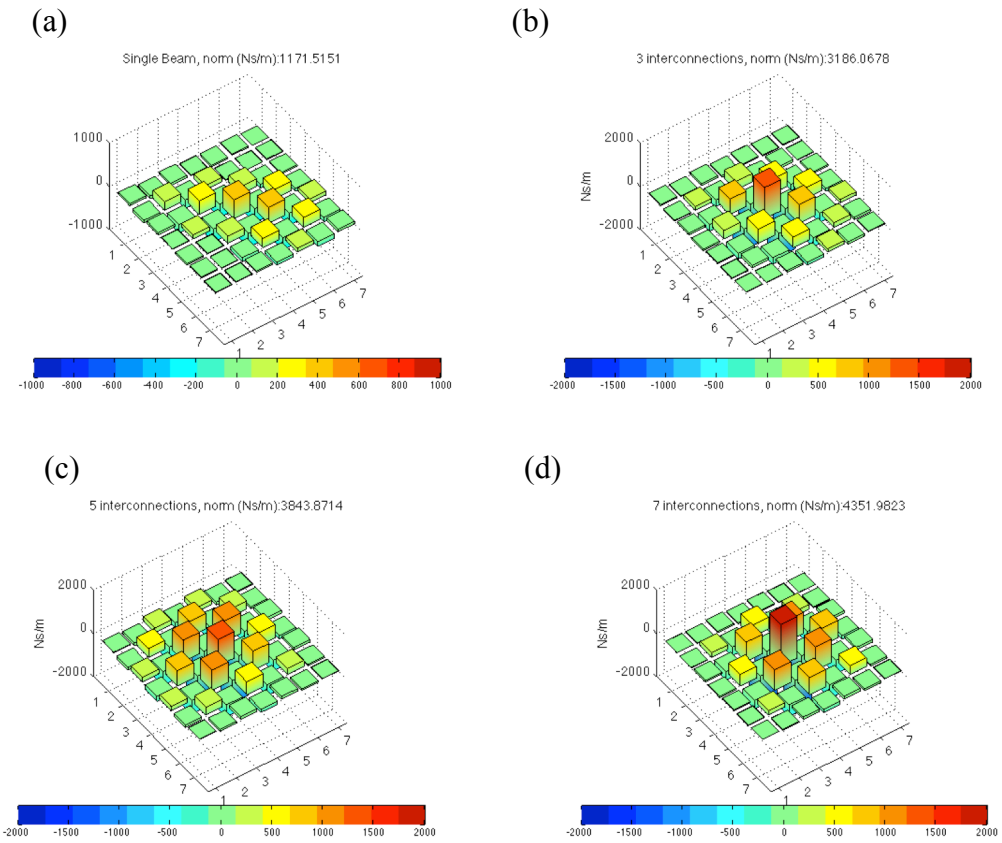

Figure 45 The matrix norm comparison of viscous damping matrices

(a) Single beam, (b) 3 interconnections, (c) 5 interconnections, (d) 7 interconnections

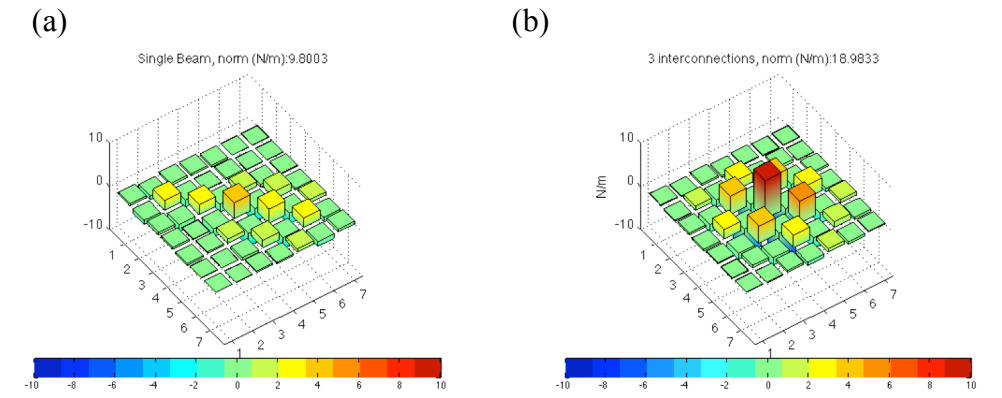

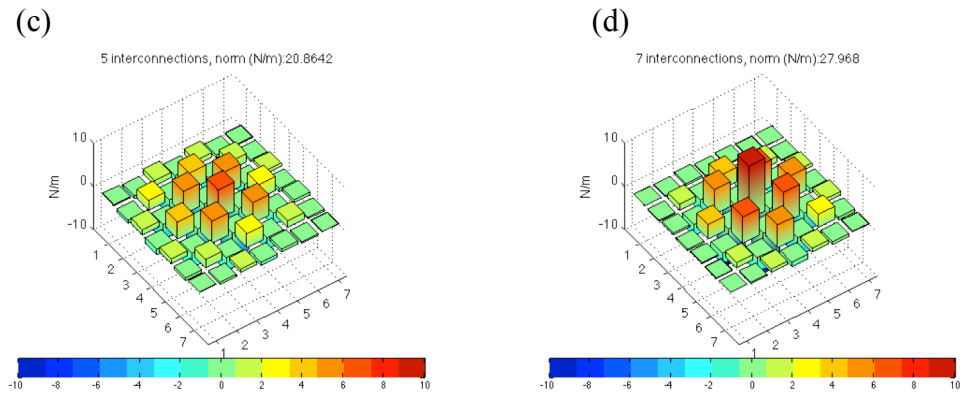

Figure 46 The matrix norm comparison of structural damping matrices

(a) Single beam, (b) 3 interconnections, (c) 5 interconnections, (d) 7 interconnections

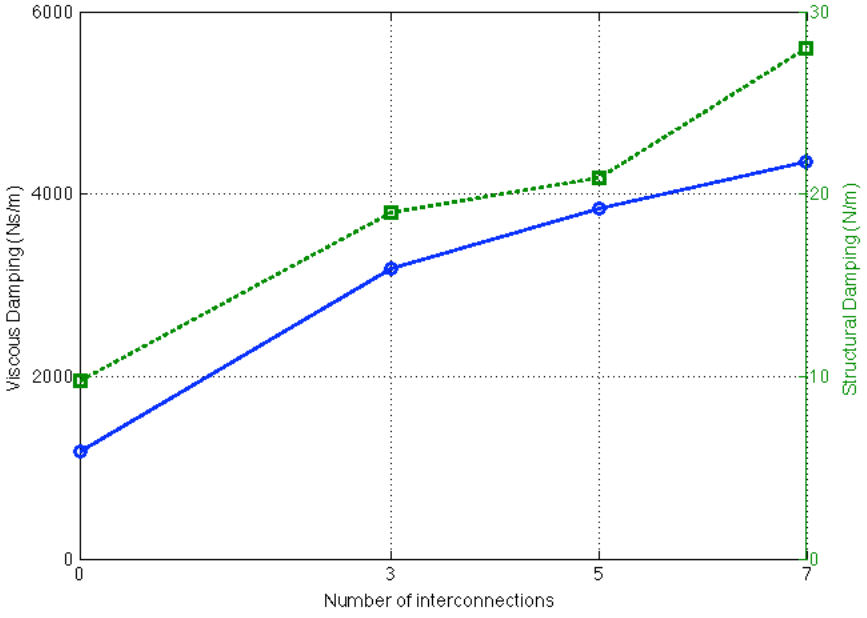

Figure 47 Comparison of the norm of damping matrices with 4 different connection numbers

The measured FRFs are shown in Figure 44. The viscous and structural damping matrices were calculated as shown in Figure 45 and Figure 46. The *x*-axis and *y*-axis represent the dimension of the damping matrices and the *z*-axis represents the magnitude of damping matrix components. Figure 45 and Figure 46 show the increase of both damping matrices as the number of connections increases. In Figure 47, the norms of the

viscous damping and structural damping matrices were compared. Again this shows that damping increases in both damping matrices when the number of connections increases. Therefore, the test results clearly indicate that the damping of the system increases as the number of connections increases.

5.2.3 The effects of the type of attached cables

To look into the effects of the attached cables, modal tests were conducted with the single beam with 3 different attached cables. The cables were attached with 3 connections. The type of cables and connection structure are summarized in Table 16.

Table 16 Connection structure and 3 attached cables

Connection structure	Copper beam	Actual satellite cable	Electric cable
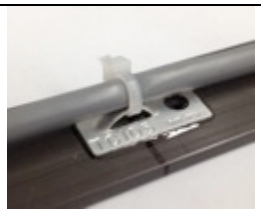			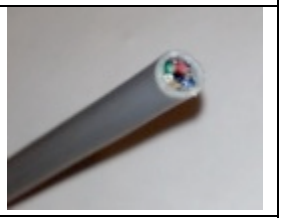
- T&B TC105 tie-down - Zip tie	- Copper Tube - Dia. 0.1265” - Thickness 0.04”	- 18 inner cables, - Length 29.5” - Dia. 0.5”	- Commercial cable - Length 29.5” - Dia. 0.2”

Figure 48 shows the driving point FRFs that were measured at the 3rd nodal point. In Figure 48, the FRFs with an actual satellite cable and an electric cable show that the resonance peaks have a smoother shape and move to the right-hand side. Thus these results show the increase in damping induced by the attached cables. But the FRF with the copper beam shows a different tendency. The measured FRF of the case with the copper beam shows sharp peaks and additional peaks compared with the single beam case. So it is hard to figure out the change in damping of the system structure with the

copper beam. To investigate the details, Kim's method was applied to obtain the damping matrices.

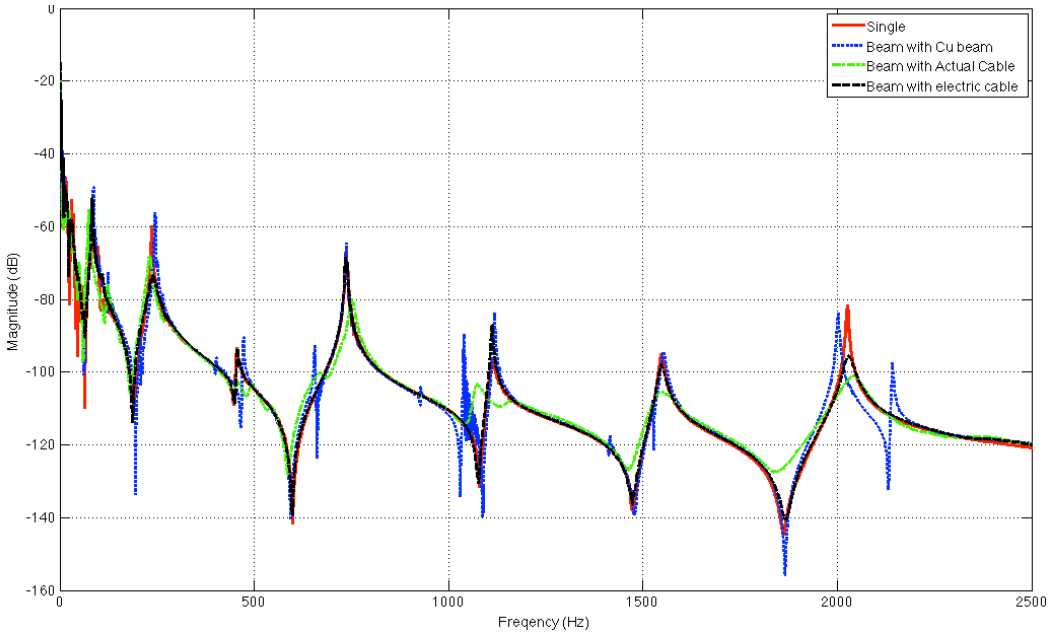

Figure 48 Driving point FRFs, measured at 3rd point

The damping matrices were obtained by using Equation (12). The calculated viscous damping and structural damping matrices are shown in Figure 49 and Figure 50. The *x*-axis and *y*-axis represent the dimension of the damping matrices and the *z*-axis indicates the magnitudes of damping matrix components. In Figure 49 and Figure 50, plots (a), (b), (c) and (d) represent the damping matrices from a single beam, beam with a copper beam, a beam with an actual cable, and a beam with an electric cable. Plots **(c)** and **(d)** on Figure 49 show the increase of viscous damping compared with plot **(a)**. But plot **(b)** shows the similar or smaller damping matrix compared with plot **(a).** Figure 50 also shows the similar tendency of structural damping compared with the viscous damping.

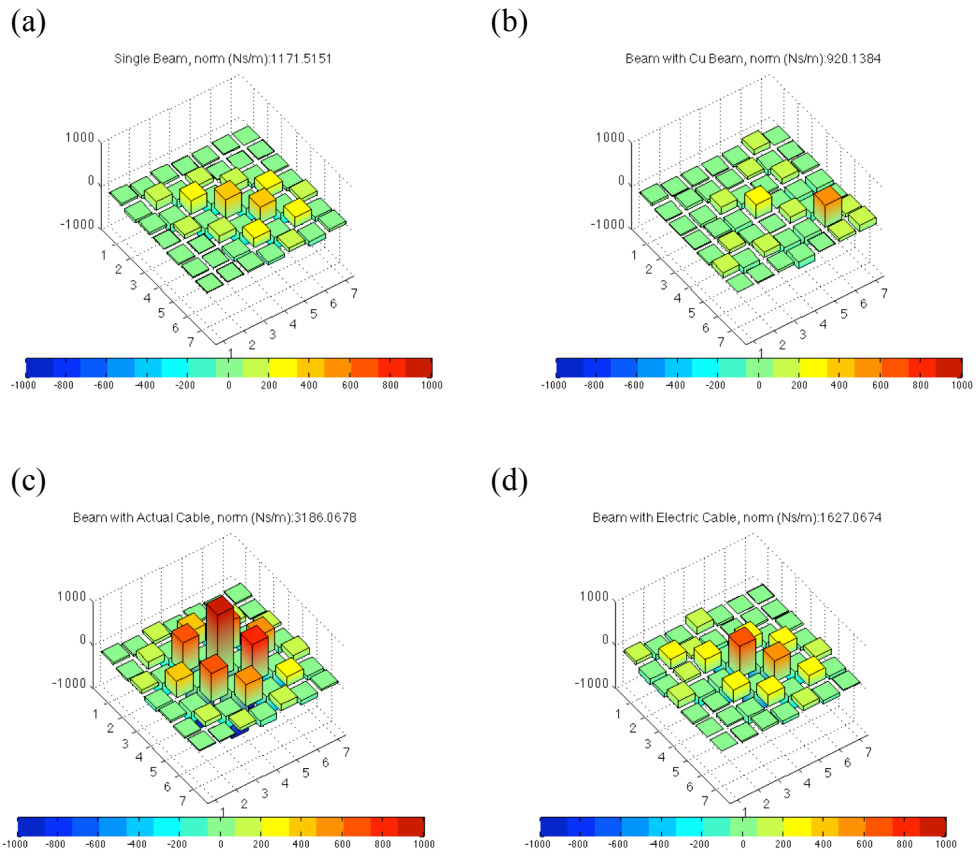

Figure 49 The matrix norm comparison of Viscous Damping Matrices

(a) Single beam, (b) Beam with attached Cu beam, (c) Beam with attached actual cable, (d) Beam with attached electric cable

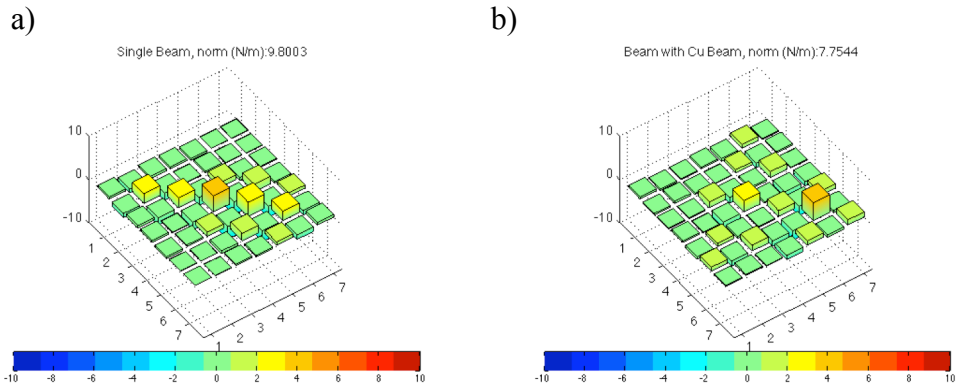

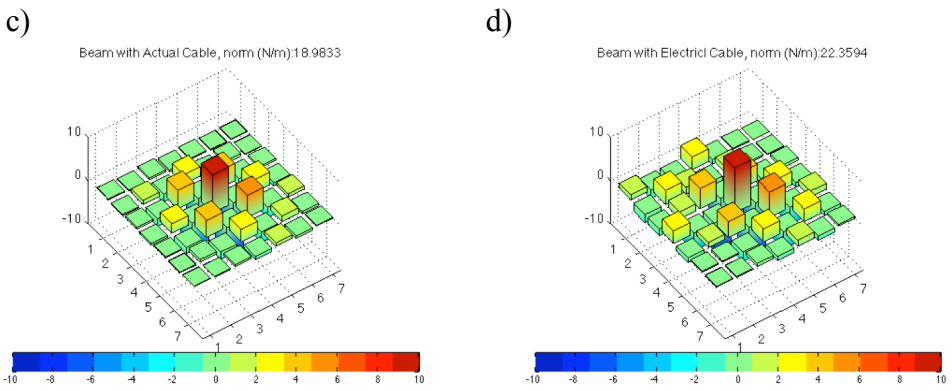

Figure 50 The matrix norm comparison of Structural Damping Matrices

a) Single beam, b) Beam with attached Cu beam, c) Beam with attached actual cable, d) Beam with attached electric cable

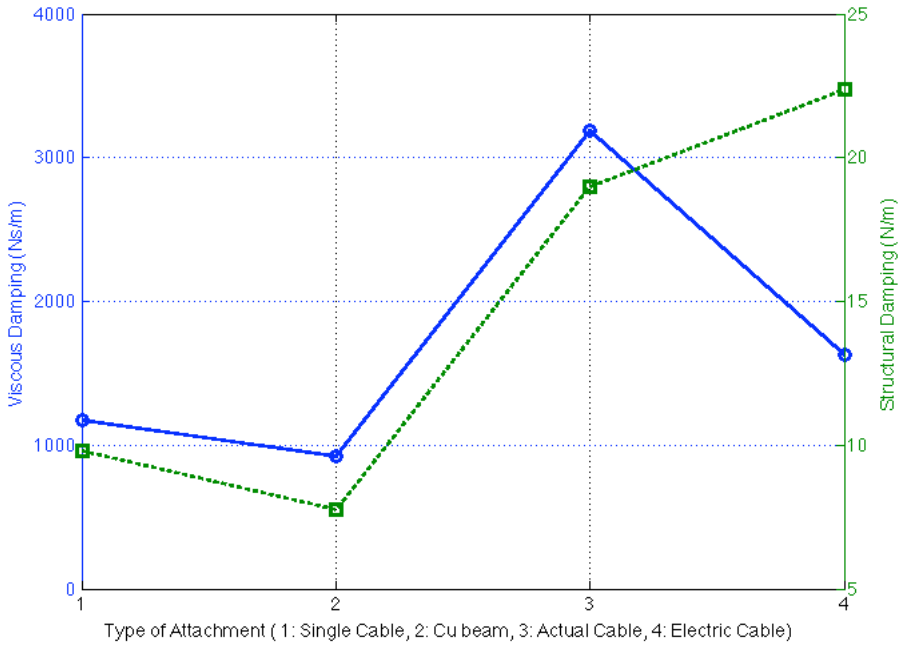

Figure 51 The matrix norm comparison of Damping Matrices with 4 different attachments

In Figure 51, the norms of the viscous damping and structural damping matrices were compared. The beam with the actual satellite cable shows the increase in damping in both damping matrices. The beam with an electric cable shows the biggest increase in the structural damping. However, considering the viscous damping, the actual cable increases

the damping most. The damping is decreased when attached with the copper beam. From these results, it can be concluded that the type of cables can affect the damping differently. The flexibility effect on the damping of a host structure will be investigated further in the next section.

5.3 The effect of flexibility of an attached cable

In previous section 5.2.3, it was found that the flexibility of an attached cable could affect the damping of a combined system. Here, to verify this phenomenon, the change of the damping ratio was investigated with a simple lumped mass system as shown in Figure 52. One DOF system in the left-hand side of Figure 52 represents the host structure without any attached cables. The right-hand side of Figure 52 represents the host structure with the attached cable. A 2 DOFs example serves to illustrate what can be expected to happen to the system damping ratio as subsystems are added with different amounts of damping. A total of 5 arrangements were numerically examined. For each analysis, the damping coefficient of the host structure was fixed and that of attachment was changed. The changes in system natural frequencies and damping ratios were observed using a state-space model [3].

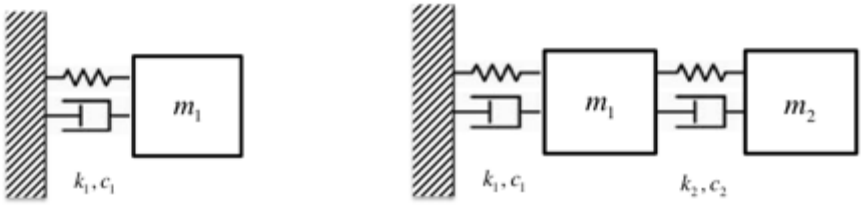

Figure 52 1 DOF (host structure) and 2 DOFs system (cable-harnessed structure)

Analysis 1)

The first analysis was conducted with following system parameters. The mass, stiffness and damping coefficient of the host structure were fixed as c_1=1 N.s/m. Then the damping coefficient of the attached system was changed from c_2=10^{1}~10^{-4} N.s/m. The system parameters are shown in Table 17.

Table 17 System parameters

m_1	m_2	k_1	k_2	c_1	c_2
10 kg	10 kg	10 N/m	10 N/m	1 Ns/m	10^{1}~10^{-4} Ns/m

The natural frequency of the host structure is $\omega_n = 1$ (rad/s). The damping ratio of the host structure $\zeta = c_1/2m_1\omega_n$ is 0.05. **Figure 53** shows the FRFs of each case. **Figure 54** shows the comparison of damping ratios. A black vertical line represents the damping coefficient of the host structure and the *x*-axis represents the damping coefficient of the attached system. Thus the left-hand side of a black vertical line means that the attached system is less flexible than the host structure. A red horizontal line represents the damping ratio of the host structure without attachment. So the range, in the left of the black vertical line and below the red horizontal line, means that the less flexible attachment decreases the system damping compared to the initial damping in the host structure. The results show the damping ratios of the combined system are located in left-bottom area with less flexible attachment and in right-top area with a more flexible attachment. Therefore, it can be concluded that the damping increases with the more flexible attachment and decreases with the less flexible attachment. The calculated damping ratios are summarized in Table 18.

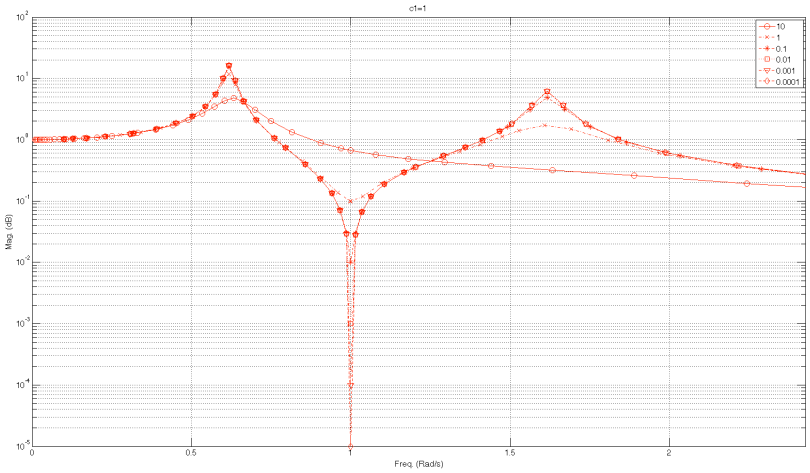

Figure 53 FRFs of a combined system (C_1=1, C_2=10^1 ~10^{-4})

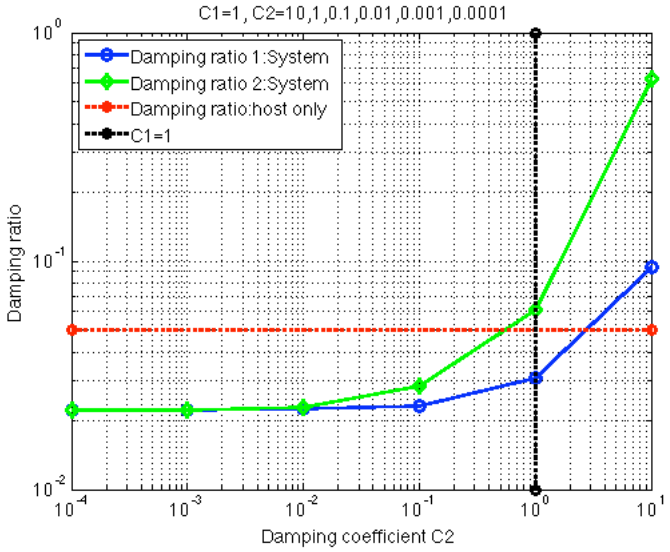

Figure 54 Damping ratios of a combined system (C_1=1, C_2=10^1 ~10^{-4})

Table 18 Natural frequencies and damping ratio of 2 DOFs system

Case	C_1	C_2	ω_1	ω_2	Damping ratio : host	Damping Ratio : Combined system	
					ζ	ζ_1	ζ_2
1		10	0.638088186543253	1.56718149793268	**0.05**	**0.0936878837028963**	**0.631846961882319**
2	1	1	0.618033988749895	1.61803398874989	0.05	0.0309016994374951	**0.0608031210133728**
3		0.1	0.618258129800398	1.61744739260096	0.05	0.0232169221630696	0.0282209791382072
4		0.01	0.618305212463104	1.61732422732838	0.05	0.0224502965153918	0.0229507874895974
5		0.001	0.618310167354544	1.61731126673612	0.05	0.0223736688226819	0.0224237188176527
6		0.0001	0.618310665309685	1.61730996423803	0.05	0.0223660064185265	0.0223710114270435

Analysis 2)

The analysis 2 was conducted with the following system parameters. The mass, stiffness and damping coefficient of the host structure were fixed at c_1=0.1 N.s/m. Then the damping coefficient c_2 of the attached system was changed from 10^{-4} N.s/m to 10^{1} N.s/m. The system parameters are shown in Table 19.

Table 19 System parameters

m_1	m_2	k_1	k_2	c_1	c_2
10 kg	10 kg	10 N/m	10 N/m	0.1 N.s/m	10^{-4}~10^{1} N.s/m

The natural frequency of the host structure is $\omega_n = 1$ (rad/s). The damping ratio of the host structure $\zeta = c_1/2m_1\omega_n$ is 0.005. Figure 55 and Figure 56 show the FRFs of each cases and the damping ratio comparison. The same tendency of analysis 1 is found. The results show that the damping ratios of the combined system are located in the left-bottom area with a less flexible attachment and in right-top area with a more flexible attachment. The calculated damping ratios are summarized in Table 20.

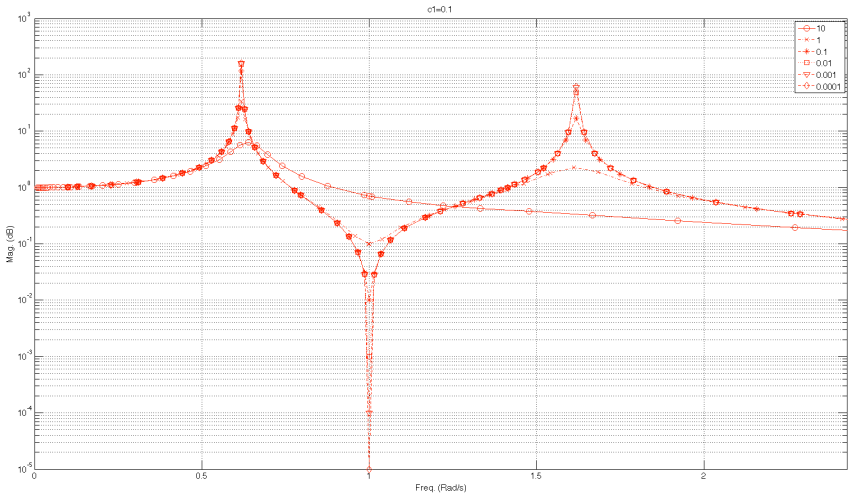

Figure 55 FRFs of a combined system (C_1=0.1, C_2=10^{1}~10^{-4})

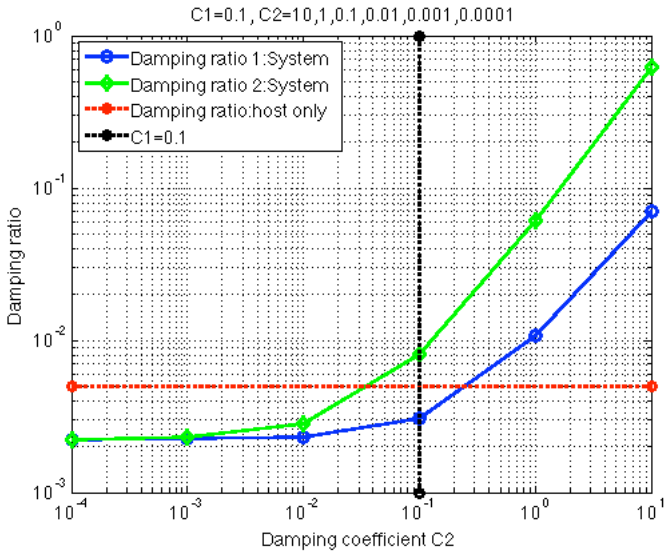

Figure 56 Damping ratios of a combined system (C_1=0.1, C_2=10^1 ~10^{-4})

Table 20 Natural frequencies and damping ratio of 2 DOFs system

Case	C_1	C_2	ω_1	ω_2	Damping ratio : host	Damping Ratio : Combined system	
					ζ	ζ_1	ζ_2
1		10	0.642182685989629	1.55718928868187	**0.005**	**0.0700577407871673**	**0.61650188504672**
2		1	0.618257685499062	1.61744855495455	0.005	**0.0107626317250269**	**0.0608031210133728**
3	0.1	0.1	0.618033988749895	1.6180339887499	0.005	0.0030901699437494	**0.00809016994374944**
4		0.01	0.618036227561052	1.61802812748742	0.005	0.00232148031491537	0.00282148436498537
5		0.001	0.618036697712694	1.6180268966243	0.005	0.00224461320105147	0.00229461369111087
6		0.0001	0.618036747190557	1.61802676709072	0.005	0.00223692652443761	0.00224192657433878

Analysis 3)

Analysis 3 was also conducted with the following system parameters. The damping coefficient of the host structure was changed and fixed at c_1=0.01 N.s/m. Then the damping coefficient c_2 of the attached system was changed from 10^{-4} N.s/m to 10^1 N.s/m. The system parameters are shown in Table 21.

Table 21 System parameters

m_1	m_2	k_1	k_2	c_1	c_2
10 kg	10 kg	10 N/m	10 N/m	0.01 N.s/m	10^{-4} ~10^1 N.s/m

The natural frequency of the host structure is $\omega_n = 1$ (rad/s). The damping ratio of the host structure $\zeta = c_1/2m_1\omega_n$ is 0.0005. Figure 57 and Figure 58 show the FRFs of each case and the damping ratio comparison. Similar to analysis 1 and 2, the results show the damping ratios of the combined system are located in the left-bottom area with a less flexible attachment and in the right-top area with a more flexible attachment. The calculated damping ratios are summarized in Table 22.

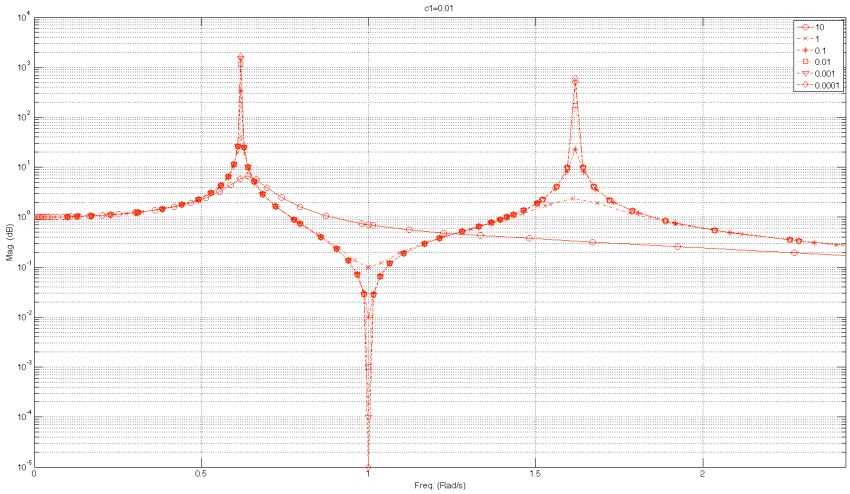

Figure 57 FRFs of a combined system (C_1=0.01, C_2=10^1 ~10^{-4})

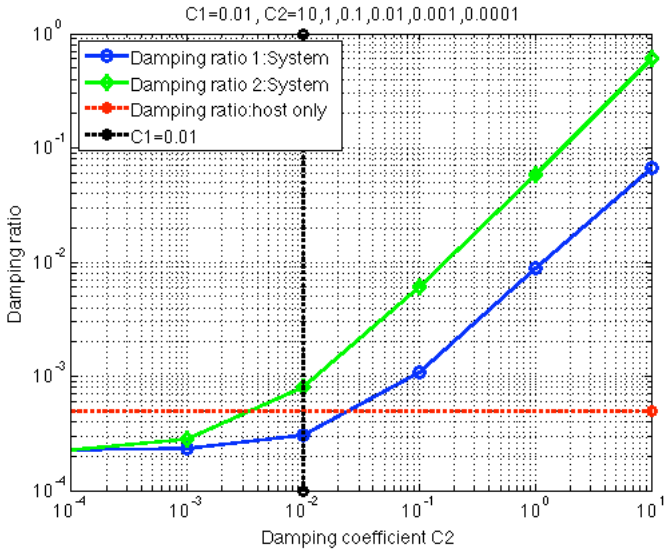

Figure 58 Damping ratios of a combined system (C_1=0.01, C_2=10^1 ~10^{-4})

Table 22 Natural frequencies and damping ratio of 2 DOFs system

Case	C_1	C_2	ω_1	ω_2	Damping ratio : host	Damping Ratio : Combined system	
					ζ	ζ_1	ζ_2
1		10	0.64261300415889	1.55614653536134	**0.0005**	**0.067666178091174**	**0.614991462738217**
2		1	0.618304669219827	1.61732564831153	0.0005	**0.00874673691128266**	**0.0587957359277592**
3		0.1	0.618036227516723	1.61802812760348	0.0005	**0.00107769430986937**	**0.00607773480976355**
4	0.01	0.01	0.618033988749895	1.6180339887499	0.0005	0.000309016994375097	**0.000809016994375**
5		0.001	0.618034011137747	1.61803393013774	0.0005	0.000232147819553291	0.000282147823603307
6		0.0001	0.618034015839196	1.61803391782919	0.0005	0.000224460903920328	0.000229460904410095

Analysis 4)

In analysis 4, the damping coefficient of the host structure is fixed at c_1=0.001 N.s/m. Then the damping coefficient c_2 of the attached system was changed from 10^{-4} N.s/m to 10^{0} N.s/m. The system parameters are shown in Table 23.

Table 23 System parameters

m_1	m_2	k_1	k_2	c_1	c_2
10 kg	10 kg	10 N/m	10 N/m	0.001 N.s/m	10^{-4}~10^{0} N.s/m

The natural frequency of the host structure is $\omega_n = 1$ (rad/s). The damping ratio of the host structure $\zeta = c_1/2m_1\omega_n$ is 0.00005. Figure 59 and Figure 60 show the FRFs of each cases and the damping ratio comparison. A similar result is found in that the damping ratios of the combined system decrease with a less flexible attached subsystem and increase with a more flexible subsystem. The calculated damping ratios are summarized in Table 24.

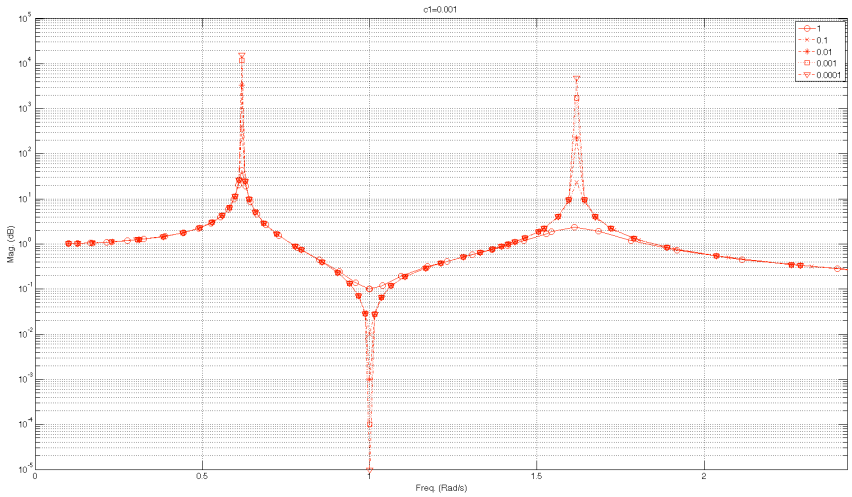

Figure 59 FRFs of a combined system (C_1=0.001, C_2=10^0 ~10^{-4})

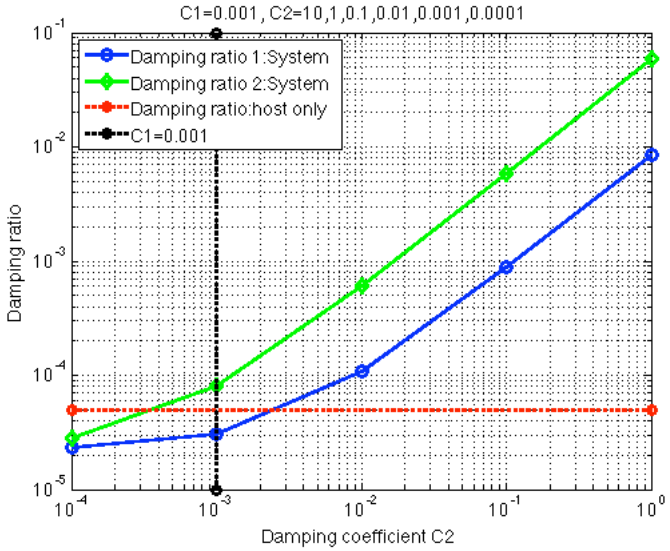

Figure 60 Damping ratios of a combined system (C_1=0.001, C_2=10^0 ~10^{-4})

Table 24 Natural frequencies and damping ratio of 2 DOFs system

Case	C_1	C_2	ω_1	ω_2	Damping ratio : host	Damping Ratio : Combined system	
					ζ	ζ_1	ζ_2
1		1	0.6183096141063	1.61731271386649	0.00005	**0.00854512349905834**	**0.0585950182511394**
2		0.1	0.618036697658519	1.61802689676613	0.00005	**0.000876444762009859**	**0.00587649376695221**
3		0.01	0.618034011137742	1.61803393013775	0.00005	**0.000107770861946026**	**0.000607770902445872**
4	0.001	0.001	0.618033988749895	1.61803398874989	0.00005	3.09016994374872e-05	**8.09016994374942e-05**
5		0.0001	0.618033988973773	1.61803398816377	0.00005	2.32147817434008e-05	2.82147817474208e-05

Analysis 5)

In this analysis, the damping coefficient of the host structure is fixed at c_1=0.0001 N.s/m. Then the damping coefficient c_2 of the attached system was changed from 10^{-4} N.s/m to 10^{0} N.s/m. The system parameters are shown in Table 25.

Table 25 System parameters

m_1	m_2	k_1	k_2	c_1	c_2
10 kg	10 kg	10 N/m	10 N/m	0.0001 N.s/m	10^{-4}~10^{0} N.s/m

The natural frequency of the host structure is $\omega_n = 1$ (rad/s). The damping ratio of the host structure $\zeta = c_1/2m_1\omega_n$ is 0.000005. Figure 61 and Figure 62 show the FRFs and the damping ratios. In this analysis, most of the damping ratios of the combined system are located in left-bottom area. Therefore, the damping increases with the attachment of larger damping. The calculated damping ratios are summarized in Table 26.

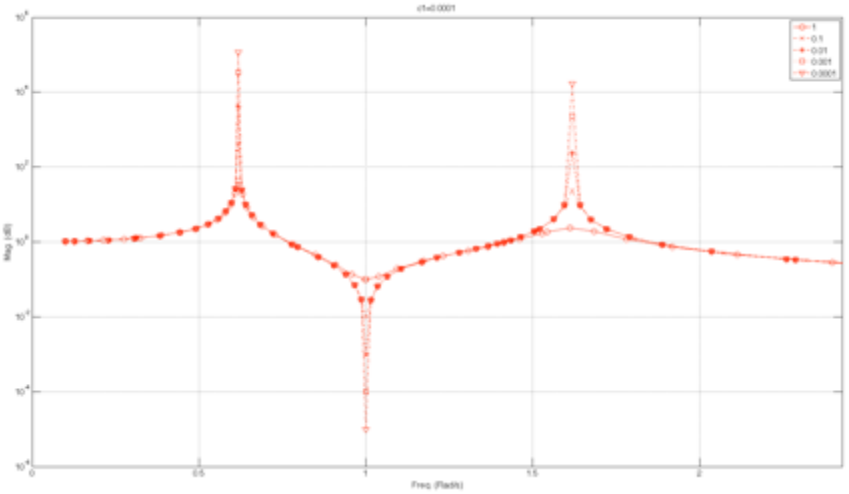

Figure 61 FRFs of a combined system (C_1=0.0001, C_2=10^{0}~10^{-4})

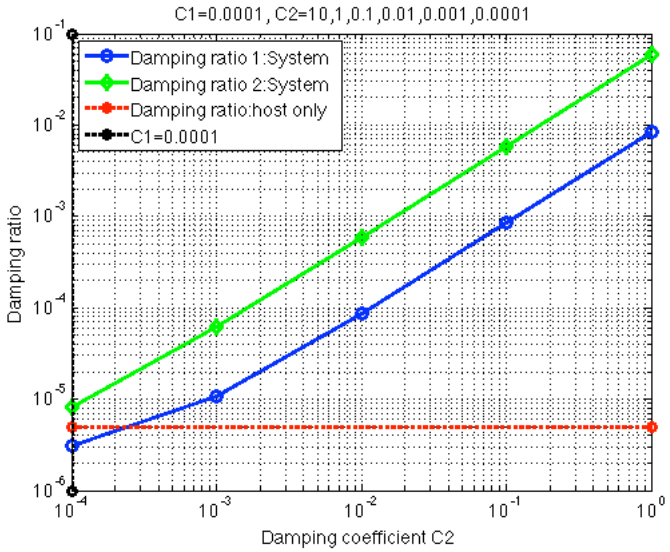

Figure 62 Damping ratios of a combined system (C_1=0.0001, C_2=10^0 ~10^{-4})

Table 26 Natural frequencies and damping ratio of 2 DOFs system.

Case	C_1	C_2	ω_1	ω_2	Damping ratio : host	Damping Ratio : Combined system	
					ζ	ζ_1	ζ_2
1		1	0.618310111060765	1.61731141398353	0.000005	**0.00852496191443892**	**0.0585749466879478**
2		0.1	0.618036747135388	1.61802676723515	0.000005	**0.000856319783398108**	**0.00585636968339716**
3		0.01	0.61803401583919	1.6180339178292	0.000005	**8.76462467185581e-05**	**0.000587646295723526**
4		0.001	0.618033988973774	1.61803398816377	0.000005	**1.07770876252591e-05**	**6.07770876661031e-05**
5	0.0001	0.0001	0.618033988749895	1.61803398874989	0.000005	3.09016994355617e-06	**8.09016994370718e-06**

From case 5, the effect on damping due to the flexibility of an attached subsystem was investigated. The damping ratio decreased in the case where the attached system is less flexible than a host structure. In contrast, the damping ratio increased when a host structure was less flexible than the attached subsystem. Finally, the results show that an increase in the flexibility of an attached cable causes an increase of damping.

5.4 Reduction of noise

Damping matrix identification approaches are mostly based on the inverse problem of the measured FRF. Even a small noise can make a significant effect on a matrix inverse. Thus, it is very easy to find papers struggling with measurement noise in the literature. In

the previous section, the author used Kim's method [32-34]. It is very straightforward and attractive. But it also cannot present the accurate damping matrices when the noise is present. Ozgen and Kim [35] tried to reduce the noise effect by selecting the specific frequency range and improving the measurement setup. But it was hard to reduce the noise effect on a general case. The Instrumental Variable (IV) method is an excellent approach to reduce the noise effect on identified damping matrices. The IV method is an iterative method. Here, the initial guess of the iteration of the IV method is obtained from Kim's method.

5.4.1 Instrumental Variable (IV) method

Wang [39] has presented the iterative approach of the IV method on the damping identification problem as shown in Figure 63.

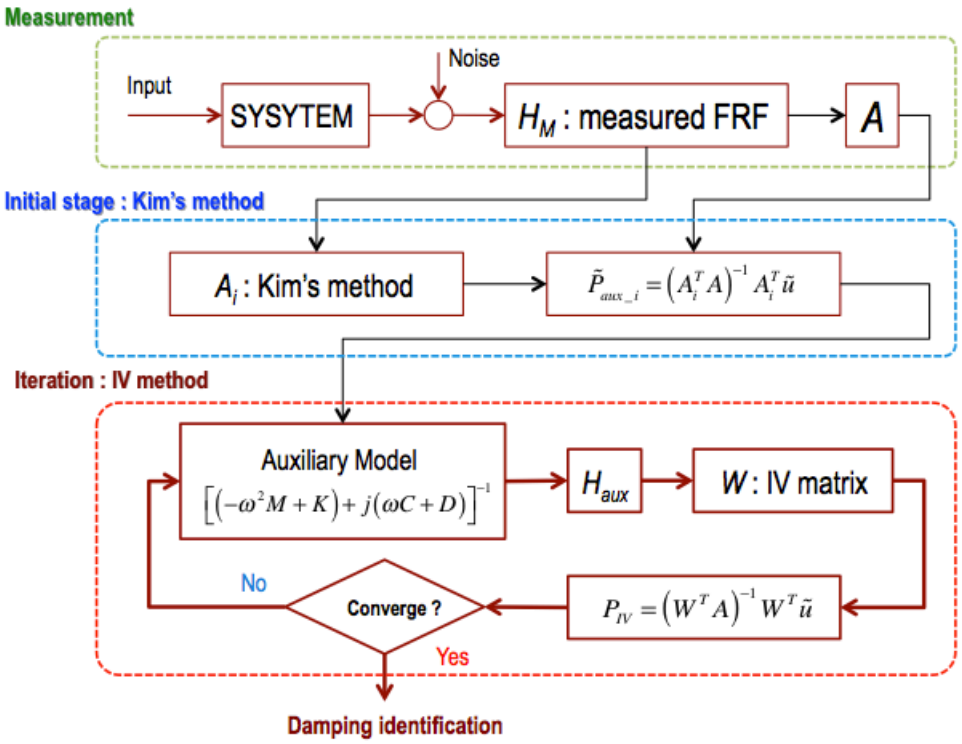

Figure 63 IV method on Kim's damping matrix identification

In Wang's approach [39], the IV algorithm starts with the Least-Square estimation as an initial auxiliary model. However, the identified matrices from Kim's method are used to construct an initial auxiliary model in this research. This choice enables us to indicate the performance of the IV method by comparing with Kim's method. For convenience, this approach will be denoted by the 'Kim+IV' method.

The IV method was applied to the simulated model. First, the mass, stiffness and damping matrices as shown Figure 64 were obtained. Then, the complex FRF matrices were calculated and simulated noise was added to the calculated FRF matrices by using the Gaussian random number generator [48] as shown in Figure 65 and Figure 68.

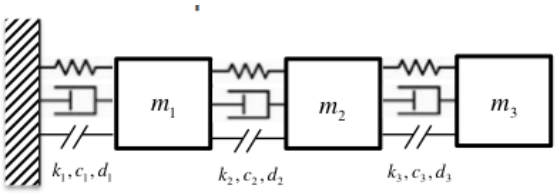

m (kg)	10	14	12
k (N/m)	2000	3000	2500
c (N.s/m)	20	30	25
d (N/m)	100	150	200

Figure 64 Simulated model

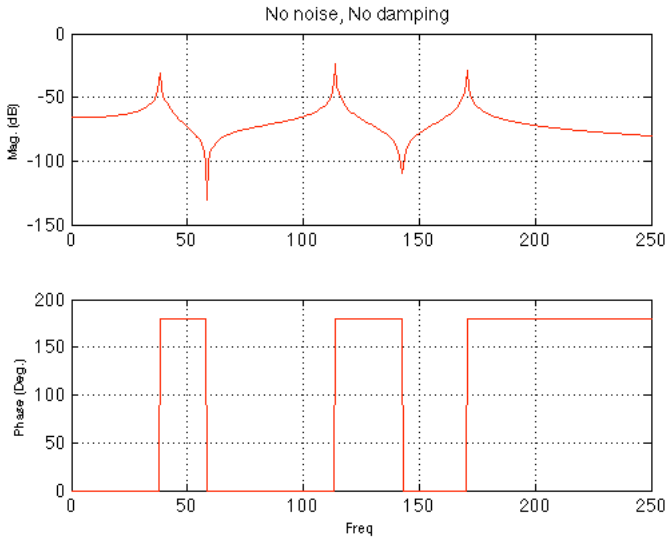

Figure 65 FRF of simulated model (no noise and no damping)

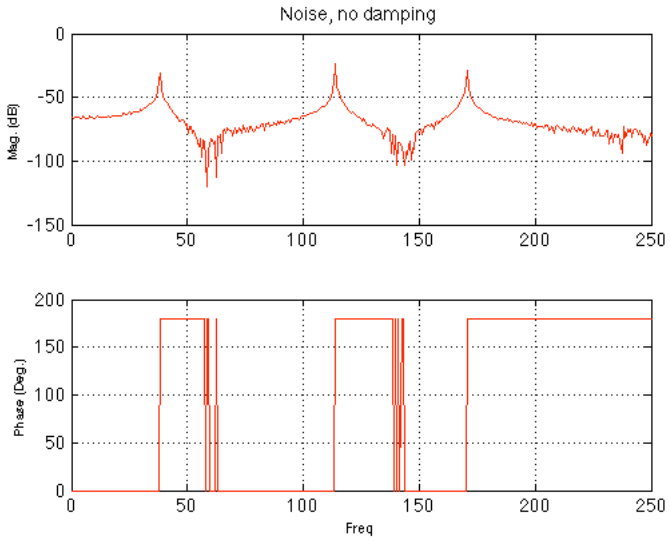

Figure 66 FRF of simulated model (5% noise and no damping)

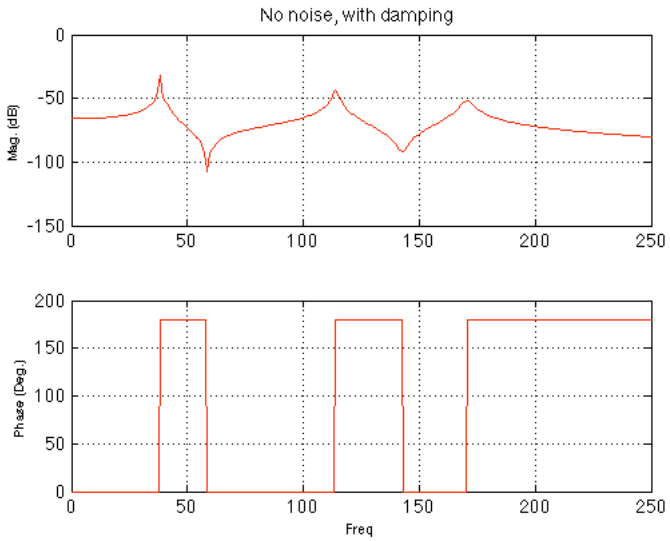

Figure 67 FRF of simulated model (no noise and damping)

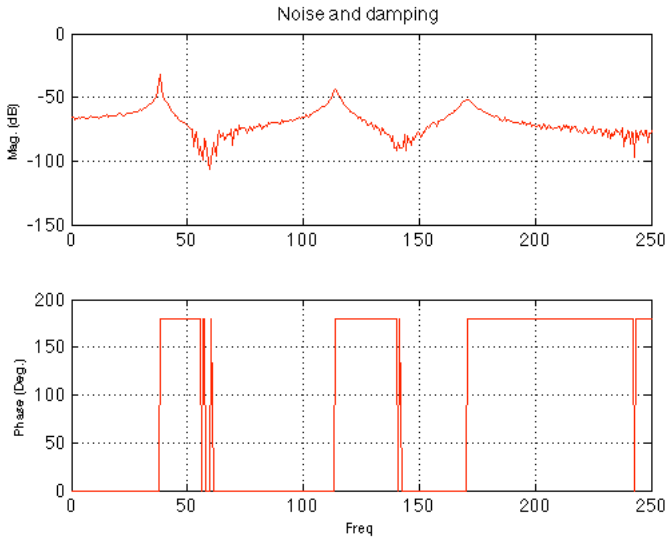

Figure 68 FRF of simulated model (5% noise and damping)

Figure 65 represents the ideal FRF without damping and noise. The simulated FRF with noise only is shown in Figure 66. Figure 67 shows the simulated FRF with damping only. The FRF in Figure 68 shows the noise and damping together. The FRF shown in Figure 68 was utilized in identifying the damping matrices by using the Kim+IV method. The results are shown in Figure 69 and Figure 70.

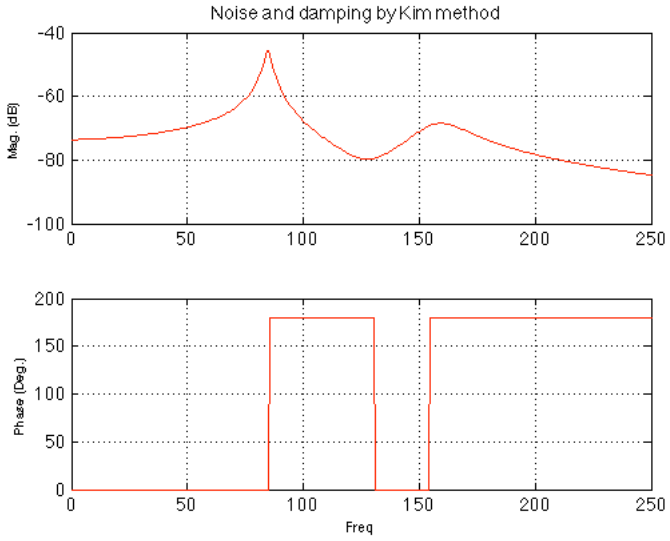

Figure 69 FRF of simulated model (Kim's method)

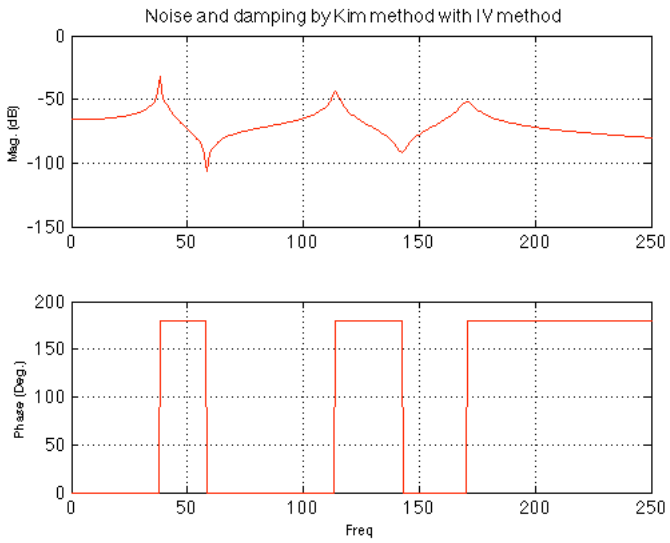

Figure 70 FRF of simulated model (Kim+IV method)

As shown in Figure 69, Kim's method resulted in a severely modified FRF contaminated by noise. But Figure 70 shows almost the same FRF as the FRF without noise as shown in Figure 67. Therefore, our approach found that the IV method could reduce or eliminate the noise effects. Figure 71 andFigure 72 show the comparison of FRFs before and after applying the IV method.

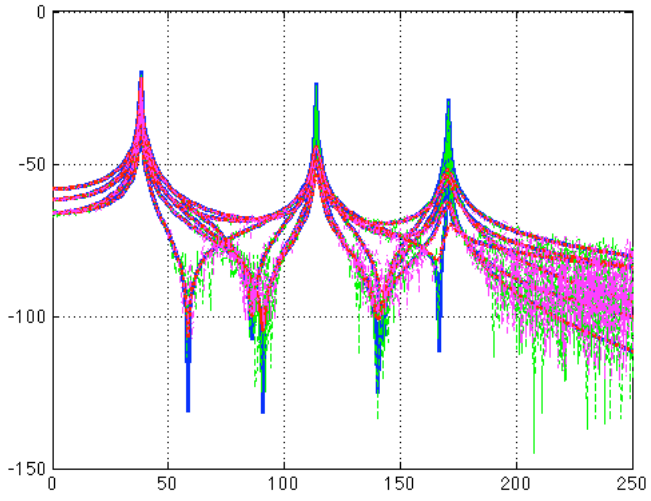

Figure 71 FRF of simulated model with noise (5%)

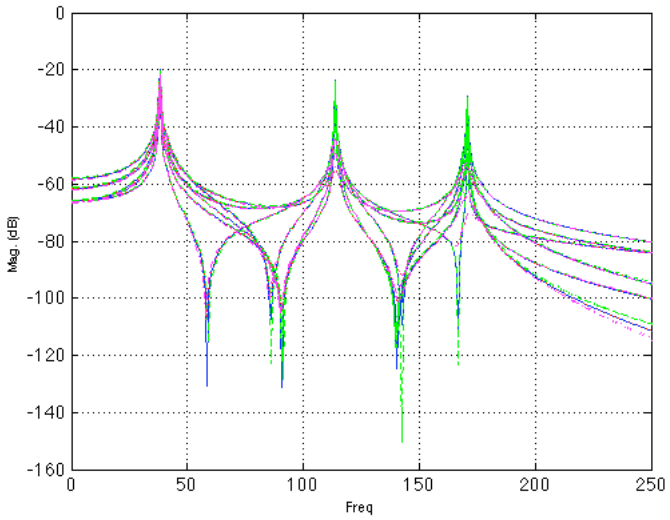

Figure 72 Reconstructed FRF of simulated model with noise reduction by IV method

The simulated results show good noise reduction. Based on good noise reduction performance in a lumped mass system, the Kim+IV method will next be applied to real measurement data.

5.4.2 Damping identification with Kim+IV algorithm

In this section, The Kim+IV method was applied to identify the damping from real measurement data. The results with the single beam test data are shown in Figure 73. Kim's method cannot reconstruct the FRF well as shown in Figure 74. IV algorithm presents closely reconstructed results to the measurement data shown in Figure 75. Figure 76 shows the comparison of results from Kim's method, the Kim+IV method and real measurement.

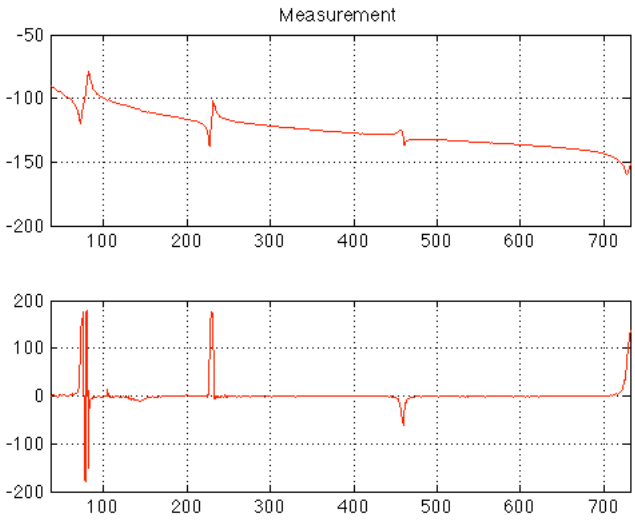

Figure 73 Measured FRF

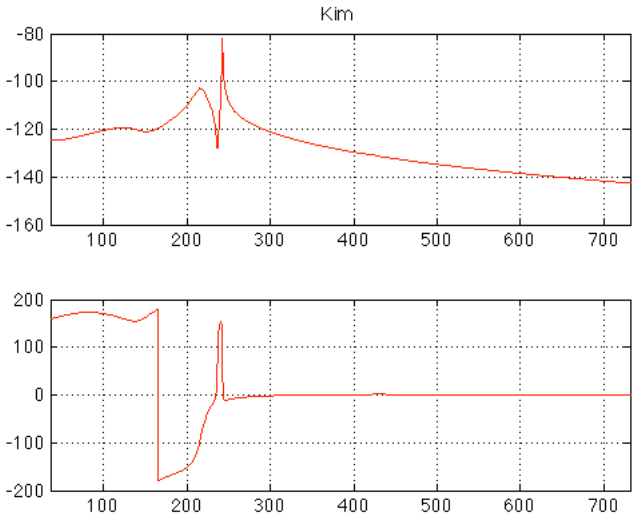

Figure 74 Reconstructed FRF from Kim's method

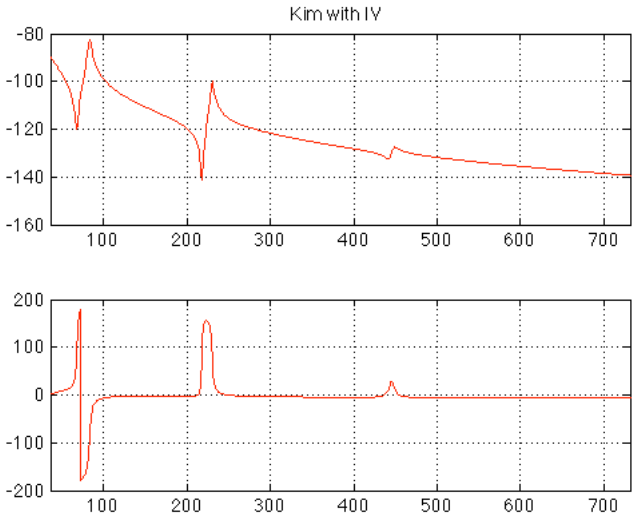

Figure 75 Reconstructed FRF from Kim+IV method

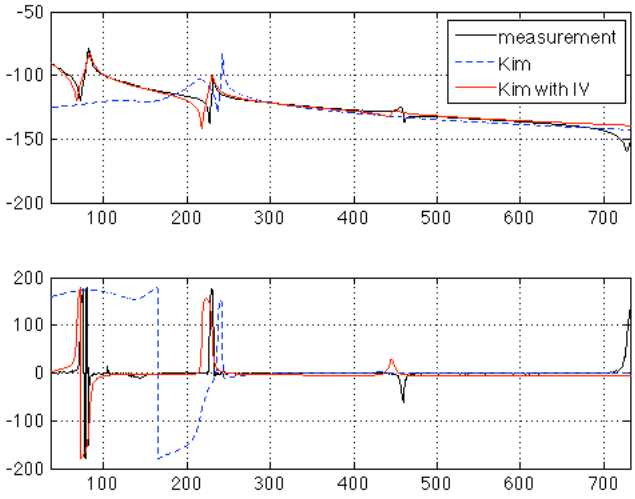

Figure 76 Comparisons of FRFs (Measurement, Kim, and Kim+IV)

The Kim+IV method shows better identification results than Kim's method alone. However, obtaining the damping matrix that contains all resonance frequencies is difficult. Therefore, the Kim+IV method was applied in the narrow band near each resonance frequency. Then the resonance frequency and damping ratio were obtained from the state-space form.

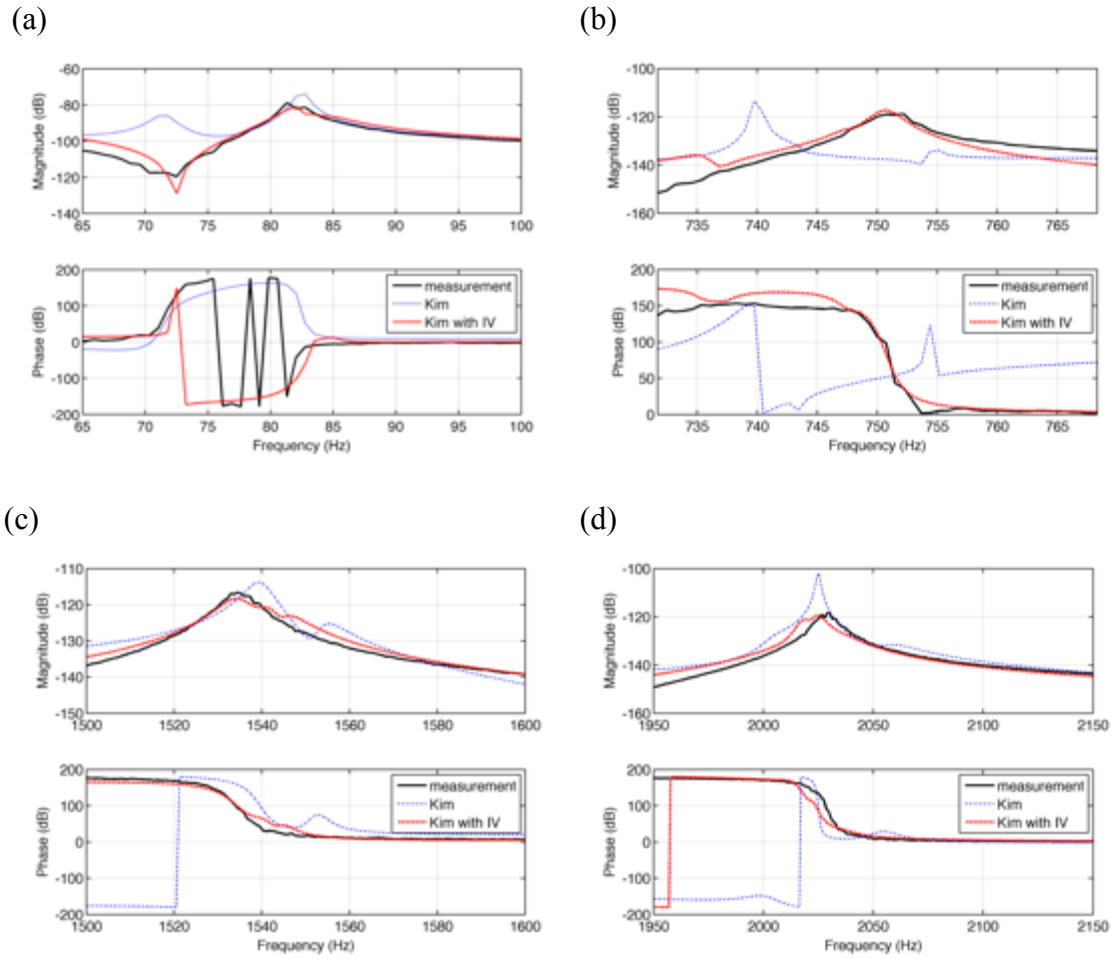

Figure 77 Measured and reconstructed FRFs (Kim and Kim+IV) of a single beam

(a) 1st mode, (b) 4th mode, (c) 5th mode, (d) 7th mode

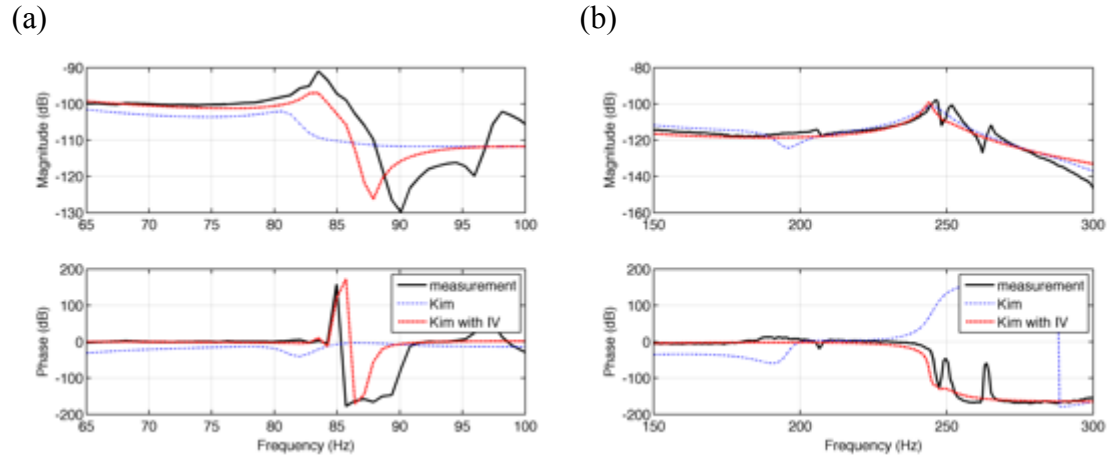

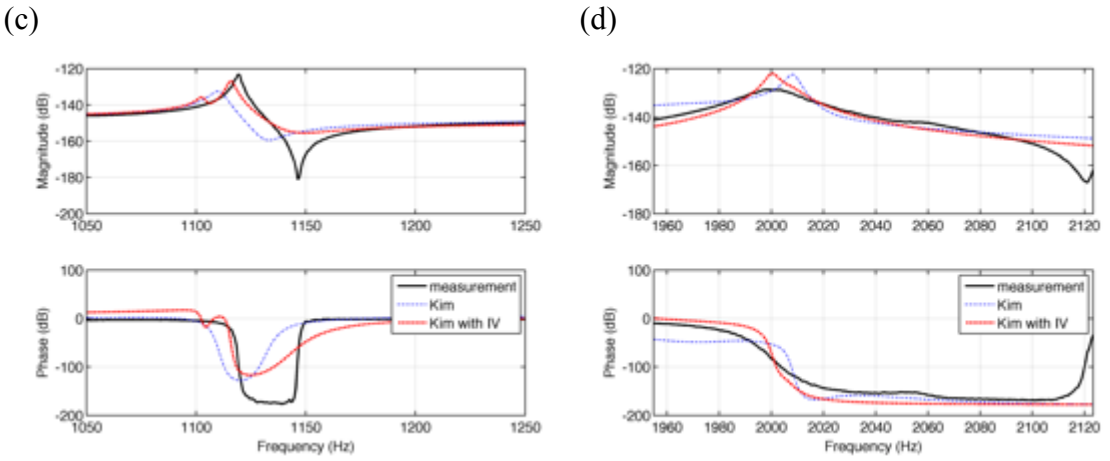

Figure 78 Measured and reconstructed FRFs (Kim and Kim+IV) with an attached Cu beam: (a) 1st mode, (b) 2th mode, (c) 5th mode, (d) 7th mode

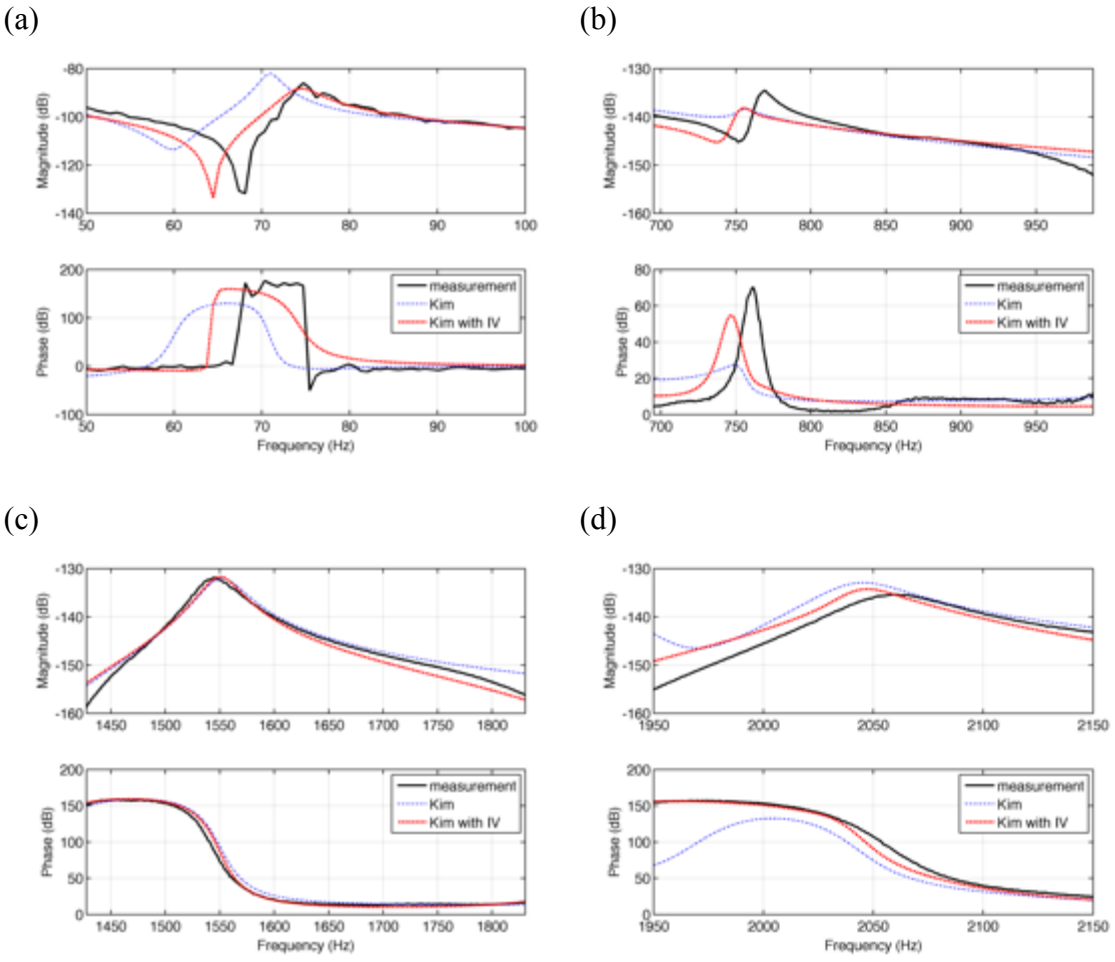

Figure 79 Measured and reconstructed FRFs (Kim and Kim+IV) with an actual satellite cable: (a) 1st mode, (b) 4th mode, (c) 6th mode, (d) 7th mode

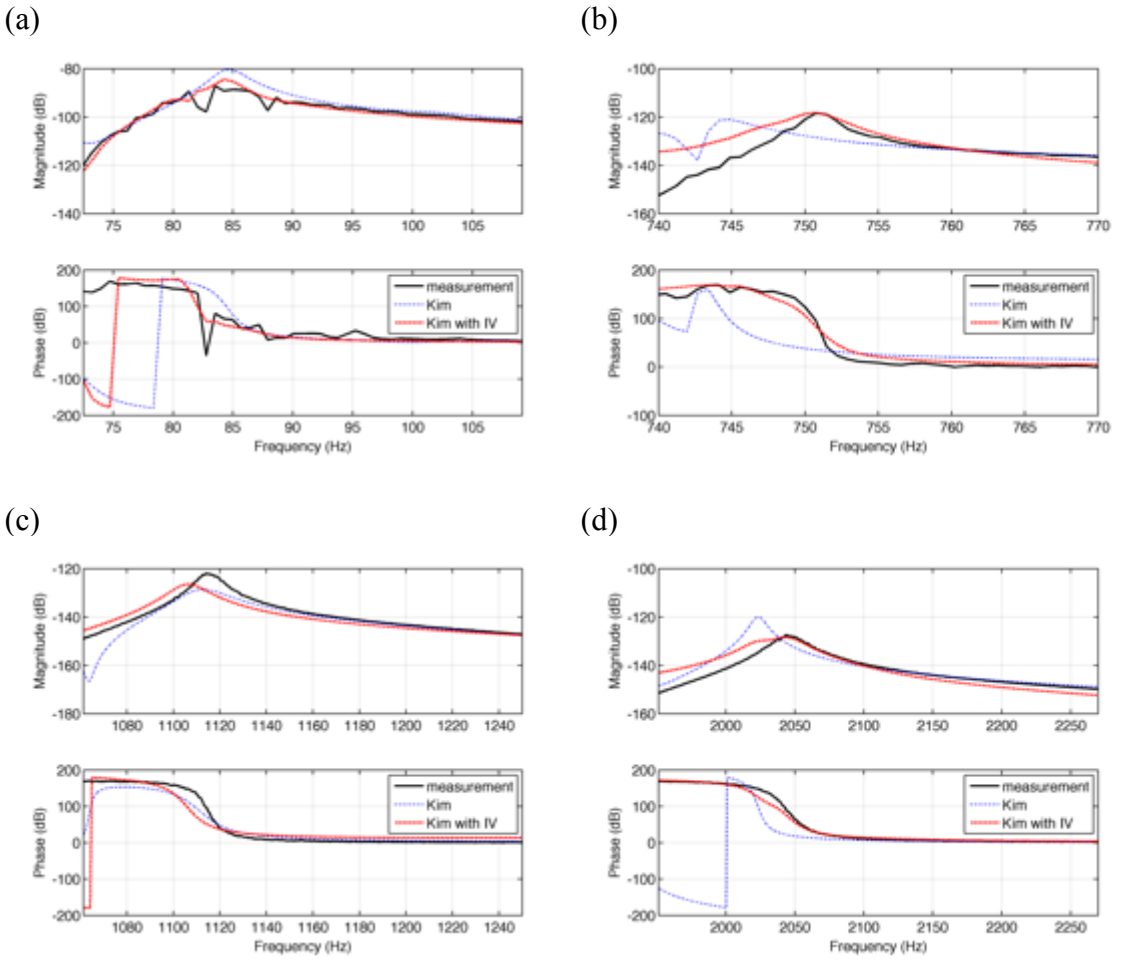

Figure 80 Measured and reconstructed FRFs (Kim and Kim+IV) with an electric cable: (a) 1st mode, (b) 4th mode, (c) 5th mode, (d) 7th mode

Table 27 Comparisons of damping ratios

Mode	Single		Cu Beam		Actual Cable		Electrical Cable		No Damping
	Freq.	Damping ratio	Freq.	Damping ratio	Freq.	Damping ratio	Freq.	Damping ratio	Freq.
1	83.06	0.015747	83.62	0.017786	75.44	0.030612	83.505	0.038531	85.866
2	230.44	0.011358	246.94	0.010096	231.33	0.024685	234.85	0.031585	236.88
3	447.4	0.010504	464.77	0.005195	447.79	0.092503	451.65	0.01966	465.51
4	749.4	0.004488	736.87	0.005496	751.94	0.023745	750.61	0.004738	773.34
5	1112	0.0061043	1115.8	0.003258	1069.2	0.039355	1106	0.014205	1165.7
6	1533.7	0.003955	1545.4	0.0028568	1549	0.02261	1542.9	0.010908	1709.5
7	2030	0.003582	1999.4	0.0015551	2046	0.024566	2043.6	0.013816	2201.4

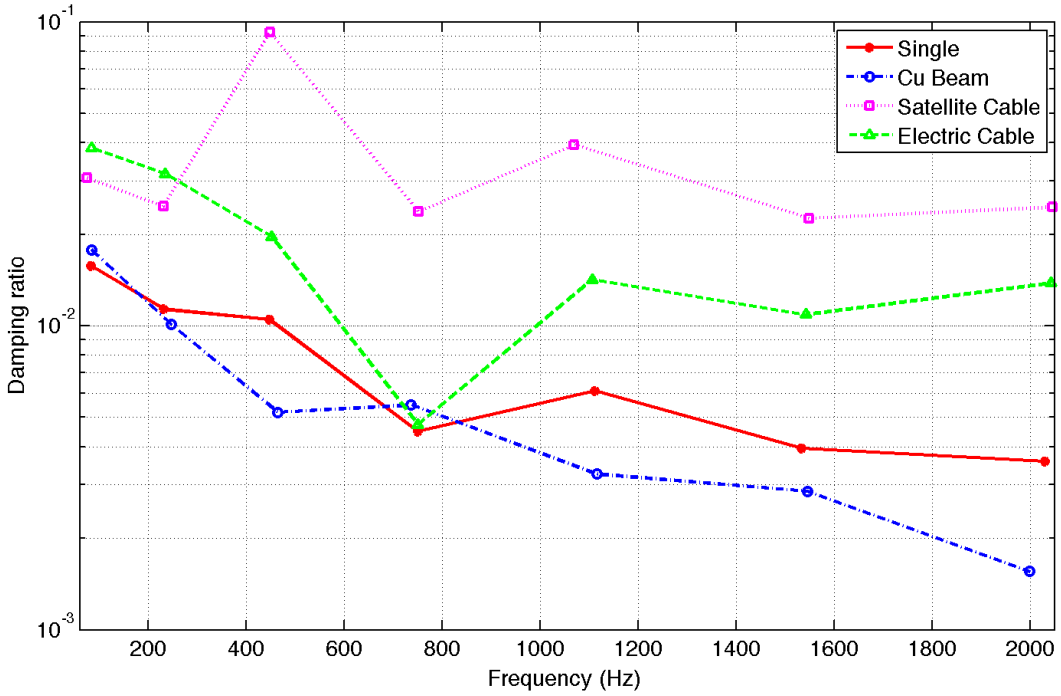

Figure 81 Comparisons of damping ratios

Considering the single beam, the reconstructed FRFs of four-selected modes are shown in Figure 77. In Figure 78, the reconstructed FRFs of the four-selected modes are shown when the system is attached to a copper beam. Figure 79 and Figure 80 present the four reconstructed FRFs of the system attached with an actual satellite cable and an electric cable. The obtained damping ratios from the reconstructed FRFs are summarized in Table 27. Kim's method obtains good identification results when dealing with real test data. In contrast, the Kim+IV method shows much better identification results. In Figure 81, the damping ratios are compared. Similar to the damping matrix identification in section 5.2.3, the damping of the total system increased mostly when attached by the satellite cable. The electric cable also increases the damping. However, when attached with a copper beam, the damping decreased. Therefore, the results indicate that the system damping is affected by the flexibility of an attached subsystem.

Even though, the Kim+IV method shows good identification results, it cannot present a unique damping matrix over the frequency range of interest. Thus, we need to identify the damping matrices near every natural frequency. To overcome this weakness of the Kim+IV method, the author will consider an identification approach that can generate the unique damping matrix over the whole frequency range of interest in next chapter.

Chapter 6

Two-step damping identification approach

6.1 Introduction

In chapter 5, the damping of the host structure is investigated using Kim's method and the IV method. Both methods identify the system matrices from measured FRF results from experiments. However, both methods need to be applied over a narrow band of frequency range in order to get accurate results. Thus the identified system matrices from both methods cannot generate the reconstructed FRFs that are matched well with the original measured FRFs over the entire frequency range of interest. To consider the whole frequency range of interest in an identification process, the modal parameters from measurements have to be considered. However, the modal parameters are only determined at the locations of resonance frequencies and of the magnitude of FRFs. Thus the remaining parts of FRFs are not reflected in identifying the damping matrix. Here, the author proposes a two-step damping identification approach that considers the full FRF and modal parameters together. First, experimental eigenvalues and eigenvectors are obtained by a combination of the System Equivalent Reduction-Expansion Process (SEREP*)* model reduction [76, 77] and the Incomplete Data Handling Method (IDHM) [65] for model updating. Then, the calculation of the damping matrix is performed.

6.2 Model reduction

In experiments, the measurement is conducted only at a limited number of locations and thus the measured data include information from a limited frequency range.

Therefore a small number of DOFs can be measured compared with the infinite number of DOFs in the analytical model. To compare the analytical results with measurement data, the DOFs of the analytical model need to be reduced to the size of the measurement data. Friswell and Mottershead [54] present the excellent summary of various model reduction methods.

Static Reduction

The most common and classical reduction method has been proposed by Guyan [73]. It is referred to as static reduction. From the equation of motion, the mass and stiffness matrices **M** and **K** and the response and input vectors **x** and **f** are partitioned as

$$\left[\begin{array}{c|c} \mathbf{M}_{mm} & \mathbf{M}_{sm} \\ \hline \mathbf{M}_{sm} & \mathbf{M}_{ss} \end{array}\right]\left\{\begin{array}{c} \ddot{\mathbf{x}}_m \\ \hline \ddot{\mathbf{x}}_s \end{array}\right\}+\left[\begin{array}{c|c} \mathbf{K}_{mm} & \mathbf{K}_{ms} \\ \hline \mathbf{K}_{sm} & \mathbf{K}_{ss} \end{array}\right]\left\{\begin{array}{c} \mathbf{x}_m \\ \hline \mathbf{x}_s \end{array}\right\}=\left\{\begin{array}{c} \mathbf{f}_m \\ \hline \mathbf{0} \end{array}\right\} \tag{71}$$

The subscript *m* presents the master or measured degrees of freedom, and *s* refers to the slave or unmeasured degrees of freedom. Neglecting the inertia term in lower part of equation yields

$$\mathbf{K}_{sm}\mathbf{x}_m + \mathbf{K}_{ss}\mathbf{x}_s = \mathbf{0} \tag{72}$$

The response vector **x** can be expressed using a static transformation matrix $\mathbf{T}_s$ as

$$\left\{\begin{array}{c} \mathbf{x}_m \\ \hline \mathbf{x}_s \end{array}\right\} = \mathbf{T}_s\mathbf{x}_m = \left[\begin{array}{c} \mathbf{I} \\ \hline -\mathbf{K}_{ss}^{-1}\mathbf{K}_{sm} \end{array}\right]\{\mathbf{x}_m\} \tag{73}$$

Finally, the reduced mass and stiffness matrices, $\mathbf{M}_R$ and $\mathbf{K}_R$ can be shown as

$$\mathbf{M}_R = \mathbf{T}_s^T\mathbf{M}\mathbf{T}_s, \ \mathbf{K}_R = \mathbf{T}_s^T\mathbf{K}\mathbf{T}_s \tag{74}$$

Dynamic Reduction

Paz [74] introduced the dynamic reduction method that includes the inertia forces. In dynamic reduction method, the equation (73) at the chosen frequency ω_i is changed and given by:

$$\left\{\begin{array}{c}\mathbf{x_m}\\ \hline \mathbf{x_s}\end{array}\right\} = \mathbf{T_d x_m} = \left[\begin{array}{c}\mathbf{I}\\ \hline -\left(\mathbf{K_{ss}} - \omega_i^2\mathbf{M_{ss}}\right)^{-1}\left(\mathbf{K_{sm}} - \omega_i^2\mathbf{M_{ss}}\right)\end{array}\right]\left\{\mathbf{x_m}\right\} \tag{75}$$

where $\mathbf{T_d}$ is the dynamic transformation matrix, and the reduced matrices can be obtained using the same approach as in the equation (74) above.

Improved Reduced System (IRS) method

O'Callahan [75] introduced the *Improved Reduction System* that improve the static reduction method. The transformation matrix $\mathbf{T_i}$ is given by:

$$\mathbf{T_i} = \mathbf{T_s} + \mathbf{SMT_s M_R^{-1} K_R} \tag{76}$$

where singular matrix $\mathbf{S} = \begin{bmatrix} \mathbf{0} & \mathbf{0} \\ \mathbf{0} & \mathbf{K_{ss}^{-1}} \end{bmatrix}$ and $\mathbf{T_s}$, $\mathbf{M_R}$ and $\mathbf{K_R}$ are the static transformation matrix, reduced mass, and stiffness matrices from the static reduction, respectively.

System Equivalent Reduction Expansion Process (SEREP)

The system equivalent reduction expansion process (SEREP) [76] uses the computed eigenvectors to reduce the transformation between the master and slave coordinates. The analytical eigenvectors are partitioned into the master and slave coordinates so that

$$\Phi = \left[\begin{array}{c}\Phi_m\\ \hline \Phi_s\end{array}\right] \tag{77}$$

and the generalized or pseudo inverse of Φ_m is used to compute the transformation, when the number of master coordinates is greater than the number of modes. This yields

$$\mathbf{T} = \begin{bmatrix} \Phi_m \\ \hline \Phi_s \end{bmatrix} \Phi_m^+ \tag{78}$$

where '+' denotes the pseudo inverse. The reduced mass and stiffness matrices can be obtained by

$$\mathbf{M}_R = \mathbf{T}^T\mathbf{M}\mathbf{T}, \ \mathbf{K}_R = \mathbf{T}^T\mathbf{K}\mathbf{T} \tag{79}$$

Comparison

Avitable et al. [77] compared the model reduction methods. The natural frequencies of the reduced model that use static reduction are higher than those in the original model. The dynamic reduction can generate accurate results, but the reduction results depend on the selection of frequency ω_i. The IRS method yields natural frequencies close to those of the original analytical model. The SEREP has given the same natural frequencies as those of the original model. Based on the comparison results, the author has applied SEREP to reduce the model in this research.

6.3 IDHM model updating

Carvalho et al. [65] presents a new direct method for a finite element matrix updating approach that can handle incomplete measured data conveniently in an algorithmic way without using standard modal expansion or reduction techniques. The method is also capable of preserving the large number of eigenvalues and eigenvectors of the finite element model that are not affected by updating. The latter has an effect of preventing the appearance of spurious modes in the frequency range of interest.

6.3.1 Introduction

Consider the finite element model of an undamped vibrating system such as

$$\mathbf{M}\ddot{x}(t) + \mathbf{K}x(t) = \mathbf{0} \tag{80}$$

Assuming a solution $x(t) = ue^{\lambda t}$ yields a quadratic eigenvalue problem as

$$\left(\lambda^2\mathbf{M} + K\right)u(t) = \mathbf{0} \tag{81}$$

The matrix $P(\lambda) = \lambda^2\mathbf{M} + \mathbf{K}$ is called a quadratic matrix pencil, and has *2n* eigenvalues and *2n* eigenvectors where *n* is the total degree of freedoms. And the finite eigenstructure of P can be represented as

$$\mathbf{M}X\Lambda^2 + \mathbf{K}X = \mathbf{0} \tag{82}$$

where $\mathbf{X} \in R^{n\times n}$ and $\Lambda^2 \in R^{n\times n}$. The matrix Λ^2 is a diagonal matrix of eigenvalue and its components are non-positive real numbers. And the matrix $\mathbf{X}$ and Λ^2 can be partitioned as

$$X = \begin{bmatrix} X_1 & X_2 \end{bmatrix}, \qquad \Lambda^2 = \begin{bmatrix} \Lambda_1^2 & \mathbf{0} \\ \mathbf{0} & \Lambda_2^2 \end{bmatrix} \tag{83}$$

where $\mathbf{X}_1 \in R^{n\times p}$, $\Lambda_1^2 \in R^{p\times p}$ and p is the number of measured modes. Substituting equation (89) into (88) yields

$$\mathbf{M}X_2\Lambda_2^2 + \mathbf{K}X_2 = \mathbf{0} \tag{84}$$

And we can also obtain the eigenvalue and eigenvector matrices from experimental data such as

$$\mathbf{Y} = \begin{bmatrix} \mathbf{Y_1} & \mathbf{Y_2} \end{bmatrix}, \qquad \Sigma^2 = \begin{bmatrix} \Sigma_1^2 & \mathbf{0} \\ \mathbf{0} & \Sigma_2^2 \end{bmatrix} \tag{85}$$

Where $\mathbf{Y}_1 \in \boldsymbol{R}^{n\times p}$ and $\Sigma_1^2 \in \boldsymbol{R}^{p\times p}$. The updated stiffness matrix should satisfy the orthogonality and eigenstructure preserving updating feature in the following theorems [65].

Theorem 1. *If* Λ_1^2 *and* Λ_2^2 *has no common eigenvalues, then*

$$\mathbf{X}_1^T\mathbf{M}\mathbf{X}_2 = \mathbf{0}, \mathbf{X}_1^T\mathbf{K}\mathbf{X}_2 = \mathbf{0} \tag{86}$$

Theorem 2. *If* Λ_1^2 *and* Λ_2^2 *has no common eigenvalue, for every symmetric matrix* ψ *, the updated pencil* $\boldsymbol{P}_U(\lambda) = \lambda^2\mathbf{M} + \mathbf{K}_U$ *, where*

$$\mathbf{K}_U = \mathbf{K} - \mathbf{M}\mathbf{X}_1\psi\mathbf{X}_1^T\mathbf{M} \tag{87}$$

And we can also obtain the relation such as

$$\mathbf{M}\mathbf{X}_2\Lambda_2^2 + \mathbf{K}_U\mathbf{X}_2 = \mathbf{0} \tag{88}$$

This relation is identical with equation (84)*. Thus, the (2n-p) eigenvalues and its corresponding eigenvectors are not affected by the updating procedure.*

Theorem 3. *There exists a symmetric matrix* ψ *such that* $\mathbf{M}\mathbf{Y}_1\Sigma_1^2 + \mathbf{K}_U\mathbf{Y}_1 = \mathbf{0}$ *, if and only if* $\mathbf{Y}_1 = \mathbf{X}_1\mathbf{T}$ *for some nonsingular matrix* **T**. **T** *can be expressed as* $\mathbf{T}=\mathbf{V}\mathbf{D}_1$ *where* $\mathbf{D}_1=\mathbf{X}^T\mathbf{M}\mathbf{X}$ *and* **V** *are orthogonal.*

Using theorems 1-3, we can define an updated stiffness matrix. Now we need to construct the unknown part $\mathbf{Y}_{12}$ of measured eigenvector $\mathbf{Y}_1$. From equation (82) and (85), we can obtain

$$\mathbf{M}\mathbf{Y}_1\Sigma_1^2 + \mathbf{K}_U\mathbf{Y}_1 = \mathbf{0} \tag{89}$$

$\mathbf{Y}_1$ is an experimental eigenvector matrix. And the part $\mathbf{Y_{11}}$ has been only measured from $\mathbf{Y_1} = \begin{bmatrix} \mathbf{Y_{11}} \\ \hline \mathbf{Y_{12}} \end{bmatrix}$ where $\mathbf{Y}_{11} \in \boldsymbol{R}^{p \times p}$. Then, substituting the equation (87) into (89), we have

$$\mathbf{M}\begin{bmatrix} \mathbf{Y_{11}} \\ \hline \mathbf{Y_{12}} \end{bmatrix}\Sigma_1^2 + \mathbf{K}\begin{bmatrix} \mathbf{Y_{11}} \\ \hline \mathbf{Y_{12}} \end{bmatrix} = \mathbf{M}\mathbf{X}_1\psi\mathbf{X}_1^T\mathbf{M}\begin{bmatrix} \mathbf{Y_{11}} \\ \hline \mathbf{Y_{12}} \end{bmatrix} \tag{90}$$

If we define the QR factorization of $\mathbf{MX}_1$ as

$$\mathbf{M}\mathbf{X}_1 = \begin{bmatrix} \mathbf{U}_1 \vdots \mathbf{U}_2 \end{bmatrix}\begin{bmatrix} \mathbf{Z} \\ \hline \mathbf{0} \end{bmatrix} \tag{91}$$

From the QR factorization in equation (91), the orthogonal matrices $\mathbf{U_1} \in \boldsymbol{R}^{n \times p}$ and $\mathbf{U}_2 \in \boldsymbol{R}^{n \times (n-p)}$ and an upper triangular matrix $\mathbf{Z} \in \boldsymbol{R}^{p \times p}$ can be obtained. Let's partition the matrices $\mathbf{M}$ and $\mathbf{K}$ as $\mathbf{M} = \begin{bmatrix} \mathbf{M_1} & \mathbf{M_2} \end{bmatrix}$ and $\mathbf{K} = \begin{bmatrix} \mathbf{K_1} & \mathbf{K_2} \end{bmatrix}$ where $\mathbf{M_1}, \mathbf{K_1} \in \boldsymbol{R}^{n \times p}$. Pre-multiplying $\begin{bmatrix} \mathbf{U_1} & \mathbf{U_2} \end{bmatrix}^T$ on both sides of equation (90) and applying relation in equation (91) with partitioned $\mathbf{M}$ and $\mathbf{K}$ yields,

$$\begin{bmatrix} \mathbf{U}_1^T \\ \hline \mathbf{U}_2^T \end{bmatrix}\left(\mathbf{M}_1\mathbf{Y}_{11} + \mathbf{M}_2\mathbf{Y}_2\right)\Sigma_1^2 + \begin{bmatrix} \mathbf{U}_1^T \\ \hline \mathbf{U}_2^T \end{bmatrix}\left(\mathbf{K}_1\mathbf{Y}_{11} + \mathbf{K}_2\mathbf{Y}_{12}\right) = \begin{bmatrix} \mathbf{Z} \\ \hline \mathbf{0} \end{bmatrix}\psi\mathbf{X}_1^T\mathbf{M}\mathbf{Y}_1 \tag{92}$$

The lower part of equation (92) returns the following

$$\mathbf{U}_2^T\left(\mathbf{M}_1\mathbf{Y}_{11} + \mathbf{M}_2\mathbf{Y}_2\right)\Sigma_1^2 + \mathbf{U}_2^T\left(\mathbf{K}_1\mathbf{Y}_{11} + \mathbf{K}_2\mathbf{Y}_{12}\right) = \mathbf{0} \tag{93}$$

Rearranging (93) yields

$$\mathbf{U}_2^T\mathbf{M}_2\mathbf{Y}_{12}\Sigma_1^2 + \mathbf{U}_2^T\mathbf{K}_2\mathbf{Y}_{12} = -\mathbf{U}_2^T\left(\mathbf{K}_1\mathbf{Y}_{11} + \mathbf{M}_1\mathbf{Y}_{11}\Sigma_1^2\right) \tag{94}$$

And equation (94)(117) is a descriptor Sylvester equation for $\mathbf{Y}_{12}$. After calculation of $\mathbf{Y}_{12}$, we can obtain the complete $\mathbf{Y_1} = \begin{bmatrix} \mathbf{Y}_{11} \\ \hline \mathbf{Y}_{12} \end{bmatrix}$. To apply a mass normalization condition, we need to calculate matrix L and the diagonal matrix $\mathbf{J} \in \boldsymbol{R}^{p \times p}$ by satisfying the $\mathbf{LJL}^T = \mathbf{Y}_1^T \mathbf{M} \mathbf{Y}_1 = \mathbf{D}$, where $\mathbf{D}$ is a diagonal matrix. $\mathbf{L}$ and $\mathbf{J}$ can be calculated by using the Singular Value Decomposition (SVD). And $\mathbf{Y}_1$ is updated as

$$\mathbf{Y}_1 = \mathbf{Y}_1 \left(\mathbf{L}^{-1} \right)^T \tag{95}$$

Now, the symmetric matrix ψ can be calculated by solving

$$\left(\mathbf{Y}_1^T \mathbf{M} \mathbf{X}_1 \right) \psi \left(\mathbf{Y}_1^T \mathbf{M} \mathbf{X}_1 \right)^T = \mathbf{Y}_1^T \mathbf{M} \mathbf{Y}_1 \Sigma_1^2 + \mathbf{Y}_1^T \mathbf{K} \mathbf{Y}_1 \tag{96}$$

Finally, the updated stiffness matrix $\mathbf{K}_U$ can be acquired and becomes

$$\mathbf{K}_U = \mathbf{K} - \mathbf{M} \mathbf{X}_1 \psi \mathbf{X}_1^T \mathbf{M} \tag{97}$$

6.3.2 Experimental validation

Here, the IDHM has been applied to the experimental data and validated. The experiments were conducted with an aluminum beam with dimension $15" \times 1" \times 1/8"$. The natural frequencies and their corresponding mode shapes are summarized in Table 28. The mode shapes are shown in Figure 82.

Table 28 Experimental natural frequencies and mode shapes

Modes	1	2	3	4	5
Natural Frequency	117.02	311.42	622.12	1027.3	1547.8
Mode shape	0.90678 0.53530 -0.78795	0.30291 -0.70992 -0.84666	0.32569 1.00000 0.7945	0.67727 1.00000 -0.68489	0.98686 1.00000 -0.96773

	-0.97051	-0.84666	-0.69758	-0.98062	-0.59224
	-1.00000	0.01706	-0.97836	0.00947	0.97894
	-0.99083	0.80577	-0.69278	0.96828	-0.78614
	-0.81283	1.00000	0.72794	0.68410	-0.96885
	0.54013	0.73403	0.99770	-0.96383	0.90887
	0.73030	-0.49683	0.27372	-0.44695	0.67415

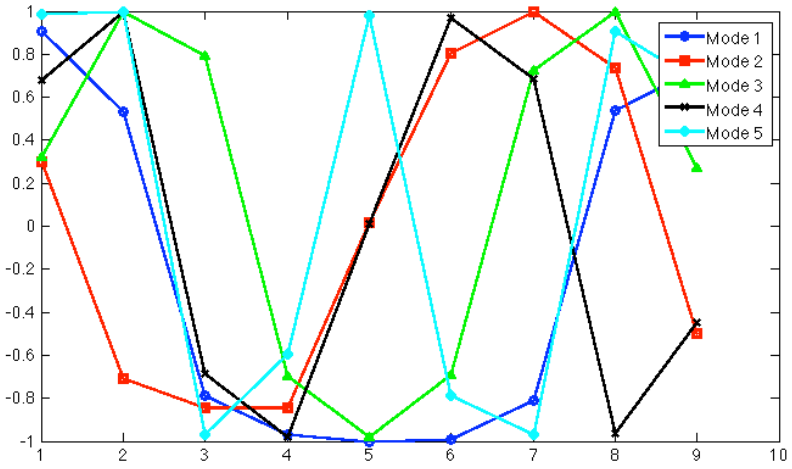

Figure 82 Experimental mode shapes (1st~5th)

From equations (96) and (97), the updated stiffness matrix can be obtained. The Eigenfrequencies of the updated analytical model are summarized in Table 29. The natural frequencies of measurement are reflected in the updated model. And the remaining eigenfrequencies after the 6th modes were not affected during the updating procedure. The Modal Assurance Criterion (MAC) between the FEM model and the updated model is summarized in

Table 30. The diagonal terms are very close to a value of 1 and the off-diagonal term is close to 0. This indicates that the updated modes correspond very well with those of the FEM model.

Table 29 Comparison of eigenfrequencies (measurement, FEM, updated)

Mode	Measure	FEM	Updated

1	**117.02**	114.48	117.02
2	**311.42**	315.64	311.42
3	**622.12**	619.24	622.12
4	**1027.3**	1025.3	1027.3
5	**1547.8**	1536.4	1547.8
6	**-**	**2156.5**	2156.5
7	**-**	**2891.2**	2891.2
8	**-**	**3742.3**	3742.3
9	**-**	**4655.4**	4655.4
10	**-**	**6211.6**	6211.6

Table 30 MAC between FEM model and updated model

Mode	1	2	3	4	5
1	**0.98612**	8.3349e-25	0.012924	3.3468e-26	0.00043515
2	4.5093e-26	**0.98263**	3.6461e-25	0.015008	2.2991e-28
3	0.01243	2.9043e-26	**0.97199**	2.6105e-27	0.01221
4	9.8406e-28	0.01522	6.6454e-27	**0.97323**	1.7146e-25
5	0.001284	5.9924e-28	0.013533	7.3024e-28	**0.97846**

6.4 Damping matrix identification

The equation of motion of a vibrating system in harmonic excitation is expressed as

$$\left[\left(\mathbf{K}-\omega^2\mathbf{M}\right)+\mathrm{j}(\omega\mathbf{C}+\mathbf{D})\right]\mathbf{X}(\omega)=\mathbf{F}(\omega) \tag{98}$$

Where the **M** and **K** are the reduced mass and stiffness matrices by SEREP, and the damping matrices **C** and **D** are required to be identified. Pre-multiplying $\left(\mathbf{K}-\omega^2\mathbf{M}\right)^{-1}$ on both side yields

$$\left[\mathbf{I}+\mathrm{j}\left(\mathbf{K}-\omega^2\mathbf{M}\right)^{-1}(\omega\mathbf{C}+\mathbf{D})\right]\mathbf{X}(\omega)=\left(\mathbf{K}-\omega^2\mathbf{M}\right)^{-1}\mathbf{F}(\omega) \tag{99}$$

The complex frequency response function $\mathbf{H}^C$ is $\mathbf{F}(\omega)/\mathbf{X}(\omega)$. Then, equation (99) can be written as

$$\left[\mathbf{I}+\mathrm{j}\left(\mathbf{K}-\omega^2\mathbf{M}\right)^{-1}\left(\omega\mathbf{C}+\mathbf{D}\right)\right]\mathbf{H}^C(\omega)=\left(\mathbf{K}-\omega^2\mathbf{M}\right)^{-1} \tag{100}$$

The real and imaginary parts of the complex frequency response function $\mathbf{H}^C$ is separable

$$\left[\mathbf{I}+\mathrm{j}\left(\mathbf{K}-\omega^2\mathbf{M}\right)^{-1}\left(\omega\mathbf{C}+\mathbf{D}\right)\right]\left(\mathbf{H}_R^C+\mathrm{j}\mathbf{H}_I^C\right)=\left(\mathbf{K}-\omega^2\mathbf{M}\right)^{-1} \tag{101}$$

And then equation (101) can be written in complex form as

$$\begin{aligned}&\left[\mathbf{H}_R^C-\left(\mathbf{K}-\omega^2\mathbf{M}\right)^{-1}\mathbf{H}_I^C\left(\omega\mathbf{C}+\mathbf{D}\right)\right]+\mathrm{j}\left[\mathbf{H}_I^C+\left(\mathbf{K}-\omega^2\mathbf{M}\right)^{-1}\mathbf{H}_R^C\left(\omega\mathbf{C}+\mathbf{D}\right)\right]\\&=\left(\mathbf{K}-\omega^2\mathbf{M}\right)^{-1}\end{aligned} \tag{102}$$

The real and imaginary parts should be satisfied with the mathematical relation in both sides and thus the equation (102) can be separated into the two equations:

$$\begin{aligned}&\mathbf{H}_R^C-\omega\left(\mathbf{K}-\omega^2\mathbf{M}\right)^{-1}\mathbf{H}_I^C\,\mathbf{C}+\left(\mathbf{K}-\omega^2\mathbf{M}\right)^{-1}\mathbf{H}_I^C\,\mathbf{D}=\left(\mathbf{K}-\omega^2\mathbf{M}\right)^{-1}\\&\mathbf{H}_I^C+\omega\left(\mathbf{K}-\omega^2\mathbf{M}\right)^{-1}\mathbf{H}_R^C\,\mathbf{C}+\left(\mathbf{K}-\omega^2\mathbf{M}\right)^{-1}\mathbf{H}_R^C\,\mathbf{D}=0\end{aligned} \tag{103}$$

Equation (103) can be expressed as the over-determined equation (104), where $\omega_i\ (\boldsymbol{i}=\mathbf{1}\sim\boldsymbol{n})$.

$$\left[\begin{array}{c|c}\omega_1\left(\mathbf{K}-\omega_1{}^2\mathbf{M}\right)^{-1}\mathbf{H}^C{}_I(\omega_1) & \left(\mathbf{K}-\omega_1{}^2\mathbf{M}\right)^{-1}\mathbf{H}^C{}_I(\omega_1)\\ \omega_1\left(\mathbf{K}-\omega_1{}^2\mathbf{M}\right)^{-1}\mathbf{H}^C{}_R(\omega_1) & \left(\mathbf{K}-\omega_1{}^2\mathbf{M}\right)^{-1}\mathbf{H}^C{}_R(\omega_1)\\ \vdots & \vdots\\ \vdots & \vdots\\ \omega_n\left(\mathbf{K}-\omega_n{}^2\mathbf{M}\right)^{-1}\mathbf{H}^C{}_I(\omega_n) & \left(\mathbf{K}-\omega_n{}^2\mathbf{M}\right)^{-1}\mathbf{H}^C{}_I(\omega_n)\\ \omega_n\left(\mathbf{K}-\omega_n{}^2\mathbf{M}\right)^{-1}\mathbf{H}_R{}^C(\omega_n) & \left(\mathbf{K}-\omega_n{}^2\mathbf{M}\right)^{-1}\mathbf{H}_R{}^C(\omega_n)\end{array}\right]\left[\begin{array}{c}\mathbf{C}\\\hline\mathbf{D}\end{array}\right]=\left[\begin{array}{c}\mathbf{H}^C{}_R(\omega_1)-\left(\mathbf{K}-\omega_1{}^2\mathbf{M}\right)^{-1}\\ -\mathbf{H}^C{}_I(\omega_1)\\ \vdots\\ \vdots\\ \mathbf{H}^C{}_R(\omega_n)-\left(\mathbf{K}-\omega_n{}^2\mathbf{M}\right)^{-1}\\ -\mathbf{H}^C{}_I(\omega_n)\end{array}\right] \tag{104}$$

Finally, The damping matrices **C** and **D** can be obtained by solving equation (105) with the pseudo inverse from:

$$\begin{bmatrix} \frac{\mathbf{C}}{\mathbf{D}} \end{bmatrix} = \left[\begin{array}{c:c} \omega_1\left(\mathbf{K}-\omega_1^2\mathbf{M}\right)^{-1}\mathbf{H}_I^C(\omega_1) & \left(\mathbf{K}-\omega_1^2\mathbf{M}\right)^{-1}\mathbf{H}_I^C(\omega_1) \\ \omega_1\left(\mathbf{K}-\omega_1^2\mathbf{M}\right)^{-1}\mathbf{H}_R^C(\omega_1) & \left(\mathbf{K}-\omega_1^2\mathbf{M}\right)^{-1}\mathbf{H}_R^C(\omega_1) \\ \vdots & \vdots \\ \vdots & \vdots \\ \omega_n\left(\mathbf{K}-\omega_n^2\mathbf{M}\right)^{-1}\mathbf{H}_I^C(\omega_n) & \left(\mathbf{K}-\omega_n^2\mathbf{M}\right)^{-1}\mathbf{H}_I^C(\omega_n) \\ \omega_n\left(\mathbf{K}-\omega_n^2\mathbf{M}\right)^{-1}\mathbf{H}_R^C(\omega_n) & \left(\mathbf{K}-\omega_n^2\mathbf{M}\right)^{-1}\mathbf{H}_R^C(\omega_n) \end{array}\right]^+ \begin{bmatrix} \mathbf{H}_R^C(\omega_1)-\left(\mathbf{K}-\omega_1^2\mathbf{M}\right)^{-1} \\ -\mathbf{H}_I^C(\omega_1) \\ \vdots \\ \vdots \\ \mathbf{H}_R^C(\omega_n)-\left(\mathbf{K}-\omega_n^2\mathbf{M}\right)^{-1} \\ -\mathbf{H}_I^C(\omega_n) \end{bmatrix} \tag{105}$$

where '+' is the pseudo inverse. Considering only the viscous damping **C** or the structural damping **D**, the damping matrix **C** or **D** can be easily expressed as

$$[\mathbf{C}] = \begin{bmatrix} \omega_1\left(\mathbf{K}-\omega_1^2\mathbf{M}\right)^{-1}\mathbf{H}_I^C(\omega_1) \\ \omega_1\left(\mathbf{K}-\omega_1^2\mathbf{M}\right)^{-1}\mathbf{H}_R^C(\omega_1) \\ \vdots \\ \vdots \\ \omega_n\left(\mathbf{K}-\omega_n^2\mathbf{M}\right)^{-1}\mathbf{H}_I^C(\omega_n) \\ \omega_n\left(\mathbf{K}-\omega_n^2\mathbf{M}\right)^{-1}\mathbf{H}_R^C(\omega_n) \end{bmatrix}^+ \begin{bmatrix} \mathbf{H}_R^C(\omega_1)-\left(\mathbf{K}-\omega_1^2\mathbf{M}\right)^{-1} \\ -\mathbf{H}_I^C(\omega_1) \\ \vdots \\ \vdots \\ \mathbf{H}_R^C(\omega_n)-\left(\mathbf{K}-\omega_n^2\mathbf{M}\right)^{-1} \\ -\mathbf{H}_I^C(\omega_n) \end{bmatrix} \tag{106}$$

Or

$$[\mathbf{D}] = \begin{bmatrix} \left(\mathbf{K}-\omega_1^2\mathbf{M}\right)^{-1}\mathbf{H}_I^C(\omega_1) \\ \left(\mathbf{K}-\omega_1^2\mathbf{M}\right)^{-1}\mathbf{H}_R^C(\omega_1) \\ \vdots \\ \vdots \\ \left(\mathbf{K}-\omega_n^2\mathbf{M}\right)^{-1}\mathbf{H}_I^C(\omega_n) \\ \left(\mathbf{K}-\omega_n^2\mathbf{M}\right)^{-1}\mathbf{H}_R^C(\omega_n) \end{bmatrix}^+ \begin{bmatrix} \mathbf{H}_R^C(\omega_1)-\left(\mathbf{K}-\omega_1^2\mathbf{M}\right)^{-1} \\ -\mathbf{H}_I^C(\omega_1) \\ \vdots \\ \vdots \\ \mathbf{H}_R^C(\omega_n)-\left(\mathbf{K}-\omega_n^2\mathbf{M}\right)^{-1} \\ -\mathbf{H}_I^C(\omega_n) \end{bmatrix} \tag{107}$$

6.5 Simulation

To verify the proposed method, the identification is performed with simulated models. In these simulations, we consider only proportional damping, $\mathbf{C} = \alpha\mathbf{M} + \beta\mathbf{K}$, to emulate

the light damped, medium damped, and high damped cases by adjusting the values of α and β. The proposed damping identification method is compared with results from Kim's method and IV methods. The simulation is executed by following procedures.

1) Establish an analytical FEM model ($\mathbf{M}_A$, $\mathbf{K}_A$) with 9 nodes with 18 D.O.Fs
2) Apply SEREP Model reduction to 7DOFs FEM model ($\mathbf{M}_{A\_R}$, $\mathbf{K}_{A\_R}$) only to consider the displacement in 7 nodes except the both of the end nodes.
3) Modify the stiffness matrix to obtain the simulated experimental model ($\mathbf{M}_E$, $\mathbf{K}_E$)
4) Update the reduced analytical FEM model by using simulated data from the experimental model ($\mathbf{M}_{A\_U}$, $\mathbf{K}_{A\_U}$)
5) Generate the proportional damping matrix C ($\mathbf{C} = \alpha\mathbf{M}_{\mathbf{A\_U}} + \beta\mathbf{K}_{\mathbf{A\_U}}$)
6) Reconstruct the complex FRF, $\left(\mathbf{K}_{\mathbf{A\_U}} - \omega^2\mathbf{M}_{\mathbf{A\_U}} + \mathbf{j}\omega\boldsymbol{C}\right)^{-1}$
7) Add a noise to the complex FRF.
8) Identified the damping matrix by the proposed approach ($\mathbf{M}_{A\_U}$, $\mathbf{K}_{A\_U}$, C)

In this simulation, an aluminum beam with dimensions **50"×1"×0.125"** with clamped-clamped boundary conditions is used. The normal FEM model represents the measured data as procedure 1). To emulate the difference between the measurement and the experimental data, the stiffness matrix K in procedure is multiplied by value of 1.5 in the procedure 3). Figure 83 shows the comparison of original FRF from FEM, a simulated experimental FRF, and reconstructed FRF from the updated FEM model. In Figure 83, there is obvious difference between original FRF and experimental FRF. After updating, an updated FRF shows good agreement with experimental data.

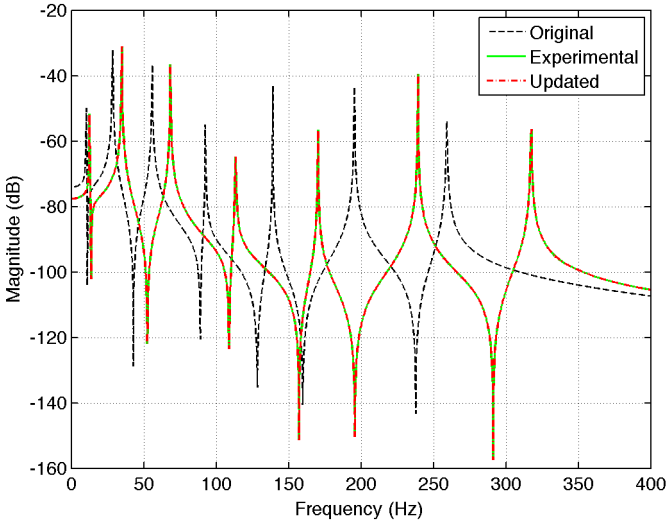

Figure 83 Comparison FRFs of original, experimental and updated models

6.5.1 Case 1: no noise and no damping

First of all, no noise and no damping are applied to the updated FRF. Figure 84 and Figure 85 show that the identified FRFs are identical because there are no damping or noise.

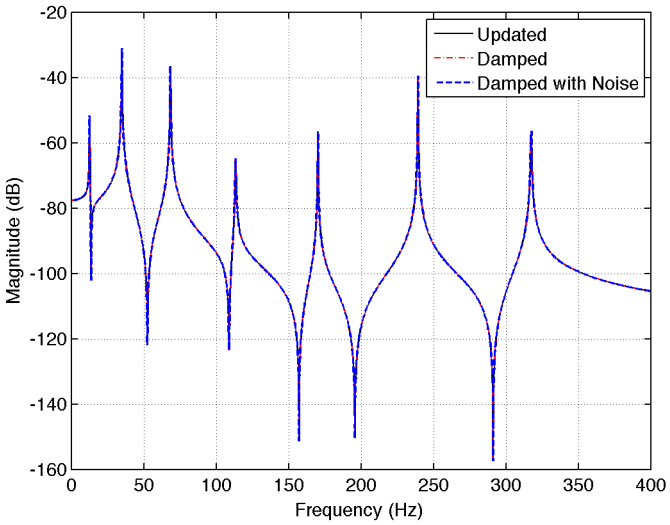

Figure 84 Comparison of noise level (no noise and no damping)

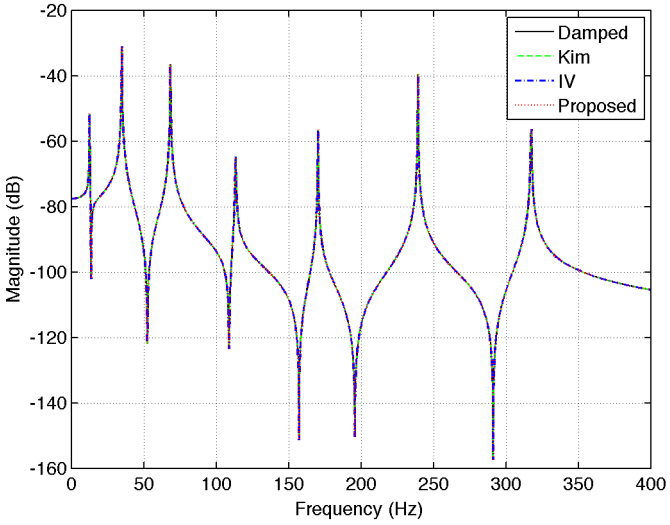

Figure 85 Comparison of identified results (no noise and no damping)

6.5.2 Case 2: light damped case, $\alpha = 10^{-7}$, $\beta = 10^{-7}$

The light damped case is considered. The proportional damping matrix **C** is obtained by using the values of $\alpha = 10^{-7}$, $\beta = 10^{-7}$.

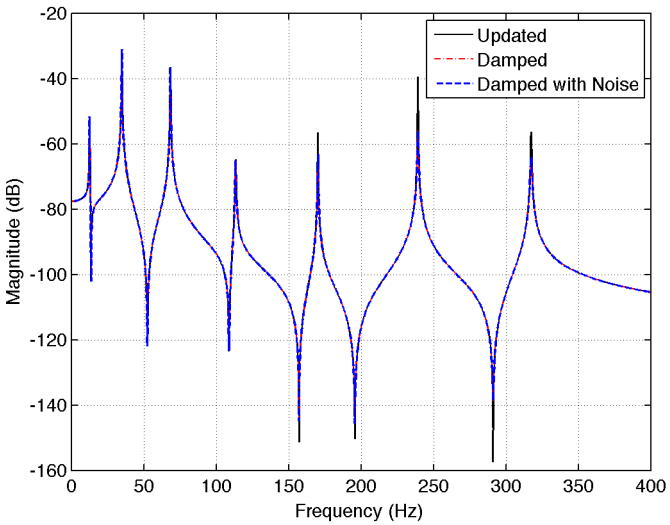

Figure 86 Comparison of FRFs (0% noise, light damped)

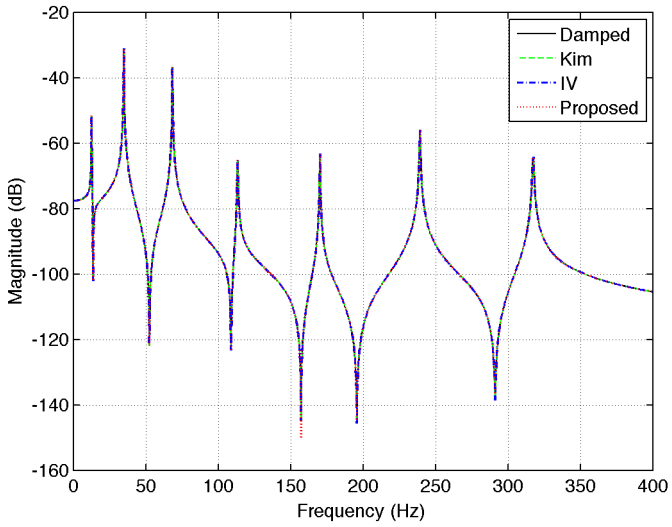

Figure 87 Comparison of reconstruct FRFs (0% noise, light damped)

Figure 86 show that the damped FRF has slightly smoother peaks than the updated FRF. In Figure 87, the reconstructed FRFs from 3 different approaches are identical because there is no noise.

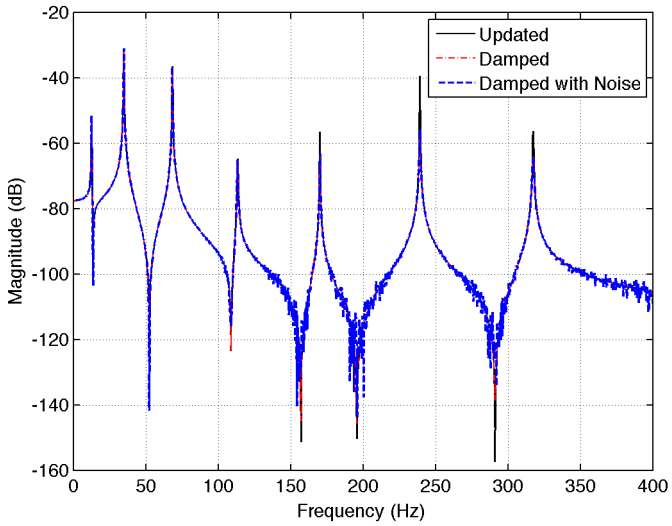

Figure 88 Comparison of FRFs (1% noise, light damped)

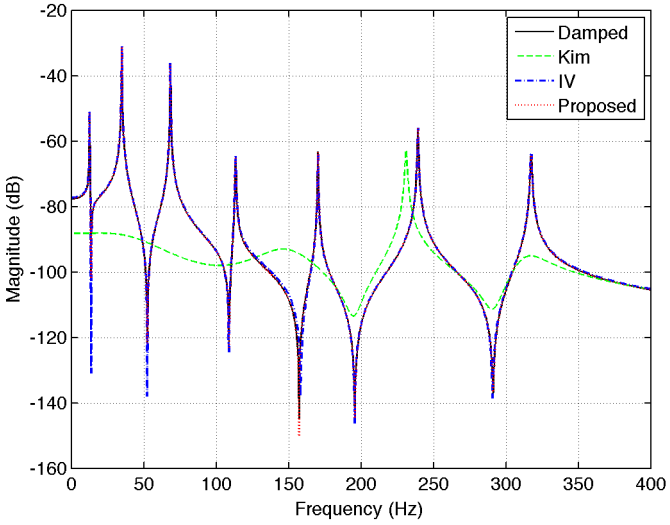

Figure 89 Comparison of reconstructed FRFs (1% noise, light damped)

A value of 1% noise is added to the updated FRF in Figure 88. Figure 89 shows the reconstructed FRFs. Identification results from Kim's method is different from the original FRF due to noise effect. As expected, the IV method and the proposed method show good identification results.

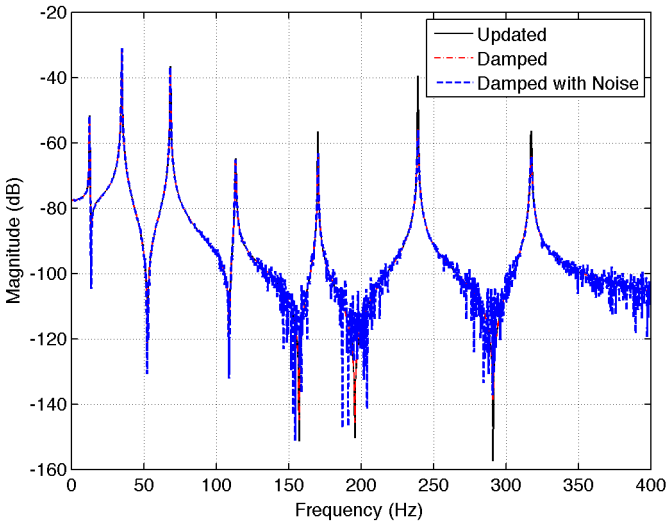

Figure 90 Comparison of FRFs (5% noise, light damped)

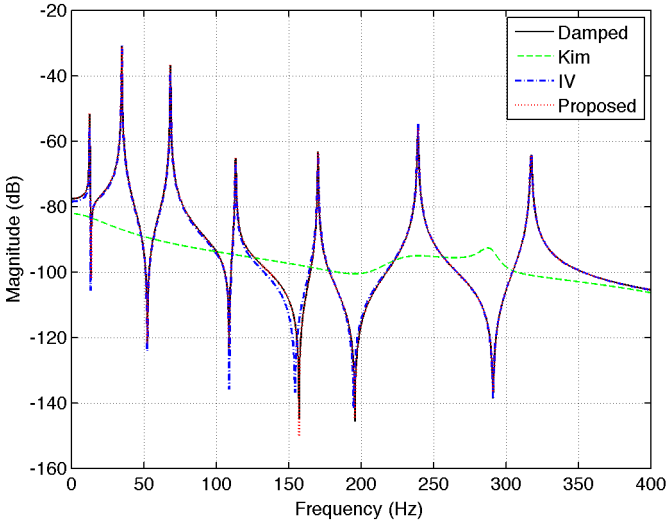

Figure 91 Comparison of reconstructed FRFs (5% noise, light damped)

In Figure 90, the noise level is increased to 5%. Figure 91 shows the reconstructed FRFs. Identification results from Kim's method is totally different from the original FRF. The IV method and the proposed method show good identification results.

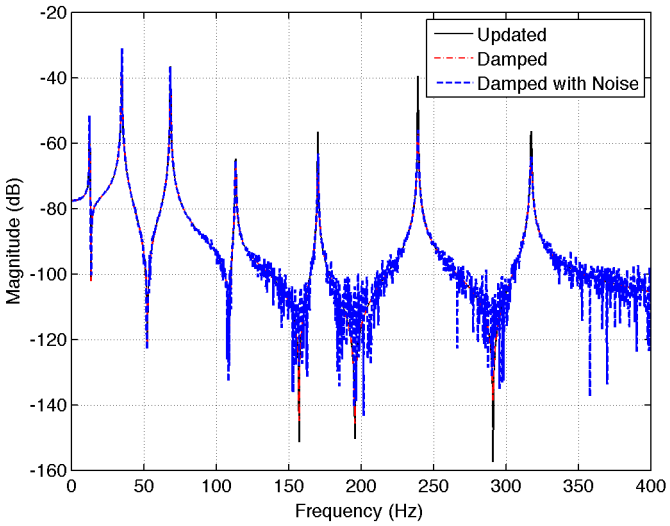

Figure 92 Comparison of FRFs (10% noise, light damped)

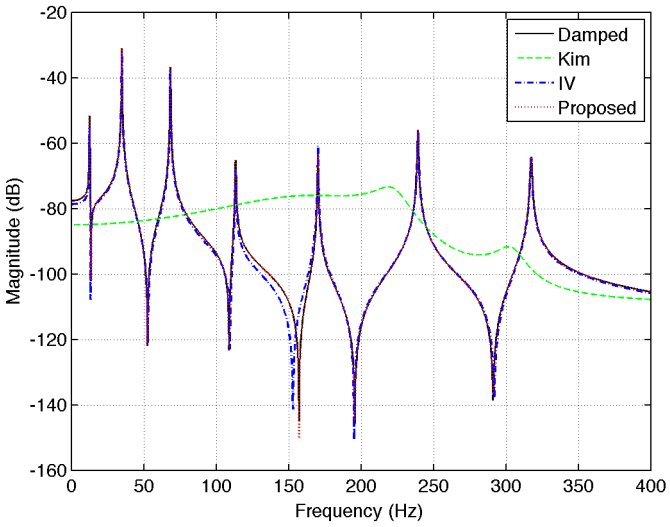

Figure 93 Comparison of reconstructed FRFs (10% noise, light damped)

In Figure 92, the noise level is increased to 10%. Figure 93 shows the reconstructed FRFs. Identification results from Kim's method are totally different from the original FRF. The IV method and the proposed method show good identification results.

6.5.3 Case 3: medium damped case, $\alpha = 10^{-6}, \beta = 10^{-6}$

To emulate the medium damped case, the values of $\alpha = 10^{-6}, \beta = 10^{-6}$ are used to construct the proportional damping **C**.

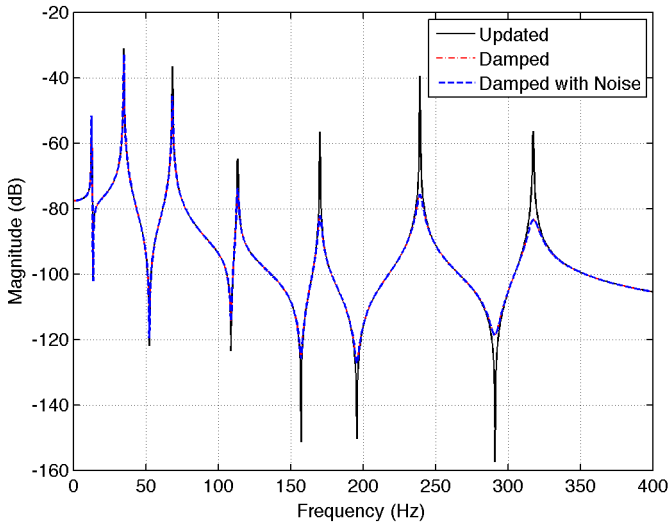

Figure 94 Comparison of FRFs (0% noise, medium damped)

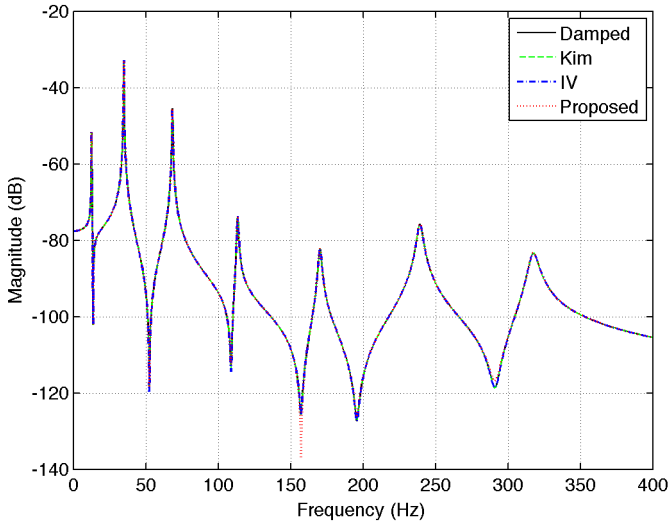

Figure 95 Comparison of reconstructed FRFs (0% noise, medium damped)

Figure 94 shows that the damped FRF has smoother peaks than the updated FRF. In Figure 95, the reconstructed FRFs from 3 different approaches are identical because there is no noise.

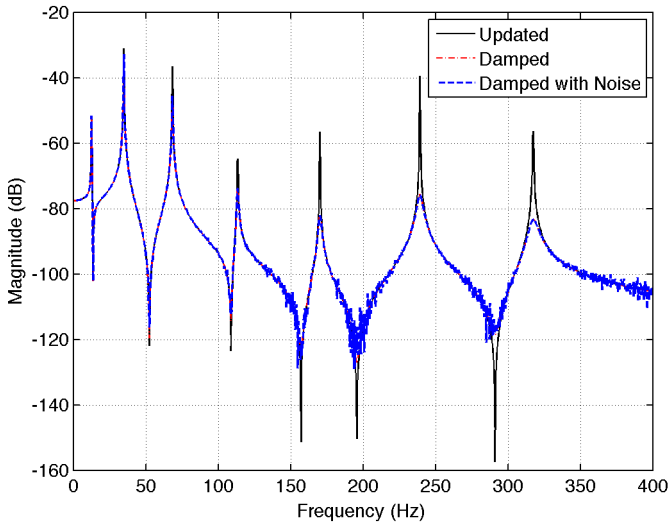

Figure 96 Comparison of FRFs (1% noise, medium damped)

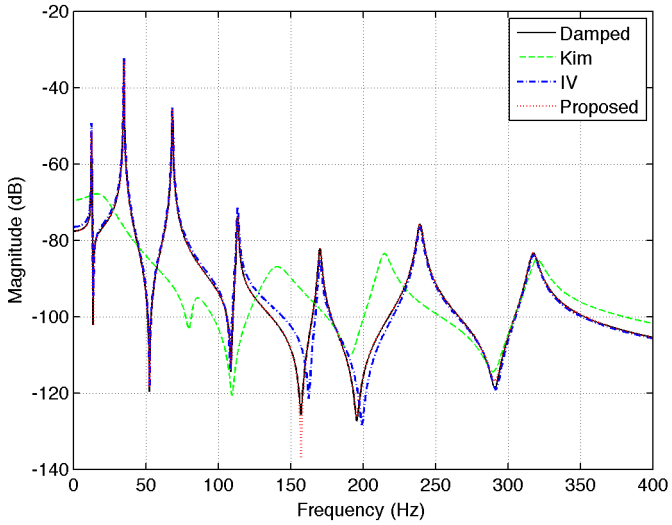

Figure 97 Comparison of reconstructed FRFs (1% noise, medium damped)

The 1% noise is added to the updated FRF in Figure 96. Figure 97 shows the reconstructed FRFs. Identification results from Kim's method cannot follow the original FRF due to the effects of noise. As expected, the IV method and the proposed method show good identification results. However, the locations of anti-peaks in FRFs from IV methods are slightly different from original FRF.

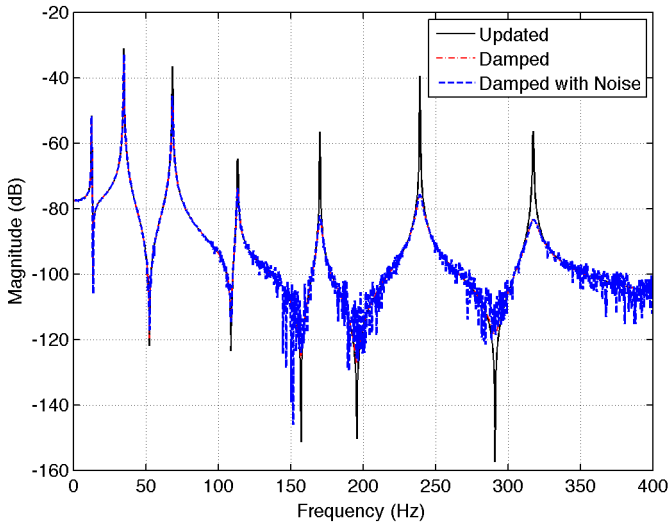

Figure 98 Comparison of FRFs (5% noise, medium damped)

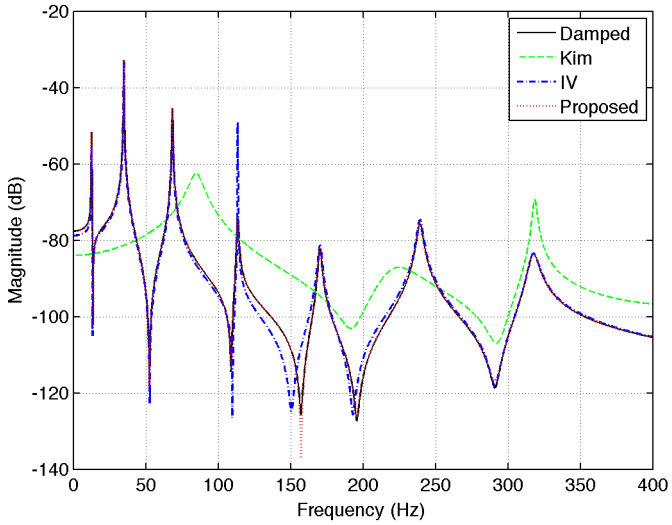

Figure 99 Comparison of reconstructed FRFs (5% noise, medium damped)

In Figure 98, the noise level is increase to 5%. Figure 99 shows the reconstructed FRFs. Identification results from Kim's method are totally different from the original FRF. The IV method and the proposed method show good identification results. Similar to what is seen in the 1% noise case, the locations of anti-peaks in FRFs from IV methods are slightly different from original FRF.

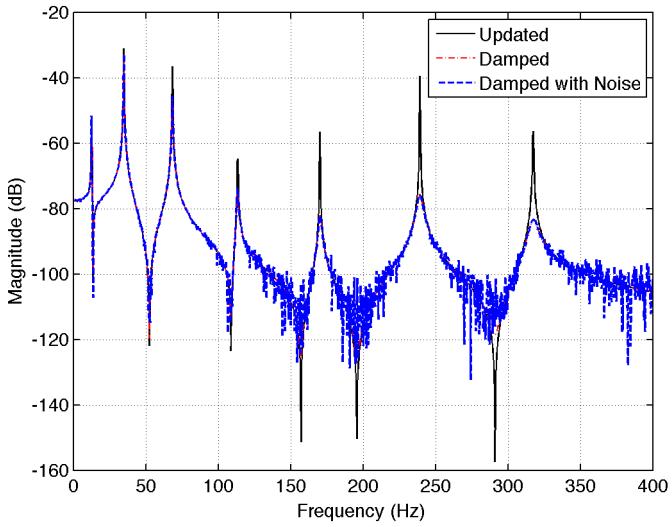

Figure 100 Comparison of FRFs (10% noise, medium damped)

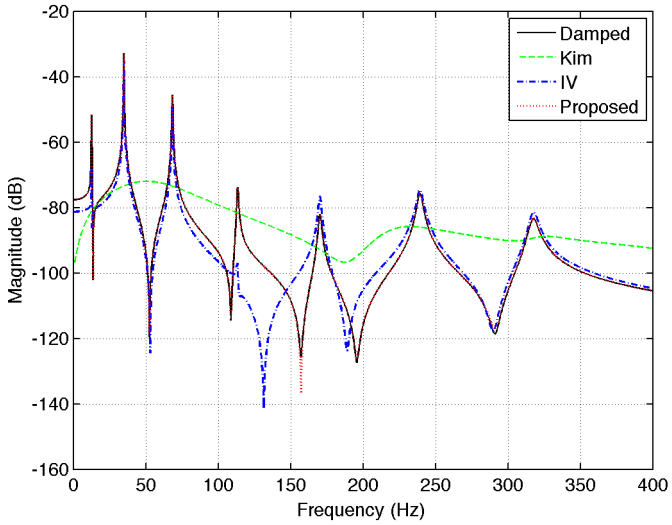

Figure 101 Comparison of reconstructed FRFs (10% noise, medium damped)

In Figure 100, the noise level is increased to 10%. Figure 101 shows the reconstructed FRFs. Identification results from Kim's method are totally different from the original FRF. The proposed method shows good identification results. But the IV method cannot reconstruct the third resonance peak.

6.5.4 Case 4: high damped case, $\alpha = 5\times10^{-6}, \beta = 5\times10^{-6}$

To emulate the high damped case, the values of $\alpha = 5\times10^{-6}, \beta = 5\times10^{-6}$ are used to construct the proportional damping **C**.

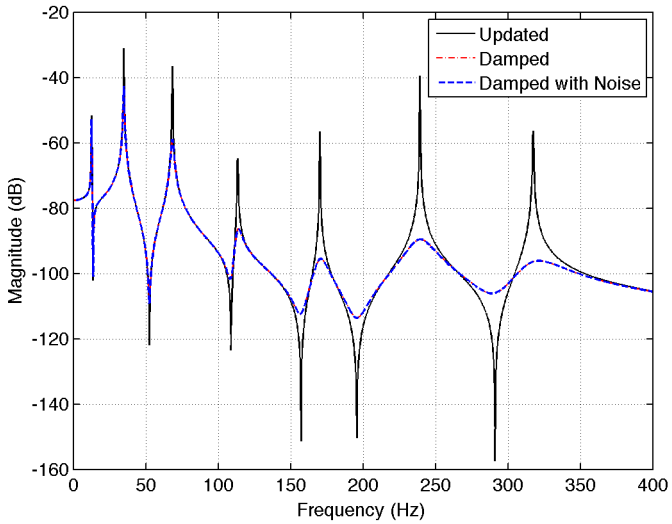

Figure 102 Comparison of FRFs (0% noise, high damped)

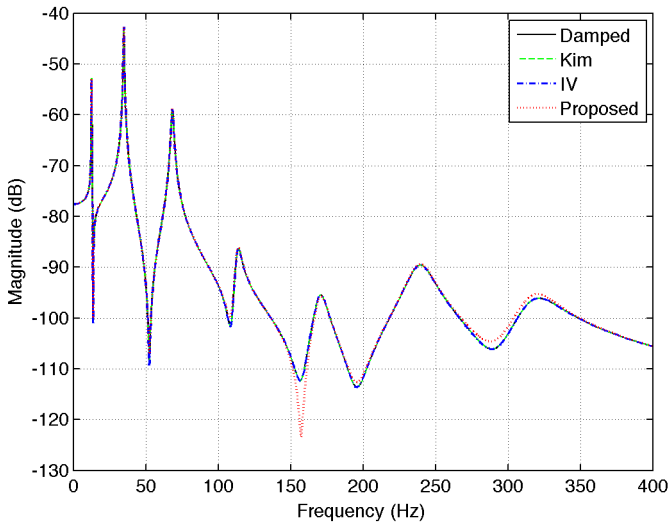

Figure 103 Comparison of reconstructed FRFs (0% noise, high damped)

Figure 102 show that the damped FRF has slightly smoother peak than the updated FRF. In Figure 103, all of identification methods can reconstructed the original FRF well.

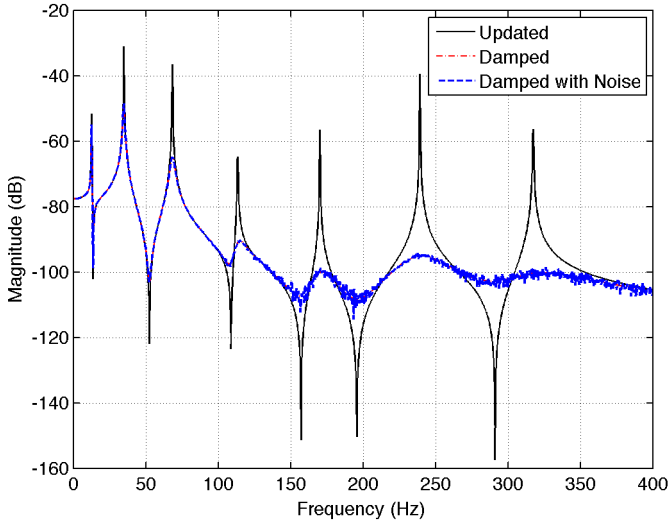

Figure 104 Comparison of FRFs (1% noise, high damped)

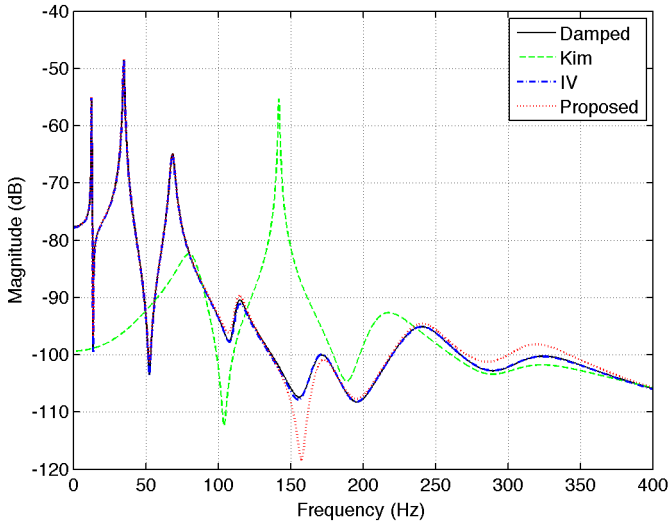

Figure 105 Comparison of reconstructed FRFs (1% noise, high damped)

The 1% noise is added to the updated FRF in Figure 104. Figure 105 shows the reconstructed FRFs. Identification results from Kim's method is different from the original FRF. As expected, the IV method and the proposed method show good identification results. However, the proposed method shows slightly a different magnitude at the 7th resonance peak.

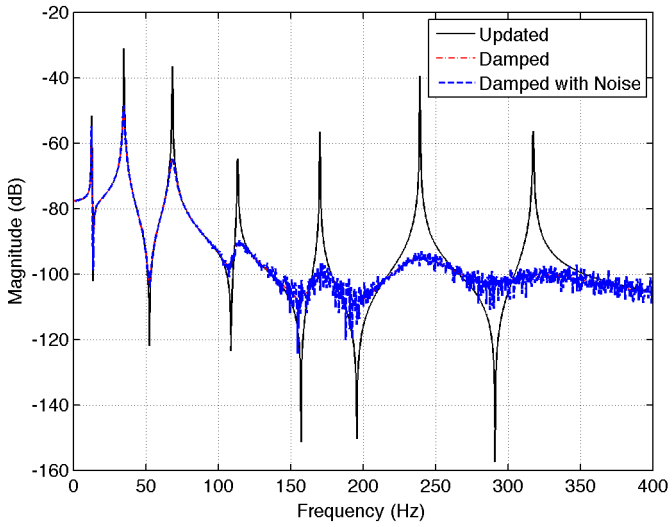

Figure 106 Comparison of FRFs (5% noise, high damped)

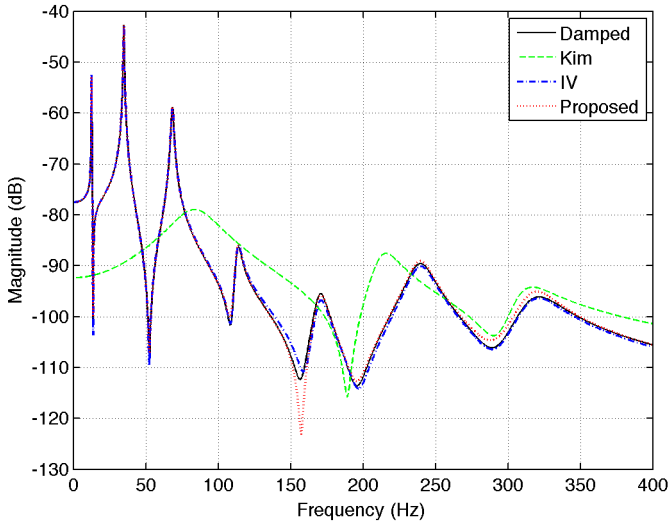

Figure 107 Comparison of reconstructed FRFs (5% noise, high damped)

In Figure 106, the noise level is increased to 5%. Figure 107 shows the reconstructed FRFs. Identification results from Kim's method are totally different from the original FRF. The IV method and the proposed method show good identification results.

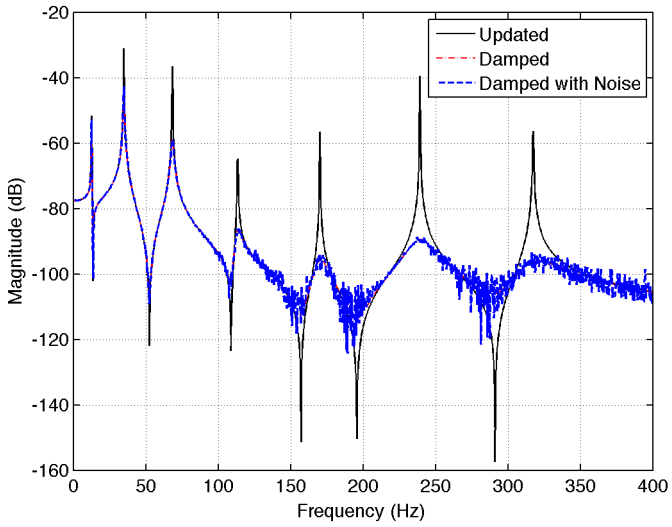

Figure 108 Comparison of FRFs (10% noise, high damped)

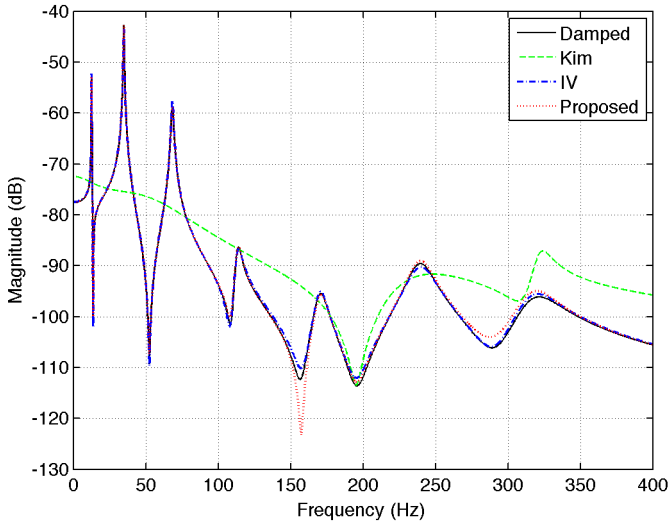

Figure 109 Comparison of reconstructed FRFs (10% noise, high damped)

In Figure 108, the noise level is increased to 10%. Figure 109 shows the reconstructed FRFs. Identification results from Kim's method cannot follow the original FRF. The IV method and the proposed method show good identification results.

6.5.5 Summary

During the simulation, the performance of the proposed method is verified in light, medium, and high damped cases with various levels of noise. A comparison between Kim's method and the IV method is given in each case. The proposed method shows good identification results in most of cases. And it can overcome the noise effect in FRFs as well as in the IV method. But the results show that the Kim's method is very sensitive to the noise in data.

6.6 Experimental validation

The proposed method is utilized to identify the damping from the experimentally obtained measurement data. The identification is conducted with an aluminum beam with the dimension of 30-inches in length, 1¼-inches in width and 3/8-inches in thickness as in chapter 5. Figure 110 shows the comparison of FRFs from the measurement data, the reduced FEM model, and the updated model by IDHM. The reduced FEM model shows different resonance peaks compared with measurement data. After the updating process, the updated FRF shows good agreement with measured FRFs. In Figure 111, the reconstructed FRFs are summarized and compared. The proposed method can generate the FRF that is very close to the measured FRF. However, Kim's method and the IV method cannot reproduce the original FRFs. This comes from the unsymmetrical measured FRF matrix and noise in measurement.

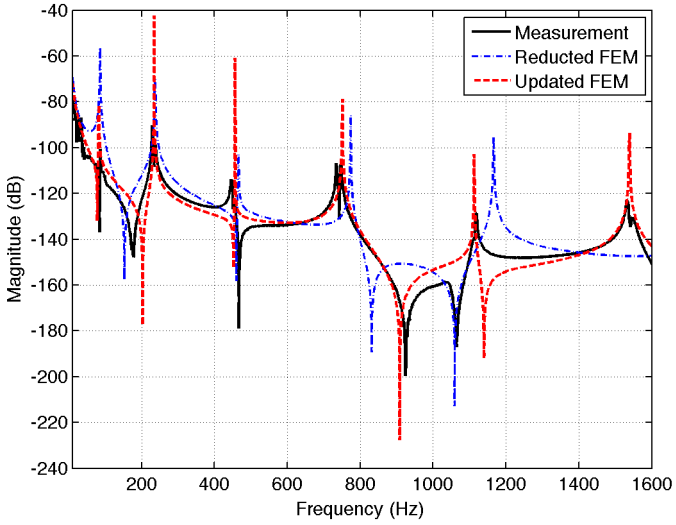

Figure 110 Comparison of H_{56} FRFs (single beam: measurement, reduced, updated)

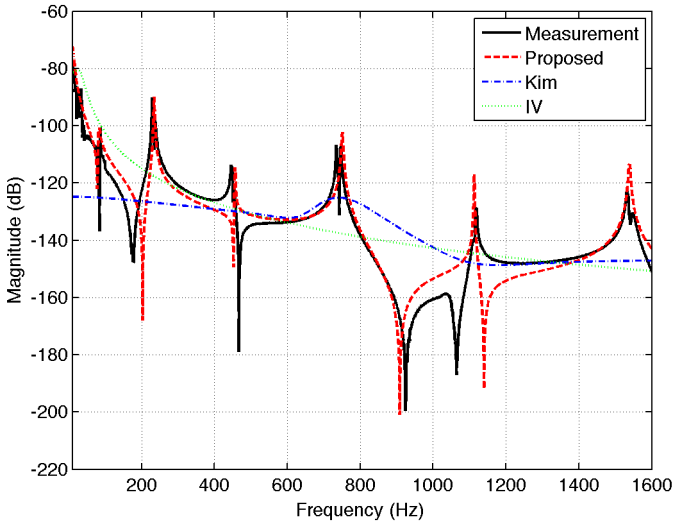

Figure 111 Comparison of reconstructed H_{56} FRFs (single beam: measurement, Proposed, Kim and IV)

The experimental data from the beam with an attached electric cable in chapter 5 is used for verification. Figure 112 shows the comparison of FRFs from measurement data, reduced FEM model and the updated model by IDHM. The updated FRF shows good agreement with measured FRF in resonance peaks. In Figure 113, the reconstructed FRFs

are summarized and compared. The proposed method can generate the FRF similar to the measured FRF. However, The proposed method shows more damping in the 2nd and 5th resonance peaks than the measured FRFs do. Kim's method and the IV method show totally different results with measurement.

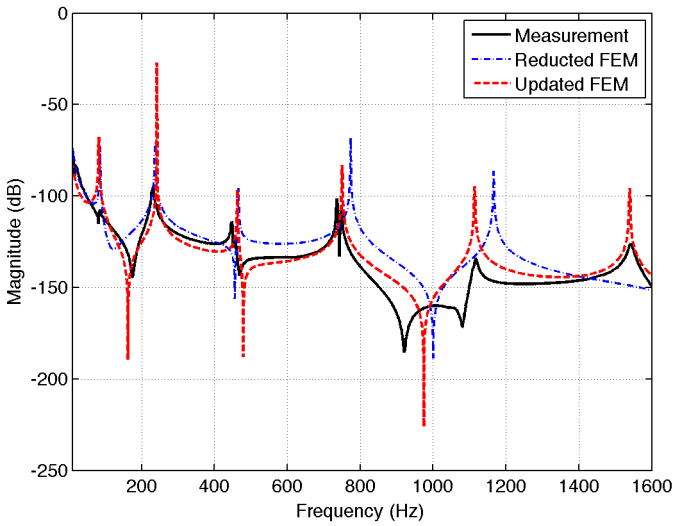

Figure 112 Comparison of H_{56} FRFs (beam with electric cable: measurement, reduced, updated)

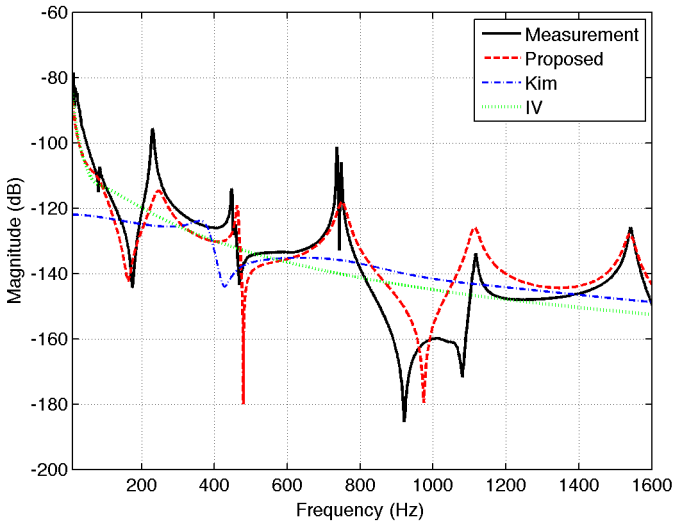

Figure 113 Comparison of reconstructed H_{56} FRFs (beam with electric cable: measurement, two step, Kim and IV)

6.7 Summary

A modified damping identification approach is proposed with a combination of SEREP model reduction and IDHM model updating. In simulation, the proposed method shows very stable results in various levels of noise. Compared with the previously published method of Kim and the IV method, the proposed approach can reconstruct the FRF that is close to the original measured FRF in the full frequency range of interest. In addition the proposed method can recover a damping matrix valid over the whole frequency range of interest.

Chapter 7

Conclusions

In this research, a change of dynamic characteristics of a cable-harnessed structure is investigated in detail. The author focused on the natural frequencies and damping of a total system. First, the natural frequencies of a combined system are observed. The simplified model of a cable-harnessed structure is presented as a double system. A spectral formulation of a double beam system is proposed using the spectral element method. The SEM modeling enables the determination of accurate results with a minimum number of degrees of freedom. Using the mesh and assembly features of SEM, the interconnections between two beams are easily defined. SEM is able to track the effect of interconnections. The SEM formulation of a double beam system is compared with the conventional FEM in numerical simulations. The numerical simulations illustrate that SEM can generate the accurate results with much smaller degrees of freedom compared with FEM. From the literature survey, the author also indicated that there are few previously published results that deal with combined distributed systems. Therefore the proposed SEM modeling is compared and validated with the experimental data. The validated modeling approach is used to investigate the effect of a stiffness of interconnection, a number of interconnections and the mass portion of an attached cable.

The damping induced by an attached cable is another issue addressed in this research. Identification of damping is a very hard task because the damping can be only determined from the measurement and thus it is not possible to obtain the general mathematical expression about damping. First of all, the method of Kim's DSM-based method is

utilized to identify the damping of a double beam system. It is investigated how the number of connections affects the damping of a total system. And the effect of type of attached cables is also observed. From the analysis of experiments, the flexibility of attached cable can cause a significant change in a total system. Thus, the effect of the flexibility of attached subsystem is checked using a lumped mass system. Kim's method shows good identification results, but is very sensitive to noise in measured data. To get the better results and to reduce the noise effect in identification, the IV method is considered using Kim's identification as an initial guess. The IV method shows good performance in reducing a noise in measurement. However, the IV method cannot guarantee accurate results over the wide range of frequency. Therefore the author proposed a two-step damping identification approach by combining the SEREP model reduction and the IDHM model updating with measurement full FRF matrix in order to consider a wide range of frequency. The proposed identification method is validated with numerical simulations and experimental data.

In conclusion, the change of the dynamic behavior of a cable-harnessed structure induced by an attached cable is investigated. During this research, the SEM modeling approach and two-step damping identification approach are proposed to observe the natural frequencies and damping of a total system. The research performed in this dissertation:

1) Produced a modeling method for considering cable harnessed structures that can produce the accurate results with minimum degrees of freedom
2) Validated a proposed modeling methodology developed here against careful experiments and against a standard FEM approach.

3) Showed that the method proposed here, allows for an understanding of how the connection ties affect the systems dynamics not obvious by standard FEM modeling.
4) Proposed a new approach to damping identification considering both of the measured FRF data and the modal parameters
5) Verified a proposed damping identification methodology developed here against careful experiments and against several damping identification methods

References

[1] D. M. Coombs, J. C. Goodding, V. Babuska, E. V. Ardelean, L. M.Robertson, S. A. Lane, Dynamic Modeling and Experimental Validation of a Cable-Loaded Panel, Journal of Spacecraft and Rockets, 48 (2011) 958-973.

[2] C.T. Sun, Y.P. Lu, Vibration damping of structural elements, Prentice Hall PTR Englewood Cliffs, 1995.

[3] D.J. Inman, Engineering vibration 4e, Pearson Prentice Hall, 2013.

[4] J. M. Seeling, W. H. Hoppmann II, Normal Mode Vibrations of Systems of Elastically Connected Parallel Bars, The Journal of the Acoustical Society of America, 36 (1964) 93-99.

[5] M. Gürgöze, On the Eigenfrequencies of A Cantilever Beam with Attached Tip Mass and a Spring-mass System, Journal of Sound and Vibration, 190 (1996) 149-162.

[6] M. Gürgöze, On the Alternative Formulations of the Frequency Equation of a Bernoulli–Euler Beam to Which Several Spring-mass Systems Are Attached In-span, Journal of Sound and Vibration, 217 (1998) 585-595.

[7] H.V. Vu, A. M. Ordóñez, B. H. Karnopp, Vibration of a Double-beam System, Journal of Sound and Vibration, 229 (2000) 807-822.

[8] J. S. Wu, H. M. Chou, Free Vibration Analysis of a Cantilever Beam Carrying Any Number of Elastically Mounted Point Masses With The Analytical-and-numerical-combined Method, Journal of Sound and Vibration, 213 (1998) 317-332.

[9] S. S. Rao, Natural vibrations of systems of elastically connected Timoshenko beams, The Journal of the Acoustical Society of America, 55 (1974) 1232-1237.

[10] J. F. Doyle, "A spectrally formulated finite element for longitudinal wave propagation," International Journal of Analytical and Experimental Modal Analysis Vol. 3, 1988, pp. 1-5.

[11] J. Doyle, T. Farris, A spectrally formulated finite element for flexural wave propagation in beams, International Journal of Analytical and Experimental Modal Analysis, 5 (1990) 99-107.

[12] S. Gopalakrishnan, M. Martin, J. Doyle, A matrix methodology for spectral analysis of wave propagation in multiple connected Timoshenko beams, Journal of Sound and Vibration, 158 (1992) 11-24.

[13] U. Lee, Vibration analysis of one-dimensional structures using the spectral transfer matrix method, Engineering structures, 22 (2000) 681-690.

[14] U. Lee, J. Kim, H. Oh, Spectral analysis for the transverse vibration of an axially moving Timoshenko beam, Journal of Sound and Vibration, 271 (2004) 685-703.

[15] J. F. Doyle, Wave propagation in structures: spectral analysis using fast discrete Fourier transforms, Springer, New York, 1997.

[16] U. Lee, Spectral element method in structural dynamics, J. Wiley & Sons Asia, Singapore; Hoboken, NJ, 2009.

[17] R. Aït-Djaoud, I. Djeran-Maigre, R. Cabrillac, Calculation of natural frequencies of beam structures including concentrated mass effects by the dynamic stiffness matrix method, Materials and Structures, 34 (2001) 71-75.

[18] J. R. Banerjee, Dynamic stiffness formulation and its application for a combined beam and a two degree-of-freedom system, Journal of Vibration and Acoustics, 125 (2003) 351-358.

[19] D.W. Chen, The exact solution for free vibration of uniform beams carrying multiple two-degree-of-freedom spring–mass systems, Journal of Sound and Vibration, 295 (2006) 342-361.

[20] J. Li, H. Hua, Spectral finite element analysis of elastically connected double-beam systems, Finite Elements in Analysis and Design, 43 (2007) 1155-1168.

[21] S. Jiao, J. Li, H. Hua, R. Shen, A spectral finite element model for vibration analysis of a beam based on general higher-order theory, Shock and Vibration, 15 (2008) 179-192.

[22] J. Li, H. Hua, Dynamic stiffness vibration analysis of an elastically connected three-beam system, Applied Acoustics, 69 (2008) 591-600.

[23] J. Choi, D.J. Inman, Spectrally formulated modeling of a cable-harnessed structure, Journal of Sound and Vibration, 333 (2014) 3286-3304.

[24] J.D. Choi, D.J. Inman, Spectral Element Method for Cable Harnessed Structure, in: Topics in Modal Analysis, Volume 7, Springer, 2014, pp. 377-387.

[25] J. D. Choi and D. J. Inman, Development of modeling for Cable Harnessed structure, 54th SDM, (2013), Boston, MA

[26] D.F. Pilkey, D.J. Inman, A survey of damping matrix identification Proceedings-SPIE, SPIE International Society for Optical, 1998, pp. 104-110.

[27] S. Pradhan, S.V. Modak, A method for damping matrix identification using frequency response data, Mechanical Systems and Signal Processing, 33 (2012) 69-82.

[28] P. Caravani, W.T. Thomson, Identification of Damping Coefficients in Multidimensional Linear Systems, Journal of Applied Mechanics, 41 (1974) 379-382.

[29] W.T. Thomson, T. Calkins, P. Caravani, A numerical study of damping, Earthquake Eng Struc, 3 (1974) 97-103.

[30] S. Chen, M. Ju, Y. Tsuei, Independent Identification of Damping Matrix from Contaminated Frequency Response Functions, Proceedings-SPIE, SPIE International Society for Optical, 1996, pp. 363-369.

[31] S.Y. Chen, M.S. Ju, Y.G. Tsuei, Estimation of Mass, Stiffness and Damping Matrices from Frequency Response Functions, Journal of vibration and acoustics, 118 (1996) 78-82.

[32] J.H. Lee, J. Kim, Identification of Damping Matrices from Measured Frequency Response Functions, Journal of Sound and Vibration, 240 (2001) 545-565.

[33] J.H. Lee, J. Kim, Development and Validation of A New Experimental Method to Identify Damping Matrices of A Dynamic System, Journal of Sound and Vibration, 246 (2001) 505-524.

[34] J.H. Lee, DEVELOPMENT OF NEW TECHNIQUE FOR DAMPING IDENTIFICATION AND SOUND TRANSMISSION ANALYSIS OF VARIOUS STRUCTURES, in, University of Cincinnati, 2001.

[35] G.O. Ozgen, J.H. Kim, Direct identification and expansion of damping matrix for experimental‐analytical hybrid modeling, Journal of Sound and Vibration, 308 (2007) 348-372.

[36] C.P. Fritzen, Identification of mass, damping, and stiffness matrices of mechanical systems, Journal of Vibration Acoustics Stress and Reliability in Design, 108 (1986) 9.

[37] M.G. Kendall, S. Alan, The advanced theory of statistics. Vols. II and III, (1961).

[38] P.C. Young, An instrumental variable method for real-time identification of a noisy process, Automatica, 6 (1970) 271-287.

[39] J.H. Wang, Mechanical parameters identification, with special consideration of noise effects, Journal of Sound and Vibration, 125 (1988) 151-167.

[40] P. Lancaster, Expressions for damping matrices in linear vibration problems, Journal of The Aerospace Science, 28 (1961) 256.

[41] S. Adhikari, Lancaster's method of damping identification revisited, Journal of vibration and acoustics, 124 (2002) 617-627.

[42] T.K. Hasselman, Method for constructing a full modal damping matrix from experimental measurements, AIAA Journal, 10 (1972) 526-527.

[43] S.R. Ibrahim, Dynamic modeling of structures from measured complex modes, AIAA Journal, 21 (1983) 898-901.

[44] C. Minas, D.J. Inman, Identification of a Nonproportional Damping Matrix from Incomplete Modal Information, Journal of vibration and acoustics, 113 (1991) 219-224.

[45] D.F. Pilkey, D.J. Inman, An iterative approach to viscous damping matrix identification, in: PROCEEDINGS-SPIE THE INTERNATIONAL SOCIETY FOR OPTICAL ENGINEERING, SPIE INTERNATIONAL SOCIETY FOR OPTICAL, 1997, pp. 1152-1157.

[46] D.F. Pilkey, Computation of a damping matrix for finite element model updating, in, Citeseer, 1998.

[47] D.F. Pilkey, G. Park, D.J. Inman, Damping matrix identification and experimental verification, in: 1999 Symposium on Smart Structures and Materials, International Society for Optics and Photonics, 1999, pp. 350-357.

[48] S. Adhikari, J. Woodhouse, Identification of damping: part 1, viscous damping, Journal of Sound and Vibration, 243 (2001) 43-61.

[49] S. Adhikari, J. Woodhouse, Identification of damping: part 2, non-viscous damping, Journal of Sound and Vibration, 243 (2001) 63-88.

[50] S. Adhikari, J. Woodhouse, Identification of damping: Part 3, symmetry-preserving methods, Journal of Sound and Vibration, 251 (2002) 477-490.

[51] M. Imregun, W. Visser, A review of model updating techniques, The Shock and vibration digest, 23 (1991) 9-20.

[52] J.E. Mottershead, M.I. Friswell, Model Updating In Structural Dynamics: A Survey, Journal of Sound and Vibration, 167 (1993) 347-375.

[53] M. Friswell, J.E. Mottershead, Finite element model updating in structural dynamics, Springer, 1995.

[54] M. Baruch. Proportional Optimal Orthogonalization of Measured Modes. AIAA Journal, 1980,18(7): 859-861.

[55] A. Berman, E. Nagy, Improvement of a large analytical model using test data, AIAA Journal(ISSN 0001-1452), 21 (1983) 1168-1173.

[56] M. Baruch., Methods of Reference Basis for Identification of Linear Dynamic Strctures, AIAA Journal, 1984(22): 561-564.

[57] B. Caesar, Updating system matrices, International Modal Analysis Conference, 5th, London, England, 1987, pp. 453-459.

[58] B. Caesar, Update and identification of dynamic mathematical models, in: International Modal Analysis Conference, 4th, Los Angeles, CA, 1986, pp. 394-401.

[59] F.S. Wei, Analytical dynamic model improvement using vibration test data, AIAA Journal, 28 (1990) 175-177.

[60] M. Friswell, D.J. Inman, D. Pilkey, Direct updating of damping and stiffness matrices, AIAA journal, 36 (1998) 491-493.

[61] C. Minas, D.J. Inman. Correcting Finite Element Models with Measured Modal Results using Eigenstructure Assignment Methods, The 6TH IMAC, 1988:583-587.

[62] C. Minas, D.J. Inman. Model Improvement by Pole Placement Methods. ASME Vibration Analysis Technique and Applications, New York, 1989:179-185.

[63] P. Tarazaga, Y. Halevi, D. Inman, Model updating with the use of principal submatrices, in: Proceedings of the 22nd International Modal Analysis Conference, 2004.

[64] P. Tarazaga, Y. Halevi, D. Inman, The quadratic compression method for model updating and its noise filtering properties, Mechanical systems and signal processing, 21 (2007) 58-73.

[65] J. Carvalho, B.N. Datta, A. Gupta, M. Lagadapati, A direct method for model updating with incomplete measured data and without spurious modes, Mechanical Systems and Signal Processing, 21 (2007) 2715-2731.

[66] R.M. Lin, D.J. Ewins, Analytical model improvement using frequency response functions, Mechanical Systems and Signal Processing, 8 (1994) 437-458.

[67] R.M. Lin, J. Zhu, Model updating of damped structures using FRF data, Mechanical Systems and Signal Processing, 20 (2006) 2200-2218.

[68] V. Arora, S.P. Singh, T.K. Kundra, Finite element model updating with damping identification, Journal of Sound and Vibration, 324 (2009) 1111-1123.

[69] V. Arora, S.P. Singh, T.K. Kundra, Damped model updating using complex updating parameters, Journal of Sound and Vibration, 320 (2009) 438-451.

[70] R.M. Lin, Identification of modal parameters of unmeasured modes using multiple FRF modal analysis method, Mechanical Systems and Signal Processing, 25 (2011) 151-162.

[71] K. Spak, G. Agnes, D. Inman, Cable Modeling and Internal Damping Developments, Applied Mechanics Reviews, 48 (2013) 010801.

[72] Brüel & Kjær, RT Pro dynamic signal analysis User Guide Rev. 7.00, 2013

[73] R.J. Guyan, Reduction of stiffness and mass matrices, AIAA journal, 3 (1965) 380-380.

[74] M. Paz, Dynamic condensation, AIAA journal, 22 (1984) 724-727.

[75] J.C. O'Callahan, A procedure for an improved reduced system (IRS) model, in: Proceedings of the 7th International Modal Analysis Conference, Union College Press, Schenectady, NY, 1989, pp. 17-21.

[76] J. O'Callahan, P. Avitabile, R. Riemer, System equivalent reduction expansion process (SEREP), in: Proceedings of the 7th international modal analysis conference, 1989, pp. 29-37.

[77] P. Avitabile, J. O'Callahan, J. Milani, Comparison of system characteristics using various model reduction techniques, in: International Modal Analysis Conference, 7th, Las Vegas, NV, 1989, pp. 1109-1115.